

ARTICLE

<https://doi.org/10.1038/s41467-018-07859-7>

OPEN

Enhancement of the gut barrier integrity by a microbial metabolite through the Nrf2 pathway

Rajbir Singh¹, Sandeep Chandrashekarappa², Sobha R. Bodduluri¹, Becca V. Baby¹, Bindu Hegde¹, Niranjana G. Kotla², Ankita A. Hiwale², Taslimarif Saiyed³, Paresh Patel³, Matam Vijay-Kumar⁴, Morgan G.I. Langille⁵, Gavin M. Douglas⁵, Xi Cheng⁴, Eric C. Rouchka⁶, Sabine J. Waigel⁷, Gerald W. Dryden⁷, Houda Alatassi⁸, Huang-Ge Zhang¹, Bodduluri Haribabu¹, Praveen K. Vemula² & Venkatakrishna R. Jala¹

The importance of gut microbiota in human health and pathophysiology is undisputable. Despite the abundance of metagenomics data, the functional dynamics of gut microbiota in human health and disease remain elusive. Urolithin A (UroA), a major microbial metabolite derived from polyphenolics of berries and pomegranate fruits displays anti-inflammatory, anti-oxidative, and anti-ageing activities. Here, we show that UroA and its potent synthetic analogue (UAS03) significantly enhance gut barrier function and inhibit unwarranted inflammation. We demonstrate that UroA and UAS03 exert their barrier functions through activation of aryl hydrocarbon receptor (AhR)- nuclear factor erythroid 2-related factor 2 (Nrf2)-dependent pathways to upregulate epithelial tight junction proteins. Importantly, treatment with these compounds attenuated colitis in pre-clinical models by remedying barrier dysfunction in addition to anti-inflammatory activities. Cumulatively, the results highlight how microbial metabolites provide two-pronged beneficial activities at gut epithelium by enhancing barrier functions and reducing inflammation to protect from colonic diseases.

¹Department of Microbiology and Immunology, James Graham Brown Cancer Center, University of Louisville, Louisville, KY 40202, USA. ²Institute for Stem Cell Biology and Regenerative Medicine (inStem), GKVK campus, Bangalore, Karnataka 560065, India. ³Centre for Cellular and Molecular Platforms (C-CAMP), GKVK campus, Bangalore, Karnataka 560065, India. ⁴Department of Physiology and Pharmacology, University of Toledo College of Medicine and Life Sciences, Toledo, OH 43614, USA. ⁵Department of Pharmacology, Dalhousie University, Halifax, B3H 4R2 Nova Scotia, Canada. ⁶Computer Engineering and Computer Science, Kentucky Biomedical Research Infrastructure Network, University of Louisville, Louisville, KY 40202, USA. ⁷Department of Medicine, University of Louisville, Louisville, KY 40202, USA. ⁸Department of Pathology, University of Louisville, Louisville, KY 40202, USA. Correspondence and requests for materials should be addressed to P.K.V. (email: praveenv@instem.res.in) or to V.R.J. (email: jvrao001@louisville.edu)

Inflammatory bowel diseases (IBD) consisting of Crohn's and ulcerative colitis are resultant of dysregulation of the immune system leading to intestinal inflammation and microbial dysbiosis. Numerous studies in recent years highlighted the pivotal role of gut microbiota and their metabolites in host physiological processes including immune, metabolic, neurological, and nutritional homeostasis^{1–4}. Thus, alterations in gut microbiota have been associated with adverse outcomes in cancer, IBD, neurological disorders, obesity, and diabetes^{1,5–7}. Microbiota and their metabolites are in close proximity to the gut epithelium that constitutes a single cell-layer separating host components from the external environment. Gut barrier integrity is maintained by the tight junction proteins such as claudins (Cldn), Zona occludin-1 (ZO1), and occludin (Ocldn) that are critical for epithelial cell barrier functions^{8,9}. Previously, it has been reported that levels of tight junction proteins are significantly down regulated under IBD conditions leading to increased gut permeability to microbial ligands and noxious metabolites resulting in systemic inflammatory responses^{8,10}. Despite the availability of large metagenomics data, the functional dynamics of microbiota and their metabolites in IBDs are unknown. Therefore, we tested the hypothesis that certain microbial metabolites will prevent gut permeability by enhancing barrier functions in addition to blocking inflammation. Treatment with such microbial metabolites will offer better therapeutic options for IBDs.

Consumption of diets containing berries and pomegranates have demonstrated significant beneficial effects on human health^{11–14}. Especially, pomegranate extract or juice containing high levels of polyphenolic compounds such as ellagitannins (ETs) and ellagic acid (EA) have been suggested to prevent hypertension¹⁵ and protect against myocardial ischemia and reperfusion injury¹⁶. They have been recognized as potential non-toxic chemo-preventive compounds against chronic diseases such as cancer, diabetes, cardiovascular and neurodegenerative disorders¹⁷. It has been suggested that further downstream metabolites of EA known as 'uroolithins' generated by gut microbiota render potential health benefits, in vivo^{18,19}. Among urolithins, Urolithin A (UroA) displayed potent anti-inflammatory, anti-oxidative and anti-ageing properties compared to other metabolites^{20–23}. Due to life style variations and antibiotic/drug usage, presence of bacteria that metabolize dietary EA to urolithins have been variable among human populations. Thus, not only the consumption of diets enriched in polyphenols is required but also the presence of microbes that convert them into beneficial metabolites is critical for manifestation of their health effects. At this time, the targets or pathways through which such microbial metabolites regulate physiological processes are largely unknown.

In this study, we examined the activities of UroA and a potent synthetic structural analogue UAS03 and identified that in addition to the anti-inflammatory activities, these compounds strongly enhanced gut barrier function. We demonstrate that both UroA and UAS03 enhance barrier function by inducing tight junction proteins through activating aryl hydrocarbon receptor (AhR)-nuclear factor erythroid 2-related factor 2 (Nrf2)-dependent pathways. Further, oral treatment with UroA/UAS03 significantly mitigated systemic inflammation and colitis suggesting potential therapeutic applications for the treatment of IBD.

Results

Synthesis and anti-inflammatory activities of UroA and UAS03. UroA (3,8-dihydroxy-6H-dibenzo[b,d]pyran-6-one) has a lactone (cyclic ester bond) that connects two mono-hydroxyl phenyl rings leading to a planar structure (Fig. 1a). Gastric pH or digestive enzymes can hydrolyze the lactone ring, which opens

the ring resulting in the loss of the planar structure and potentially its activities. To generate more stable and potent compounds, we synthesized non-hydrolyzable cyclic ether derivative, UAS03 (6H-benzo[c]chromene-3,8-diol) (Fig. 1a). The stability of both compounds was examined under conditions of gastric pH and digestive enzymes. The results showed that UAS03 indeed is stable at gastric pH and also in the presence of gastric enzymes e.g., esterases and proteases (Fig. 1a). Both UroA and UAS03 significantly decreased LPS induced IL-6 and TNF- α in mouse bone marrow derived macrophages (BMDMs) with UAS03 showing anti-inflammatory activities even at nano molar concentrations (Fig. 1b). Next, anti-inflammatory activities of UroA and UAS03 were examined in vivo in a LPS-induced peritonitis mouse model. UroA or UAS03 treatment significantly reduced the LPS-induced increase in serum IL-6 and TNF- α levels (Fig. 1c). These results suggest that UAS03 is a potent structural analogue of UroA with increased anti-inflammatory activities.

UroA/UAS03 induce tight junction proteins. Since, microbial metabolites are in close proximity to gut epithelium; we surmise that metabolites could have a direct impact on epithelial cell function. To examine such effects, we performed RNA-Seq analysis of epithelial cell line (HT29) exposed to UroA. The analysis was performed as described in methods and to determine significance of differential gene expression, cuffdiff2 algorithm was used. Based on an uncorrected *p*-value cutoff of 0.05, 1960 genes were determined to be significantly differentially expressed as a result of UroA treatment in HT29 cells. Further restricting this list, 437 genes were found to be differentially expressed at FDR corrected *q* value <0.05 in UroA treated HT29 cells (Supplementary Fig. 1 and Supplementary Data 1). The pathway analysis using this restricted gene list was performed using Ingenuity Pathway Analysis (IPA) software (Supplementary Fig. 1). The Eukaryotic Initiation Factor 2 (eIF2), mammalian target of rapamycin (mTOR) and mitochondrial dysfunction pathways were emerged as top 3 pathways. The impact of UroA on mitochondrial dysfunction (pathways of mitophagy) have been described in previously by Ryu D et al.²². They demonstrated that UroA induced mitophagy and prolonged the lifespan of *C. elegans* and increased muscle function in rodents. The impact of UroA on mTOR and eIF2 pathways need to be established in the context of colon epithelial functions. The RNA-Seq analysis showed that cytochrome P450 1A1 (*Cyp1A1*) is among the top 3 UroA upregulated genes (Supplementary Data 1). The pathways analysis further indicated that the Nrf2 and AhR signaling pathways are in top 25 (Supplementary Fig. 1). We surmise that regulation of barrier function is of critical importance in mitigating IBDs. Therefore, we examined the expression of the tight junction proteins in RNA-Seq data and found that claudin 4 (*Cldn4*) is upregulated in UroA treated cells (Supplementary Fig. 2)²⁴. In addition to *Cldn4* and *Cyp1A1*, UroA also significantly increased the expression of heme oxygenase 1 (*HMOX1* or *HO1*) (Supplementary Fig. 2). *HO1* is well known Nrf2-dependent gene, which exerts wide variety of beneficial activities including removal of toxic heme, protection against oxidative stress, regulation of apoptosis, and inflammation²⁵. Based on these observations, we hypothesized that UroA and UAS03 will induce tight junction proteins and enhance barrier function through AhR and Nrf2 pathways.

Ingenuity Pathway Analysis (IPA) revealed significant enrichment of Nrf2 and AhR signaling pathways (Supplementary Fig. 1), supporting a role for these pathways in UroA signaling. A potential therapeutic avenue in IBD is the ability to increase barrier function. It was therefore of interest that we observed a

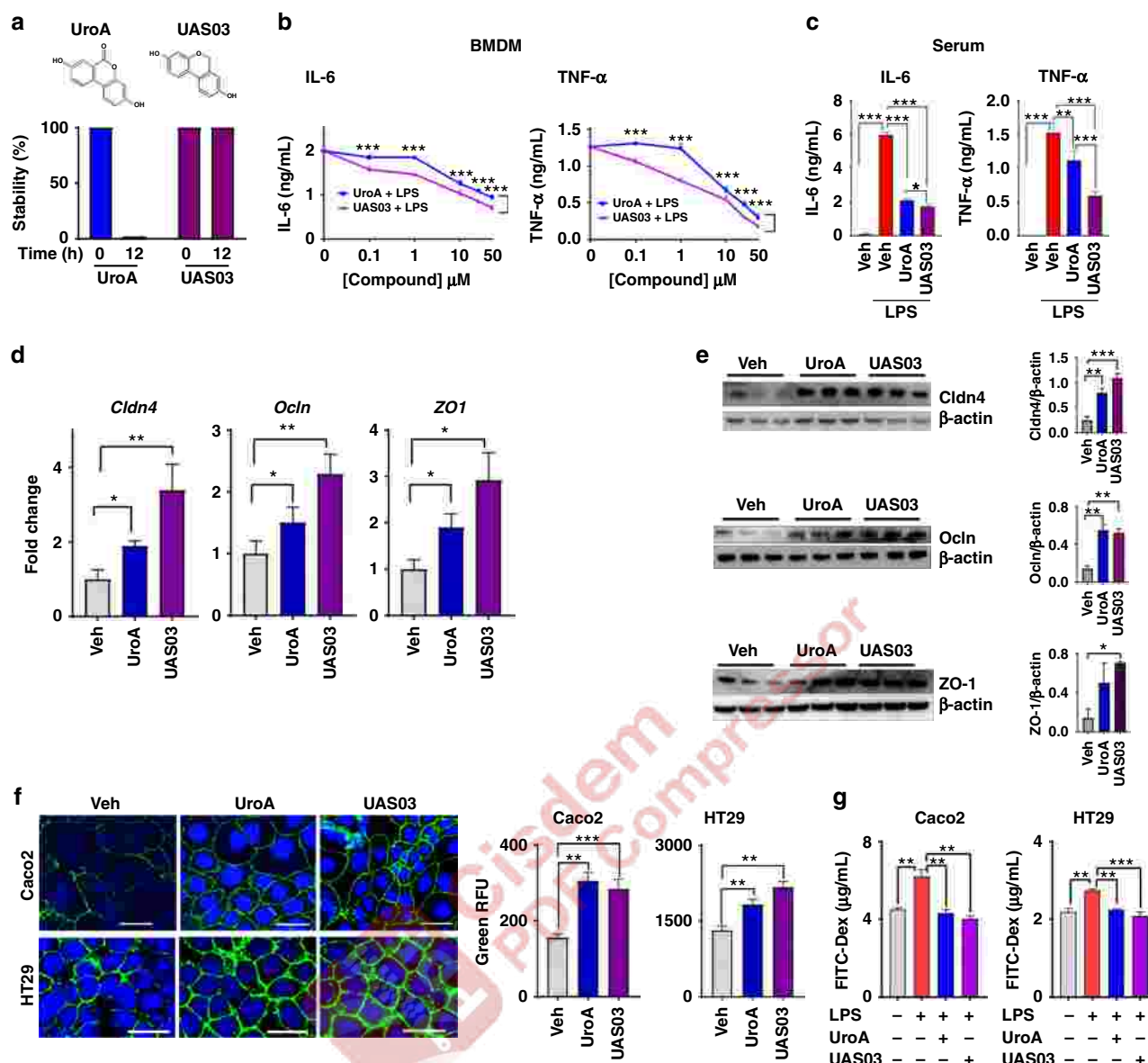


Fig. 1 UAS03 is a potent anti-inflammatory structural analogue of UroA and induces tight junction proteins. **a** Chemical structures of UroA, UAS03. UroA/UAS03 stability was examined in the presence of gastric pH 2.0 and digestive enzymes. UroA and UAS03 (0.2 mg/ml) were incubated with digestive enzymes (esterases and proteases, 100 U/ml) for 12 h at 37 °C and compound levels were quantified. **b** BMDMs were stimulated with LPS (50 ng/ml) without or with UroA (blue line)/UAS03 (purple line) (0.1, 1, 10, 25, and 50 μ M) for 6 h. IL-6 and TNF- α levels in supernatants were measured. **c** C57BL/6 mice (n = 3–4) were pretreated with UroA (20 mg/kg) and UAS03 (20 mg/kg). After 4 h, LPS (2 mg/kg) was injected intraperitoneally. Post 4 h of LPS administration, serum levels of IL-6 and TNF- α were measured. **d–f** HT29 or Caco2 cells were treated with vehicle (DMSO-0.01%) or UroA/UAS03 (50 μ M) for 24 h. **d** The fold changes in mRNA levels of claudin 4 (*Cldn4*), occludin (*Ocln*), and Zona occludens 1 (*ZO1*) in HT29 cells were determined by RT-PCR method. **e** UroA/UAS03 induced protein expression of *Cldn4*, *Ocln*, and *ZO1* in HT29 cells were determined by immunoblots and quantified by Image J software. **f** Caco2 or HT29 cells were grown on coverslip bottom FluroDish and treated with Vehicle, UroA/UAS03 for 24 h. The cells were stained with anti-*Cldn4* followed by secondary antibody tagged with Alexa-488. Nucleus was stained using DAPI. The confocal images were captured. The green intensity (n = 15–20 cell membrane regions) was measured. Scale bars for Caco2 and HT29 cells indicate 50 and 25 μ m respectively. **g** Monolayer HT29 or Caco2 cells on transmembranes were treated with vehicle or UroA/UAS03 (50 μ M) for 24 h followed by treatment with LPS (50 ng/ml) for 2 h. FITC-dextran was added to these cells (top of the membrane) and incubated for 2 h and FITC-dextran levels in bottom chamber well was measured. Results are representative of three independent experiments with triplicates for each concentration. * p < 0.05, ** p < 0.01, *** p < 0.001, unpaired t-test between Veh, UroA, or UAS03. Error bars, \pm SEM. Source Data are provided as a Source Data File

significant increase in expression of the tight junction protein *Cldn4* in UroA treated cells. Although not statistically significant in our RNA-seq dataset, we further observed an increase in expression of additional tight junction proteins *ZO-1* and *Ocln1* using real-time PCR (Fig. 1d). The increased levels of these proteins by UroA or UAS03 was confirmed by western blots (Fig. 1e) and *Cldn4* by confocal imaging (Fig. 1f) in both HT29

and another colon epithelial cell line, Caco2. Further, we observed elevated expression of *Cldn4* in the colons of mice treated with UroA/UAS03 (Supplementary Fig. 3a). The functional consequence of increased tight junction proteins was examined using in vitro FITC-dextran permeability assay in transwell plates. As shown in Fig. 1g, pretreatment of Caco2 or HT29 cells with UAS03 or UroA significantly inhibited LPS induced leakage of

FITC-dextran into bottom chambers. Overall, these results suggest that treatment with UroA/UAS03 increased the expression of tight junction proteins potentially enhancing the gut barrier integrity.

AhR mediates the activities of UroA/UAS03. RNA-Seq data and real-time PCR data suggested that UroA significantly upregulated *Cyp1A1* (Supplementary Data 1, Supplementary Fig. 2, Fig. 2a, b). The P450-Glo *Cyp1A1* assay (Fig. 2c) as well as 7-ethoxyresorufin-O-deethylase (EROD) assay (Supplementary Fig. 4) were performed to determine, whether the *Cyp1A1* enzyme activity was similarly affected. UroA/UAS03 significantly induced *Cyp1A1* activity in colon epithelial cells (Fig. 2c and Supplementary Fig. 4). Since *Cyp1A1* is a well-known downstream target of AhR signaling²⁶, we examined whether UroA/UAS03 mediate their actions through AhR. In these assays, we utilized well established potent AhR ligands [2,3,7,8-tetrachlorodibenzo-p-dioxin (TCDD) or 6-Formylindolo[3,2-b]carbazole (FICZ) and low affinity AhR ligand (beta-naphthoflavone (BNF)] to compare the *Cyp1A1* activities with UroA/UAS03. UroA/UAS03 activated *Cyp1A1* similar to low affinity AhR ligand BNF at 50 μ M. As expected, the high affinity ligands such as FICZ and TCDD showed increased *Cyp1A1* activity even at nano molar concentrations compared to UroA/UAS03/BNF (Fig. 2c and Supplementary Fig. 4). More importantly, we tested whether UroA/UAS03 induce the *Cyp1A1* activities in vivo using wild type and AhR^{-/-} mice. As shown in Fig. 2d, UroA/UAS03 significantly activated *Cyp1A1* activity in colon and liver of wild type but not in AhR^{-/-} mice. Moreover, UroA/UAS03 treated wild type mice showed relatively more *Cyp1A1* activity in colon tissues compared to BNF and FICZ treated mice (Supplementary Fig. 5a, b). Interestingly, FICZ and BNF that are delivered through intra peritoneum (i.p) showed more *Cyp1A1* activity in liver compared to UroA/UAS03 that are delivered through oral route (Supplementary Fig. 5a, b). It could be attributed to first pass effect. To directly compare the administration route, we delivered UroA or UAS03 or FICZ through i.p. and determined *Cyp1A1* enzyme activities. As expected, high affinity AhR ligand, FICZ, induced *Cyp1A1* activity ~30 fold in liver compared to 5–6 fold by UroA/UAS03 (Supplementary Fig. 5c). In colons, FICZ only increased *Cyp1A1* activity up to ~5 fold, whereas UroA/UAS03 increased by only ~3 fold. In summary, these results suggest that UroA/UAS03 upregulate expression of *Cyp1A1* and enhances the enzyme activity through AhR albeit at low levels in vivo.

The direct activation of AhR by UroA/UAS03 was examined in HT29 cells by XRE-luciferase reporter assay as well as nuclear translocation of AhR. The data showed that UroA/UAS03 treatment resulted in 2–4 fold induction of luciferase activity (Fig. 2e) compared to the high affinity ligand MeBio that caused higher levels (~15 fold) of AhR activation. Both UroA and UAS03 induced the nuclear translocation of AhR (Fig. 2f, g). AhR was upregulated in mice treated with UroA or UAS03 (Supplementary Fig. 3b). Next, we asked whether AhR or *Cyp1A1* are required for UroA/UAS03 mediated upregulation of tight junction protein, *Cldn4*. For this purpose, AhR or *Cyp1A1* expression was suppressed using siRNA knockdown and *Cldn4* expression was examined. As shown in Fig. 2h, i and Supplementary Fig. 6, UroA/UAS03 failed to induce *Cldn4* both in AhR or *Cyp1A1* knockdown cells. In addition, we also deleted *Cyp1A1* in HT29 cells using CRISPR/Cas9 methods and examined UroA/UAS03 mediated activities. Deletion of *Cyp1A1* did not show effect on basal levels of *Cldn4* compared to parental HT29 cells (Supplementary Fig. 7a). As shown in Supplementary Fig. 7b–d, UroA/UAS03 failed to upregulate *Cldn4* or NQO1 in *Cyp1A1*

deleted cells. These results suggest that UroA/UAS03 induce the expression of tight junction proteins through activation of AhR-*Cyp1A1*-dependent pathway.

UroA/UAS03 enhance gut barrier function through Nrf2. Since AhR is required for UroA mediated activities, we analyzed existing AhR-ligand Chip analysis using ChIP-Atlas (http://chip-atlas.org/target_genes) that were performed on breast cancer cell line MCF-7 (<http://dbarchive.biosciencedbc.jp/kyushu-u/hg19/target/AHR.1.html>). The analysis suggested that Nrf2 is a target of AhR signaling cascade (Supplementary Fig. 8a). Similarly, AhR also has influence on tight junction proteins such as Occludin, TJP3, *Cldn2*, 3 and 5 (Supplementary Fig. 8b). Furthermore, the pathway analysis of our RNA seq data (Ingenuity) also revealed that AhR and Nrf2 pathways are listed in top 25 (Supplementary Fig. 1). Previously, it was shown that TCDD mediates some of its activities through Nrf2 pathways^{27,28}. Therefore, we hypothesized that UroA/UAS03 induce tight junction proteins through activating AhR-Nrf2 dependent pathways. We tested this hypothesis in colon epithelial cells as well as in mice deficient in AhR and Nrf2. Treatment with UroA/UAS03 significantly upregulated Nrf2 both at mRNA and protein levels (Supplementary Fig. 9a and Fig. 3a) and induced its nuclear translocation in HT29 cells (Fig. 3b, c). Nrf2-promoter activities were validated utilizing ARE-luciferase assays, where UroA/UAS03 significantly enhanced luminescence upon treatment (Supplementary Fig. 9b) similar to known Nrf2 activator sulforaphane (SFN) albeit at lower levels. Nrf2 and its target gene HO1 are upregulated in the colons of wild type mice treated with UroA/UAS03 (Supplementary Fig. 3) as well as in HT29 cells (Supplementary Fig. 9c). To examine the precise function and interdependency of AhR-Nrf2 pathways in UroA/UAS03 induced *Cldn4* upregulation, we utilized colon explants from C57BL/6 (wild type, WT), AhR^{-/-} and Nrf2^{-/-} mice. NAD(P)H:quinone oxidoreductase (NQO1) encodes cytoplasmic 2-electron reductase and the induction is shared by both AhR and Nrf2 pathways²⁷. We examined whether UroA/UAS03 upregulate expression of NQO1 in colon explants of these mice. Treatment with UroA/UAS03 induced the expression of both Nrf2, NQO1, and *Cldn4* in WT colon explants (Fig. 3d, e and Supplementary Fig. 10). But these compounds failed to induce *Cldn4* and NQO1 in both Nrf2^{-/-} and AhR^{-/-} colon explants as well as Nrf2 in AhR^{-/-} mice colon explants (Fig. 3d, e, Supplementary Fig. 10) suggesting requirement of AhR and Nrf2 expression for UroA/UAS03 mediated activities. The basal level comparison of expression of *Cldn4* and NQO1 in WT, AhR^{-/-}, and Nrf2^{-/-} mice colon explants suggests that lack of AhR and Nrf2 reduced the expression of NQO1 and *Cldn4* (Supplementary Fig. 10a). The data suggest that expression of *Cldn4* is reduced in AhR^{-/-} and Nrf2^{-/-} but not in *Cyp1A1* knock down cells.

To define the in vivo requirement of AhR and Nrf2 for UroA/UAS03 mediated upregulation of tight junction proteins, we utilized WT, Nrf2^{-/-}, and AhR^{-/-} mice. Examination of basal level expression of *Cldn4*, NQO1 in the colon tissues of these mice suggests that lack of AhR or Nrf2 have reduced significantly NQO1 levels, but did not show statistical significance for reduction of *Cldn4* albeit there was a trend towards reduced expression. (Supplementary Fig. 11c). The mice were treated daily with UroA/UAS03 (orally, 20 mg/kg bodyweight) for 7 days and barrier functions were analyzed. Treatment with UroA/UAS03 significantly upregulated Nrf2 and tight junction proteins (*Cldn4*, NQO1, Occludin, ZO1, and TJP3) in WT mice (Fig. 3f and Supplementary Fig. 11). In contrast, UroA/UAS03 failed to induce these proteins in Nrf2^{-/-} and AhR^{-/-} mice (Fig. 3f and Supplementary Fig. 11).

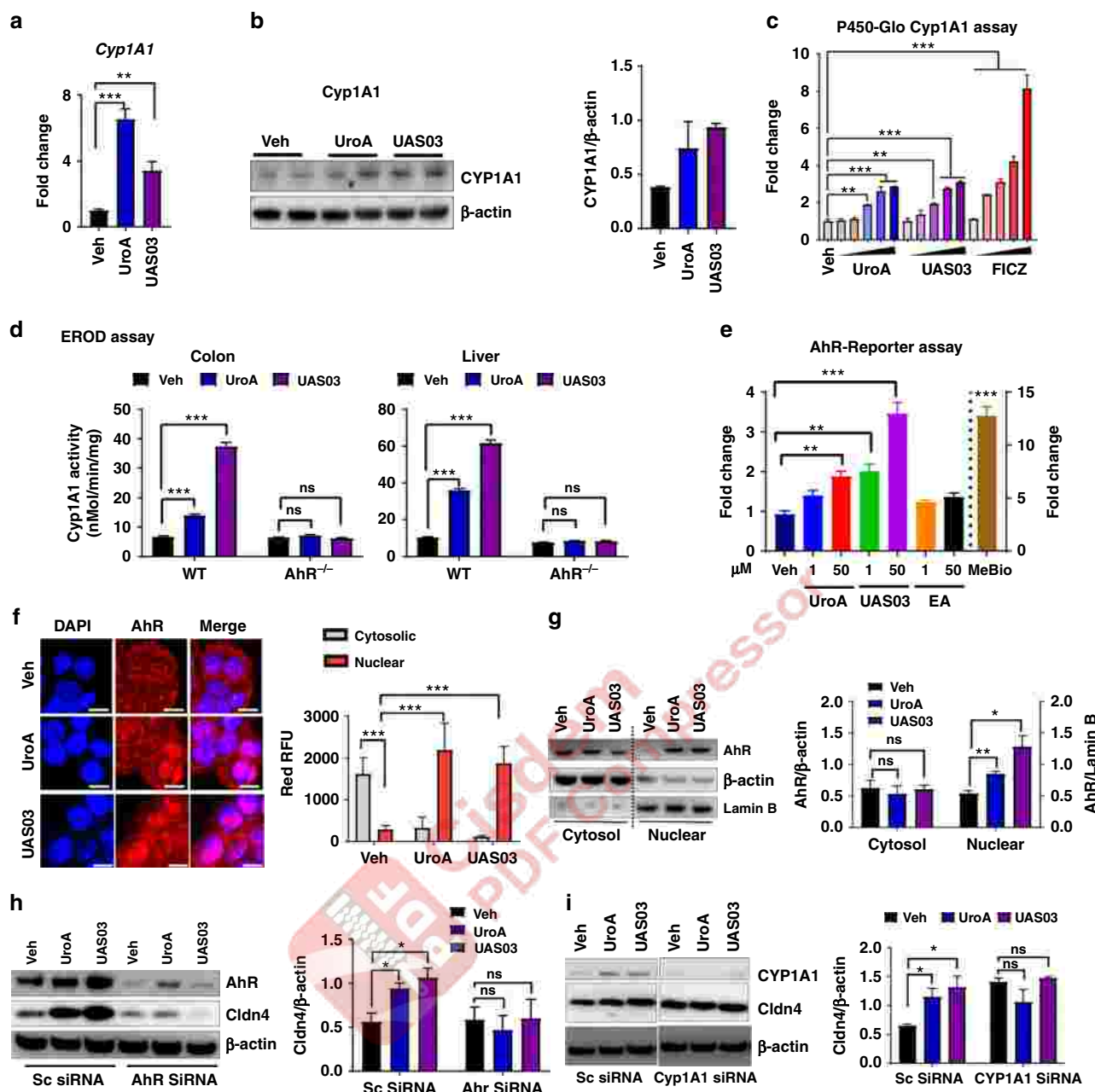


Fig. 2 UroA/UAS03 enhance tight junction proteins in AhR-dependent manner. **a** HT29 cells were treated with vehicle (DMSO-0.01%)/UroA/UAS03 (50 μ M) for 24 h. mRNA levels of Cytochrome P450 1A1 (*Cyp1A1*) was measured by RT-PCR. **b** *Cyp1A1* protein levels were measured using immunoblots and quantified band intensities by Image J software. **c** *Cyp1A1* enzyme activity was measured by P450-Glo *Cyp1A1* assay. HT29 cells were treated with UroA or UAS03 (0.1, 1, 10, 25, 50 μ M) or FICZ (0.1, 1, 10, 25, 50 nM) for 24 h and enzyme *Cyp1A1* activity was measured. **d** C57BL/6 and AhR^{-/-} ($n = 3$) mice were treated orally with Vehicle (0.25% CMC), UroA or UAS03 (20 mg/kg) for 1 week and *Cyp1A1* activity was measured in colons and livers by ethoxyresorufin-O-deethylase (EROD) assay. **e** The cells expressing AhR-reporter (luciferase) were treated with Veh or UroA/UAS03 or ellagic acid (EA) or MeBio (AhR high affinity ligand) for 6 h and fold change of luminescence over vehicle treatment was measured. **f** Immunofluorescence confocal images of HT29 cells treated with vehicle/UroA/UAS03 (50 μ M) for 6 h. The cells were stained with anti-AhR antibody (red) and DAPI (blue). Relative fluorescence ($n = 20$ cells) in the cytosol and nucleus was measured. The scale bar indicates 10 μ m. **g** AhR levels in cytosol and nuclear fractions of HT29 cells treated for 2 h with Veh or UroA/UAS03 (50 μ M). **h** AhR or **i** *Cyp1A1* was knocked down using siRNA in HT29 cells and the cells were treated with vehicle/UroA/UAS03 (50 μ M) for 24 h and immunoblots were performed to detect expression of AhR, *Cyp1A1*, and *Cldn4*. Scrambled (Sc) siRNA transfections were used as controls. Immunoblots were quantified using Image J software. The data is representative of two independent repeats with triplicate wells for each treatment. Statistics performed using unpaired *t*-test using Graphpad Prism software. All in vitro studies were performed in triplicates. Error bars, \pm SEM; ****p* < 0.001; ***p* < 0.01; **p* < 0.05. Source Data are provided as a Source Data File

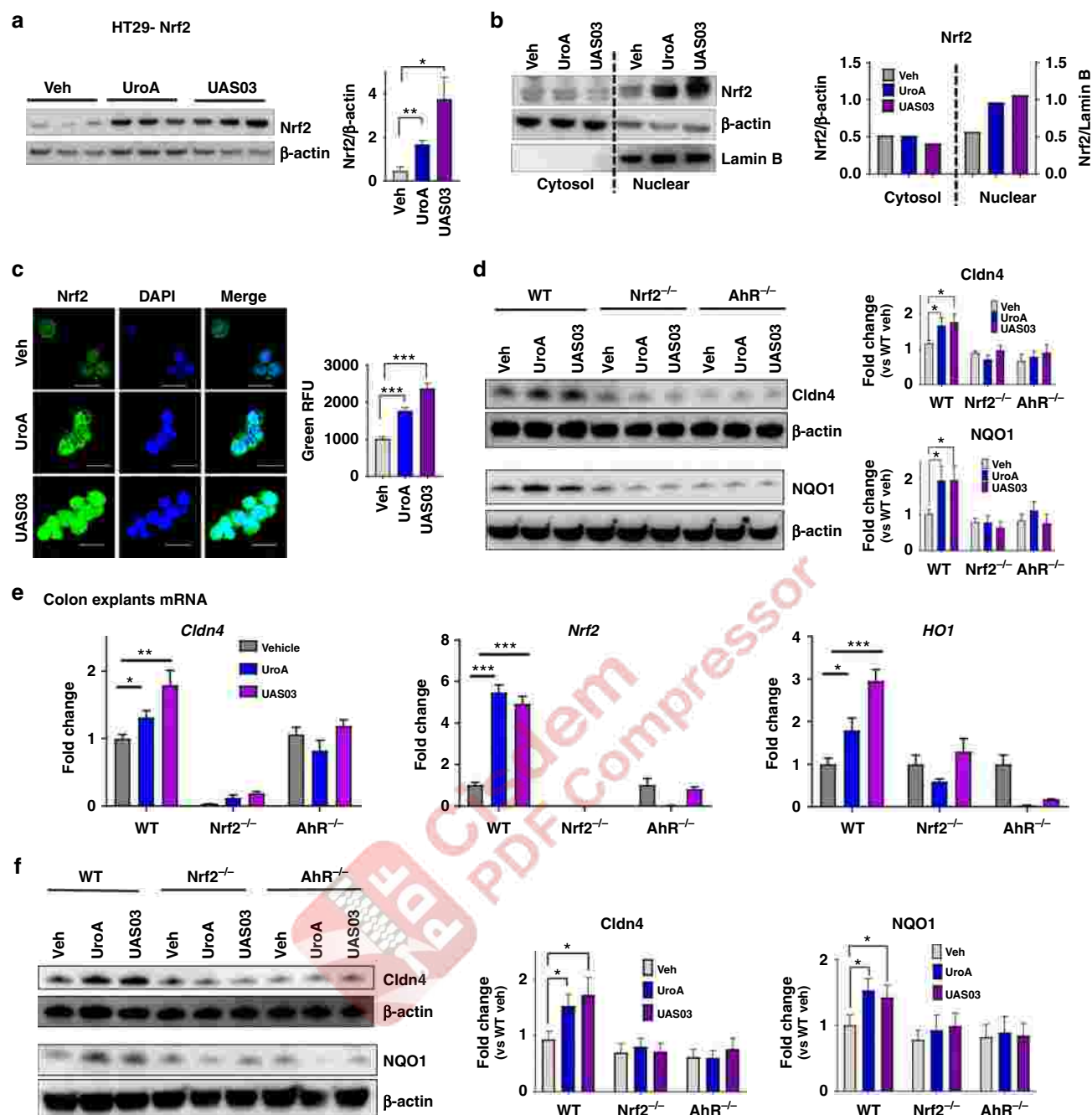


Fig. 3 Nrf2 is required for UroA/UAS03 mediated upregulation of tight junction proteins. **a** Nrf2 levels were determined by immunoblots in HT29 cells treated with vehicle/UroA/UAS03 (50 μ M) for 24 h. **b** Nrf2 expression in cytosolic and nuclear fractions of HT29 cells treated with Veh/UroA/UAS03 (50 μ M) for 6 h. **c** Immunofluorescence confocal images of HT29 cells treated with vehicle/UroA/UAS03 (50 μ M) for 6 h. The cells were stained with anti-Nrf2 antibody and DAPI. Relative green fluorescence ($n = 20$ cells) intensity was measured. Scale bars indicate 25 μ m. **d** Expression of Cldn4 and NQO1 in colon explants from WT, Nrf2^{-/-}, and AhR^{-/-} mice treated with vehicle/UroA/UAS03 (50 μ M) for 24 h. Immunoblots were quantified using Image J software. **e** mRNA levels of *Cldn4*, *Nrf2*, and *HO1* from colon explant cultures was measured by real-time PCR using SyBr green method. **f** C57BL/6, Nrf2^{-/-}, and AhR^{-/-} mice ($n = 3$) treated orally daily with veh or UroA/UAS03 (20 mg/kg) for 1 week. Cldn4 and NQO1 protein levels in colons were measured by immunoblots and quantified by Image J software. All in vitro studies were performed in triplicates. The immunoblots of colon explants and colon tissues were quantified from at least 6 independent runs. The levels of proteins were normalized to β -actin and Wild type vehicle treatment was set to 1 and calculated the fold changes. Statistics performed using unpaired *t*-test using Graphpad Prism software. Error bars, \pm SEM; * $p < 0.05$; ** $p < 0.01$; *** $p < 0.001$. Source Data are provided as a Source Data File

UroA/UAS03 induced NQO1 expression was also confirmed in HT29 cells (Supplementary Fig. 9d). Overall these results suggest that both AhR and Nrf2 are required for UroA/UAS03 mediated upregulation of tight junction proteins and NQO1.

Treatment with UroA/UAS03 mitigates colitis. The physiological relevance of UroA/UAS03 regulated barrier function was examined in the 2,4,6-Trinitrobenzenesulfonic acid (TNBS)-induced colitis model²⁹. Oral treatment with UroA/UAS03 (20 mg/kg at 12 h intervals) significantly protected from TNBS-

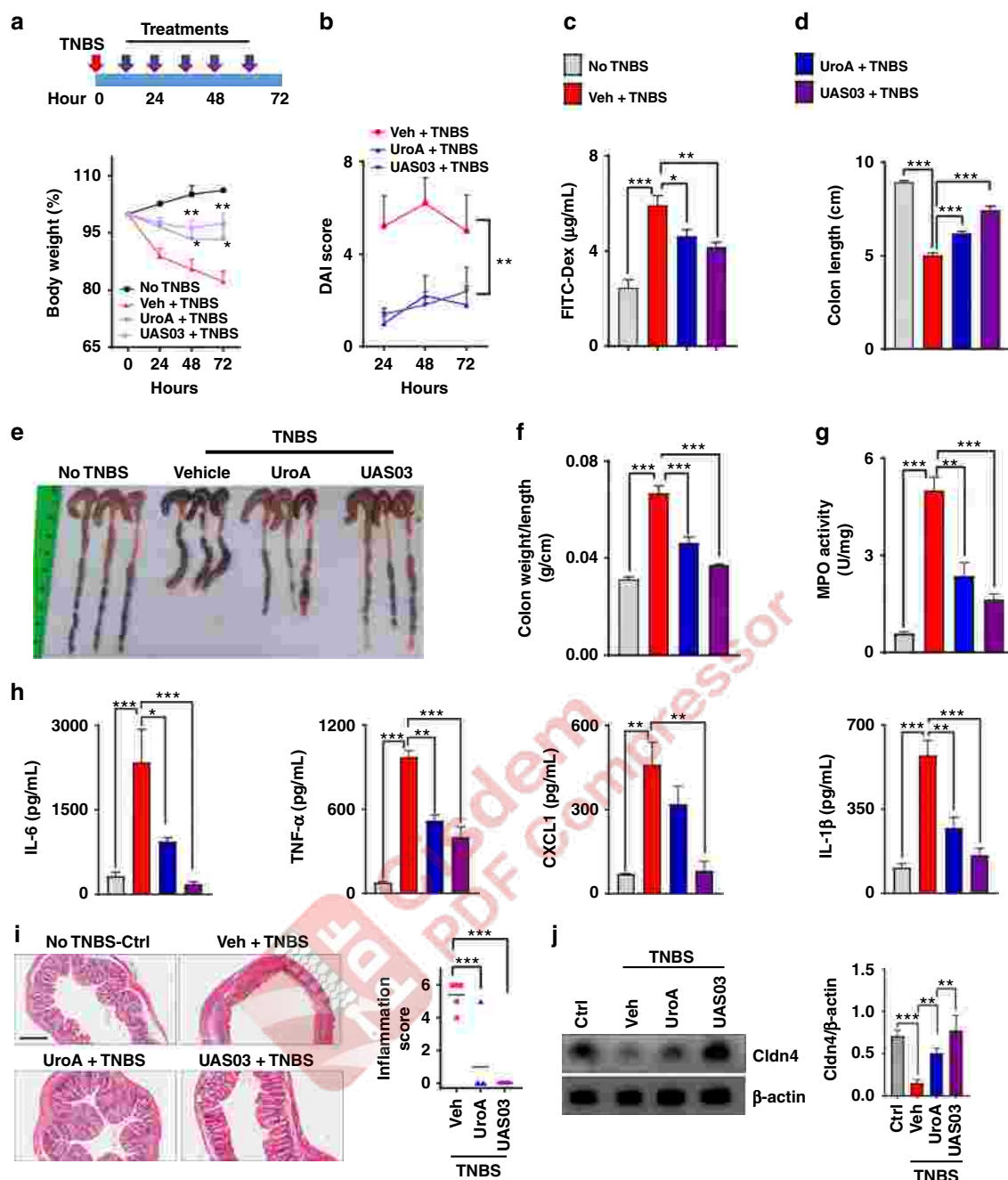


Fig. 4 UroA/UAS03 treatment attenuates TNBS-induced colitis in mice. Colitis was induced by intrarectal administration of TNBS (2.5 mg/mouse) in C57BL/6 (8 week age old, $n = 5$ /group) mice. Mice were orally treated with vehicle or UroA (20 mg/kg) or UAS03 (20 mg/kg body weight) every 12 h post-TNBS instillation for 60 h and the experiment terminated at 72 h. Representative data from one of three independent experiments is shown. **a** Percent body weight loss (No TNBS- Solid black line; Veh + TNBS- Solid red line; UroA + TNBS- Solid blue line; UAS03 + TNBS- Solid purple line). **b** disease activity index, **c** intestinal permeability, **d** colon lengths were measured. **e** Gross morphological changes of colon, **f** ratio of colon weight/length, **g** colonic myeloperoxidase (MPO) levels, **h** serum IL-6, TNF- α , CXCL1, and IL-1 β levels, **i** microphotographs of hematoxylin and eosin (H&E) stained sections of colons and inflammation scores are shown. Scale bar indicates 300 μ m. **j** Cldn4 expression in the colons of these mice ($n = 3$) was measured by immunoblots and quantified. Statistical analysis was performed (unpaired t -test) using Graphpad Prism software. Error bars, \pm SEM *** $p < 0.001$; ** $p < 0.01$; * $p < 0.05$. Source Data are provided as a Source Data File

induced body weight loss (Fig. 4a), reduced disease activity index (DAI) score (Fig. 4b) and intestinal permeability (Fig. 4c). UroA/UAS03 treatment significantly protected from TNBS-induced colon shortening (Fig. 4d, e) and reduced weight to length ratio (Fig. 4f) suggesting decreased colonic inflammation. UroA/UAS03 treatment also reduced neutrophil infiltration as evident from myeloperoxidase (MPO) activity (Fig. 4g) as well as serum

inflammatory markers such as IL-6, TNF- α , CXCL1, and IL-1 β (Fig. 4h) that are hallmarks of ulcerative colitis. Consistent with these findings, H&E analysis of colon sections showed significantly less tissue damage and inflammation scores (Fig. 4i). Furthermore, UroA/UAS03 also protected from TNBS-induced downregulation of Cldn4 in the colons of these mice (Fig. 4j). We further examined the effects of dose and frequency of UroA/

UAS03 treatments as well as their preventive efficacy in mitigating colitis. As shown in Supplementary Fig. 12, UroA/UAS03 mitigated TNBS-induced colitis with a single treatment at 4 or 20 mg/kg body weight. The comparisons bodyweights at each time points suggest that TNBS treatment in all the groups led to decrease in body weight and treatment seems to decrease the loss of body weight, but did not reach significance (Supplementary Fig. 13). However, treatments significantly showed impact on other parameters such as protecting from shortening of colons, blocking inflammatory mediators. Supplementing wild type mice with UroA or UAS03 did not exhibit any signs of toxicity as evident from no observed changes in their body weights, CBC counts as well as serum ALT and AST levels (Supplementary Fig. 14).

Since UroA/UAS03 exhibited strong barrier protective activities by upregulating tight junction proteins, we investigated whether regular exposure to these metabolites would have sustained beneficial effects in preventing colitis. The prophylactic activity profile of UroA/UAS03 was examined in the TNBS-induced colitis model. WT mice were orally fed daily with vehicle or UroA/UAS03 for 1 week followed by TNBS administration to induce colitis. These mice did not receive any further UroA/

UAS03. The treatment regimen and percent bodyweights are shown in Fig. 5a and Supplementary Fig. 15. The pre-treated mice were significantly protected from TNBS-induced colon shortening and colonic inflammation (colon length/weight) similar to a therapeutic regimen (Fig. 5b–d). Pre-treatment also significantly enhanced barrier function and decreased TNBS-induced inflammation (Fig. 5e, f). These results suggest that UroA/UAS03 mediated enhanced gut barrier function will likely have long-term beneficial effects in preventing colitis. In therapeutic regimen, mice were treated with UroA or UAS03 24 h post-TNBS, where mice develop severe colitis. In this setting, treatment with UroA/UAS03 also significantly reversed the colitis phenotype by reducing shortening of colons, gut permeability and inflammation compared to vehicle treatment.

The therapeutic applications of UroA/UAS03 were also examined in the dextran sodium sulfate (DSS)-induced colitis model. DSS chemically disrupts the epithelial cell barrier and leads to increased penetration of bacteria resulting in inflammation and colonic tissue damage. As shown in Supplementary Fig. 16, the mice treated with UroA/UAS03 were significantly protected from 3% DSS induced acute colitis. UroA/UAS03 treatment mice displayed overall decreased DAI scores during the

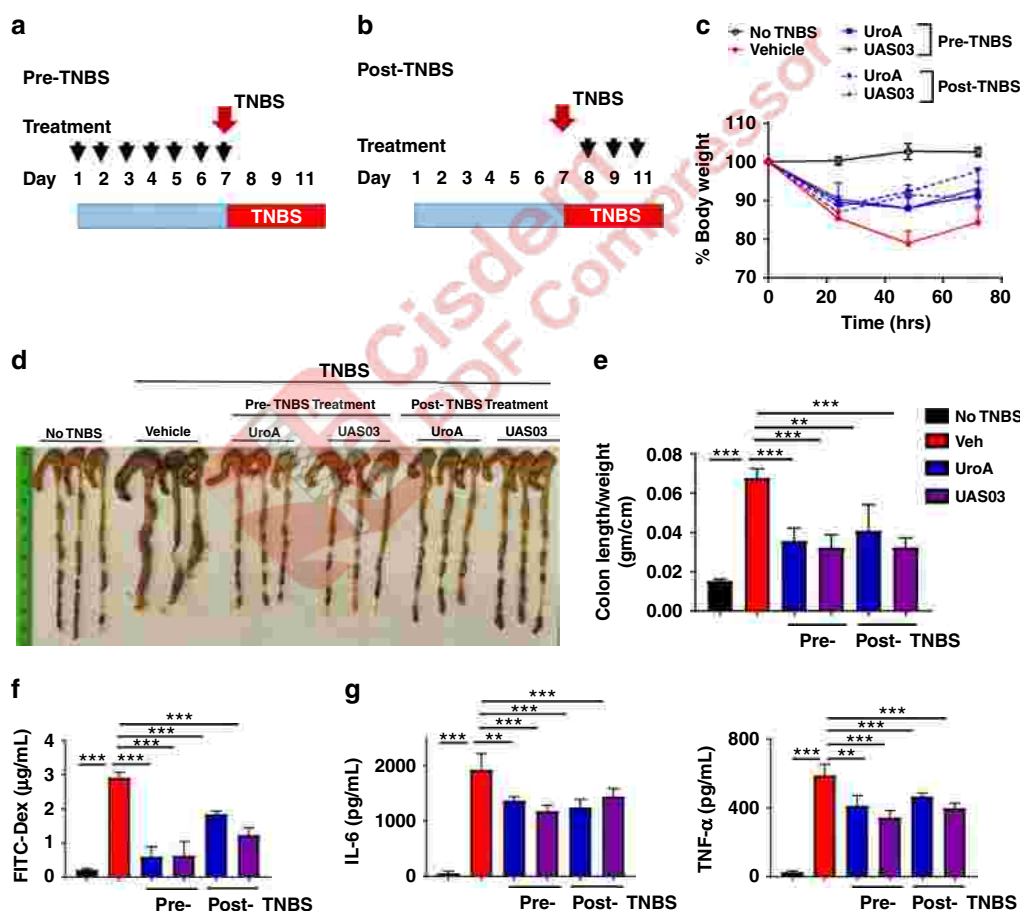


Fig. 5 UroA/UAS03 prevent TNBS-induced colitis and sustain beneficial barrier activities. **a** Pre-TNBS treatment. Male C57BL/6 mice ($n = 5$ per group at 7–8 week old age) were given orally vehicle (Veh; 0.25% sodium carboxymethylcellulose) or UroA or UAS03 (20 mg/kg/bodyweight) daily for one week followed by rectal administration of TNBS to induce colitis. These mice did not receive any treatment post-TNBS administration. Mice were euthanized 72 h post-TNBS administration and characterized. **b** Post-TNBS treatment. Another set group of C57BL/6 mice ($n = 5$ per group at 7–8 week old age) received Veh or UroA or UAS03 (20 mg/kg) 24, 48, and 72 h post-TNBS. **c** Percent body weight loss was recorded after TNBS-administration. (No TNBS- Solid black line; Veh + TNBS- Solid red line; Pre-TNBS + UroA- Solid blue line; Pre-TNBS + UAS03- solid purple line; Post-TNBS + UroA- dashed blue line; Post-TNBS + UAS03- dashed purple line). **d** Representative colon images of control (no TNBS) along with vehicle/UroA/UAS03 treated mice from pre- and post-treatment groups. **e** Ratio of colon weight/length, **f** intestinal permeability was evaluated using FITC-dextran leakage assay. **g** Serum levels of IL-6 and TNF- α were measured using standard ELISA methods. Statistical analysis was performed (unpaired t -test) using Graphpad Prism software. Error bars, \pm SEM *** $p < 0.001$. Source Data are provided as a Source Data File

disease progression. Importantly, UroA/UAS03 treatments protected from shortening of colons, decreased gut permeability and reduced inflammation compared to vehicle treatment (Supplementary Fig. 16) at the end of experiment on day 15. Further, the therapeutic efficacies of UroA/UAS03 were also examined in a chronic DSS model, where mice were given 4 cycles of 2% DSS in drinking water for 7 days with an interval of 14 days in each cycle on regular water (Fig. 6a). Treatment with UroA/UAS03 significantly protected from DSS-induced colitis as evident from decreased gut permeability (Fig. 6b), reduced shortening of colons (Fig. 6c, d), increased colon weight/length ratio (Fig. 6e), reduced inflammation (serum IL-6, IL-1 β , TNF- α as well as colonic tissue MPO levels) (Fig. 6f, g). Analysis of tight junction proteins in these mice also suggest that treatment with UroA/UAS03 enhanced the expression of Cldn4 (Fig. 6h). These results highlight the model independent beneficial activities of UroA/UAS03 in preserving the barrier integrity and mitigating colonic inflammation.

UAS03/UroA mediated protection against colitis requires AhR-Nrf2 pathways. The studies described above indicated the importance of AhR-Nrf2 pathway in UroA/UAS03 enhanced barrier function. To examine the relevance of these pathways in colitis, we tested the *in vivo* requirement for Nrf2 (Fig. 7) and AhR (Fig. 8). Treatment of Nrf2^{-/-} mice with UroA/UAS03 failed to restore body weight loss caused by TNBS-induced colitis (Fig. 7a, b and Supplementary Fig. 17) or protect from shortening

of colons (Fig. 7c). UroA/UAS03 treatment did not enhance barrier function in Nrf2^{-/-} mice as evident from similar FITC-dextran leakage in UroA/UAS03 treated mice compared to vehicle treatment (Fig. 7d). These results demonstrated that UroA/UAS03 enhanced gut barrier integrity requires the expression of Nrf2. Interestingly, UroA/UAS03 partially reduced serum inflammatory mediators such as IL-6 and TNF- α levels in Nrf2^{-/-} mice (Fig. 7e), suggesting that UroA/UAS03 could mediate some of the anti-inflammatory activities in Nrf2-independent manner. To define the role of AhR in UroA/UAS03 mediated protective activities, the TNBS-induced colitis model was executed in AhR^{-/-} mice along with wild type mice (Fig. 8a). As expected AhR^{-/-} mice were more susceptible to TNBS-induced colitis model as evident from rapid loss of body weight (Fig. 8b and Supplementary Fig. 18). Therefore, we terminated the experiment at post 60 h TNBS administration (Fig. 8a). Treatment with UroA/UAS03 failed to protect from shortening of colon lengths in AhR^{-/-} mice compared to wild type mice (Fig. 8c, d). Additionally, UroA/UAS03 failed to correct the barrier dysfunction in AhR^{-/-} mice as evident from *in vivo* permeability assays (Fig. 8e). Analysis of serum inflammatory mediators suggest that UroA/UAS03 failed to reduce IL-6 and slightly reduced the TNF- α in AhR^{-/-} mice, whereas UroA/UAS03 treatments significantly reduced IL-6 and TNF- α in wild-type mice as observed above (Fig. 8f). Based on these results we propose that UroA/UAS03 exert protective barrier functional activities through AhR-Nrf2-dependent pathways by inducing tight junction proteins (Fig. 8g).

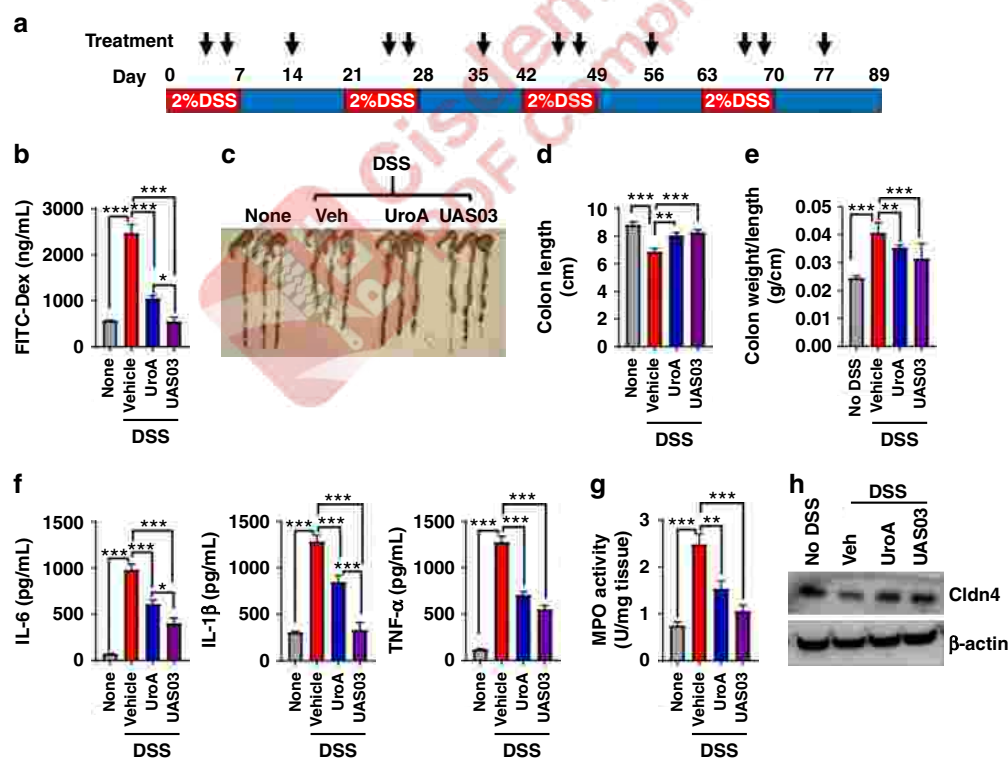


Fig. 6 Treatment with UroA/UAS03 mitigates DSS-induced chronic colitis. **a** C57BL/6 mice (7–8 week age old) were treated with four cycles of DSS (2%) with 7 days/cycle with an interval of 14 days with regular water. Control group of mice ($n = 5$) received the regular water without DSS. UroA/UAS03 (20 mg/kg/day/body weight) that was resuspended in 0.25% sodium carboxymethylcellulose (CMC) solution ($n = 9$) or vehicle (CMC) ($n = 9$) was administered on 4th and 6th day of each DSS cycle and one treatment while on regular water. $n = 5$ /control; $n = 9$ /veh and UroA; $n = 8$ /UAS03 group) Mice were euthanized at day 89 and the colitis phenotype was characterized. **b** Intestinal permeability using FITC-dextran was evaluated. **c** Representative colon images **d** colon lengths, **e** ratios of colon weight/length are shown. **f** Serum levels of IL-6, IL-1 β , and TNF- α were measured using ELISA methods. **g** MPO levels were determined in colon tissues. **h** Cldn4 expression in the colons of these mice ($n = 3$) was measured by immunoblots. Statistics performed using unpaired *t*-test using Graphpad Prism software. Error bars, \pm SEM *** $p < 0.001$; ** $p < 0.01$; * $p < 0.05$. Source Data are provided as a Source Data File

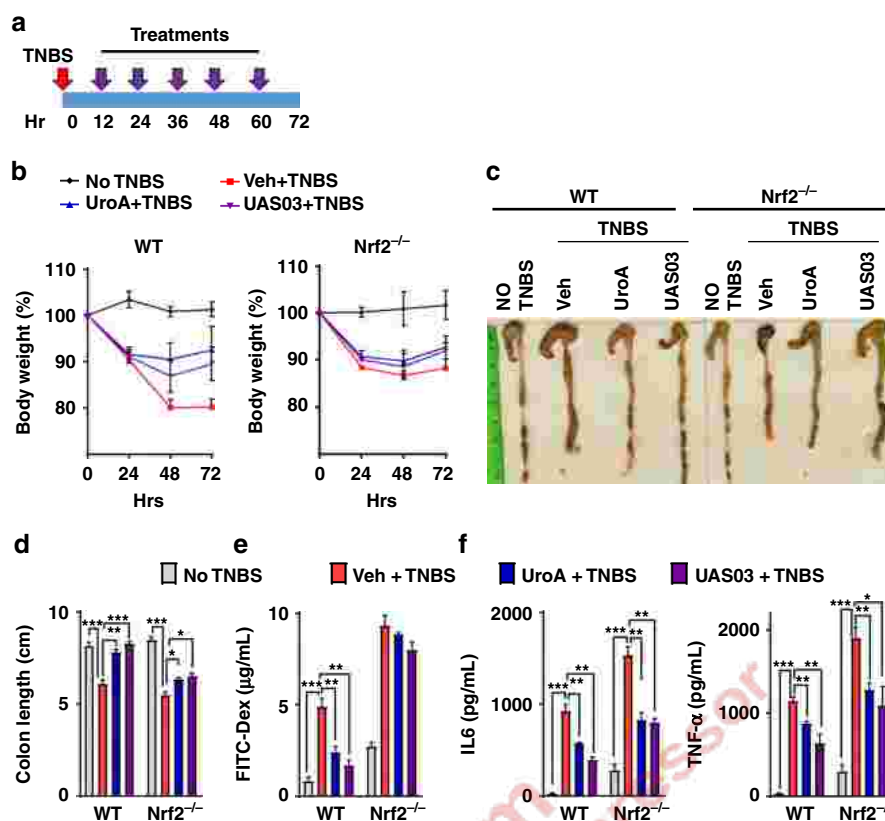


Fig. 7 UroA/UAS03 utilize Nrf2 pathways to mitigate colitis. **a–e** Colitis was induced using TNBS in C57BL/6 (WT) and Nrf2^{-/-} mice ($n = 4\text{--}5/\text{group}$ 7–8 week old age). Mice were treated with Veh or UroA/UAS03 (20 mg/kg bodyweight) every 12 h post TNBS administration ending at 72 h. Representative data from two independent experiments is shown. **a** TNBS-induced colitis experimental design and treatment regimen. **b** Percent body weight loss (No TNBS- Solid black line; Veh + TNBS- Solid red line; UroA + TNBS- Solid blue line; UAS03 + TNBS- Solid purple line), **c** representative colon images, **d** colon lengths, **e** gut permeability, **f** serum levels of IL-6 and TNF- α were determined. Statistical analysis was performed (unpaired t -test) using Graphpad Prism software. Error bars, \pm SEM *** $p < 0.001$; ** $p < 0.01$ * $p < 0.05$. Source Data are provided as a Source Data File

Since the macrophages are critical mediators of colonic inflammation in IBDs^{30,31}, we determined if UroA/UAS03 mediated anti-inflammatory activities require the AhR-Nrf2 pathways in macrophages. First, we examined whether UroA/UAS03 activates Nrf2-dependent pathways in macrophages. The results showed that treatment with UroA/UAS03 significantly upregulated Nrf2 expression and induced its nuclear translocation, as well as upregulation of Nrf2-target genes such as HO1 expression in macrophages (Supplementary Fig. 19a–e). Further, analysis of UroA/UAS03 mediated down regulation of LPS-induced IL-6 production in macrophages from WT, Nrf2^{-/-} and AhR^{-/-} mice showed that LPS-induces much higher levels of IL-6 in Nrf2^{-/-} and AhR^{-/-} macrophages relative to WT (Fig. 8h). UroA/UAS03 also reduced the NF- κ B activation in an AhR-dependent manner in macrophages (Supplementary Fig. 19f). AhR^{-/-} BMDM are hyper responsive to LPS stimulation as evident from increased NF- κ B activation as well as increased levels of IL-6 compared to wild type (Fig. 8h and Supplementary Fig. 19g). Despite significant lowering of IL-6 levels by UroA/UAS03 in Nrf2^{-/-} macrophages, these reduced levels are still higher compared to LPS-induced IL-6 in WT macrophages. When compared, the fold reduction upon treatments (Supplementary Fig. 20), UroA/UAS03 reduced IL-6 in Nrf2^{-/-} similar to WT indicating Nrf2-independent anti-inflammatory activities both in vivo (TNBS model) and in vitro BMDM (LPS-induced IL-6). In contrast, UroA/UAS03 did not block LPS-induced IL-6 production in AhR^{-/-} macrophages up to 30 μ M as well as in AhR^{-/-} mice in TNBS-induced colitis model suggesting that

UroA/UAS03 mediate anti-inflammatory activities through AhR-dependent manner. AhR^{-/-} BMDM slight decrease in IL-6 levels at 50 μ M dose may suggest some of unknown AhR-independent anti-inflammatory activities. The results presented here highlight that single microbial metabolite regulates the barrier function in epithelial cells via the activating AhR-Nrf2 signaling pathways and also anti-inflammatory activities in AhR dependent pathways.

Discussion

In this study, we identified that microbial metabolite UroA, and its analogue UAS03, increases overall gut health by enhancing barrier function in addition to their anti-inflammatory activities. UroA/UAS03 activate the phase I (AhR-Cyp1A1) and phase II (Nrf2-anti-oxidative pathways) metabolic pathways to enhance expression of tight junction proteins and inhibit inflammation. We further demonstrate that treatment with these compounds significantly mitigated colitis both in preventive and therapeutic settings.

A key physiological function of gut microbiota is to catabolize dietary components into absorbable metabolites. Despite the identification of numerous microbial metabolites, the molecular targets and mechanisms of action for many metabolites is unknown. Urolithins, derived from dietary polyphenols such as ETs, EA by microbiota are linked to the beneficial effects associated with high consumption of fruits and vegetables in humans^{11,18,19}. It was reported that the *Bifidobacterium pseudocatenulatum* INIA P815 strain was able to metabolize EA to

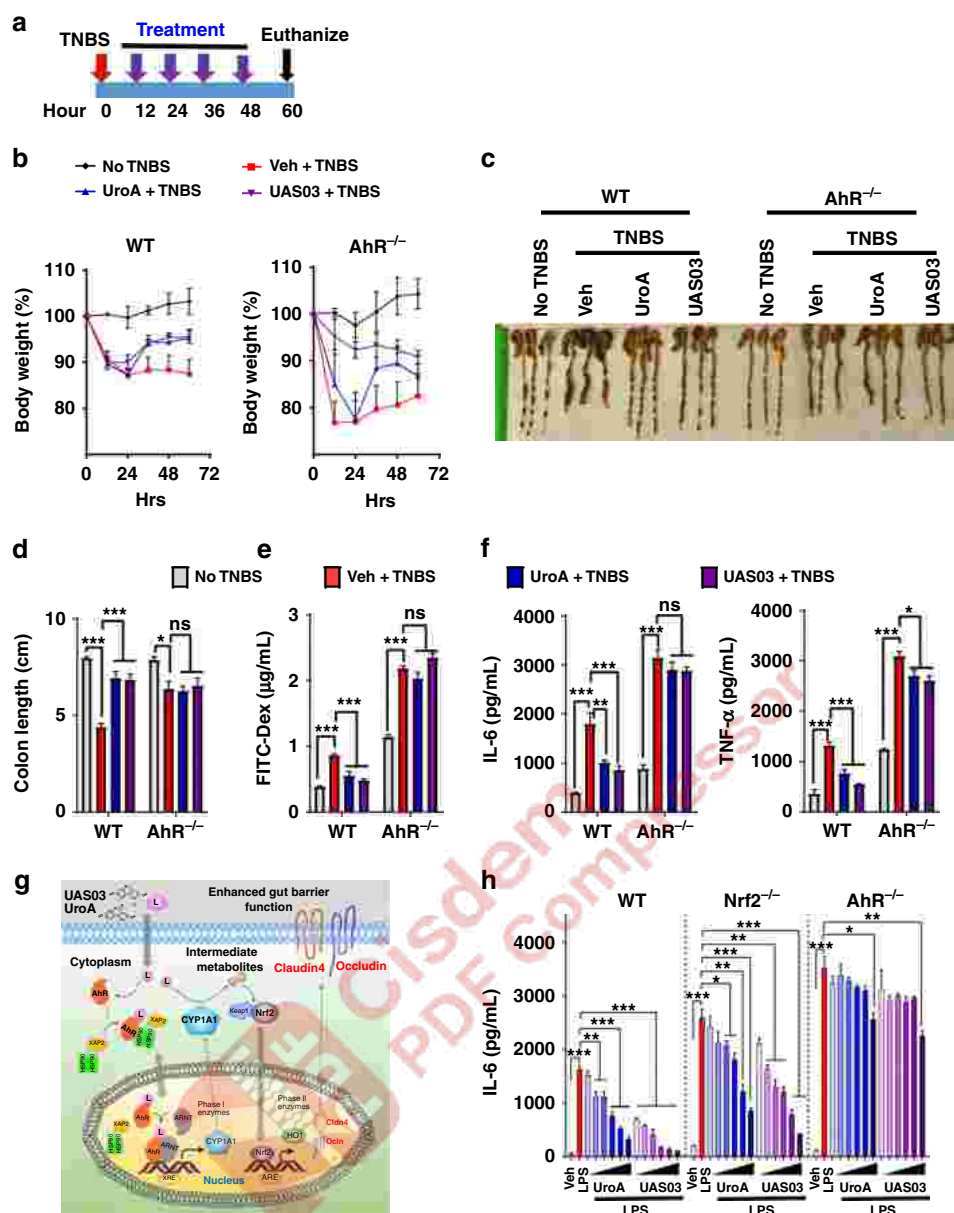


Fig. 8 UroA/UAS03 exert beneficial activities through AhR-dependent pathways. **a–e** Colitis was induced using TNBS in C57BL/6 (WT) and AhR^{-/-} mice ($n = 4$ /group 7–8 week old age). Mice were treated with Veh or UroA/UAS03 (20 mg/kg bodyweight) every 12 h post TNBS administration and mice were euthanized at post 60 h TNBS administration. **a** TNBS-induced colitis experimental design and treatment regimen. **b** Percent body weight loss (No TNBS- Solid black line; Veh + TNBS- Solid red line; UroA + TNBS- Solid blue line; UAS03 + TNBS- Solid purple line). **c** representative colon images, **d** colon lengths, **e** gut permeability, **f** serum levels of IL-6 and TNF- α were determined. Statistical analysis was performed (unpaired t -test) using Graphpad Prism software. Error bars, \pm SEM *** $p < 0.001$; ** $p < 0.01$; * $p < 0.05$. **g** AhR-Nrf2 dependent tight junction protein regulation by UroA/UAS03. UroA/UAS03 (L: ligands) bind to AhR and activate its nuclear translocation to induce expression of Cyp1A1 and Nrf2. Further, UroA/UAS03 causes Nrf2-dependent upregulation of tight junction proteins and enhanced barrier function. **h** LPS (50 ng/ml)-induced IL-6 levels were measured in the presence of Vehicle or UroA or UAS03 (0.1, 1, 10, 20, 30, and 50 μ M) in bone marrow derived macrophages (BMDM) from wild type (WT), Nrf2^{-/-} and AhR^{-/-} mice. The data is representative of two independent experiments with triplicates. Statistical analysis was performed (unpaired t -test) using Graphpad Prism software. Error bars, \pm SEM *** $p < 0.001$; ** $p < 0.01$ * $p < 0.05$. Source Data are provided as a Source Data File

produce UroA and UroB³². Large inter-individual variability in UroA levels¹⁸ suggests that bacteria responsible for UroA production may also be highly variable in humans. Urolithin levels can reach up to micro molar concentrations in human serum depending on their microbiota composition¹⁸. The premise of this study is that direct supplementation of UroA will overcome the intrinsic variation in microbiota among populations and offer health benefits. In this regard, we also successfully developed UAS03, a more stable and potent structural analogue of UroA

that displayed increased gut barrier protection and anti-inflammatory activities.

Previous studies demonstrated inhibitory activities of urolithins in inflammation, proliferation, and aging in various models^{20,22,33}. However, the molecular targets or mechanisms of action of these metabolites on pathophysiological processes are unknown. Our approach of searching for an epithelial cell function for these metabolites by RNA-Seq analysis revealed several important clues for their function and potential mechanisms.

UroA/UAS03 mediated up regulation of tight junction proteins (e.g., *Cldn4*, *Ocln*, and *ZO1*) and protection from LPS induced leakage in epithelial monolayers showed that these metabolites clearly play an important role in the regulation of barrier function. Tight junctions consist of both transmembrane proteins (e.g., occludin, claudins, junctional adhesion molecules, and tricellulin) as well as peripheral membrane proteins (e.g., ZO-1 and cingulin) to regulate paracellular permeability and maintain gut barrier function. The disruption of tight junctions leads to barrier dysfunction and is implicated in IBDs and other disorders³⁴. In particular, gut barrier dysfunction leads to bacterial invasion and excessive inflammation^{35,36}. The inflammatory cytokines and growth factors such as TNF- α , IFN γ , IL-1 β , TGF- α , and platelet derived growth factors as well as bacterial endotoxins (LPS) are known to increase permeability by disrupting tight junctions³⁷. Thus, barrier dysfunction and inflammation form a self-perpetuating loop in IBDs and blocking one of these is often insufficient for mitigating the disease process.

Our RNA-seq studies and expression analysis showed that in addition to upregulation of *Cldn4*, UroA also induced the expression of *Cyp1A1* and *HO1* in colon epithelial cells. Since *Cyp1A1* and *HO1* represent the activation of phase I and phase II drug metabolic pathways, these results suggested the potential involvement of AhR and Nrf-2 in mediating UroA/UAS03 functions. AhR is a nuclear transcription factor that responds to both xenobiotic and endogenous ligands leading to cell-specific gene regulation and cellular functions. AhR activation is responsible for the induction of multiple Phase I and Phase II xenobiotic chemical metabolizing enzymes such as *Cyp1A1*³⁸. AhR can be activated by many chemicals including environmental polycyclic aromatic hydrocarbons, coal tar, phytochemicals, and products from commensal bacteria and tryptophan metabolism³⁹. Historically, human exposure to high affinity AhR ligand, TCDD (which is not metabolized by *Cyp1A1*) displayed severe adverse events such as appearance of cysts, eruptions, pustules, and erythema as well as life threatening manifestations including liver, renal failures, myocardial degeneration³⁹. However, AhR activation by FICZ ligand (amenable to *Cyp1A1* drug metabolism) has been implicated in controlling the immune system and protection from colitis^{40,41}. Our studies revealed that UroA/UAS03 treatments induced the expression and nuclear translocation of AhR and enhanced transcription of XRE-target genes as well as induced *Cyp1A1* enzyme activities without exhibiting toxicity.

Interestingly, UroA/UAS03 failed to induce *Cldn4*/NQO1 in *Cyp1A1* knockdown cells. Previously, it was reported that overexpression of *Cyp1A1* in mice resulted in depletion of natural AhR ligands and deletion of *Cyp1*-enzymes in mice (*Cyp1A1*, *Cyp1A2*, *Cyp1B1* triple knockout mice) led to increase in availability of AhR ligands and increased their activities⁴². Similarly, we also anticipated that deletion of drug metabolizing and detoxifying enzyme, *Cyp1A1*, would enhance the availability of UroA/UAS03 and enhance their activities. However, we did not observe increased activities upon deletion of *Cyp1A1* in colon epithelial cells. We still do not understand the complete mechanisms for these observations. It may be necessary to delete all *Cyp* enzymes to avoid compensation mechanisms to detect increased activities. It also is possible that UroA/UAS03 undergo *Cyp1A1* drug metabolism and generates unknown active phase I metabolites, which could activate Nrf2 pathways. It was reported by Gimenez-Bastida et al.⁴³ that UroA-glucuronide (UroA-Gluc) forms displayed beneficial activities, where treatment with UroA-Gluc ameliorated the TNF- α induced inflammation and associated molecular markers in human aortic endothelial cells. UroA is known to circulate as glucuronide and sulfate conjugates as well as parent form (UroA) in plasma²⁰. Therefore, it is possible that

products from UroA drug metabolism Phase I and II intermediates could also exert certain beneficial activities. Alternatively, UroA/UAS03 could induce basal ROS that is dependent on expression of *Cyp1A1* and leading to activation of Nrf2-pathways. Additional studies are required to support these possibilities and to define precise role of *Cyp1A1* in UroA/UAS03 mediated activities using *Cyp1*-enzyme whole body and intestinal epithelial cells (villin) specific knock out mice.

UroA/UAS03 failed to exert their activities in cells lacking AhR or in AhR^{-/-} colon explants as well as in AhR^{-/-} mice suggesting a critical role for the AhR pathway in mediating UroA/UAS03 activities. While the regulation of immune cell function by AhR has been previously demonstrated^{41,44}, our current studies highlight the importance of this pathway in epithelial cells to regulate tight junction proteins and barrier function.

Previous studies suggested that interdependency of AhR and Nrf2 pathways^{28,45,46}. Nrf2, a basic region-leucine zipper transcription factor, protects cells and tissues from oxidative stress by inducing the expression of antioxidant and phase II-enzymes such as glutathione S-transferase and NQO1⁴⁷ as well as controlling LPS-induced inflammation⁴⁸. Our studies both in vitro and in vivo suggest that UroA/UAS03 significantly induced the expression of Nrf2 as well as its target genes such as *HO1* and *NQO1* in colon epithelium. Furthermore, our results also showed that AhR-*Cyp1A1*-Nrf2 pathways are essential for UroA/UAS03 mediated upregulation of tight junction proteins (Figs. 2 and 3).

Our extensive studies in colitis models revealed that treatment with UroA/UAS03 significantly enhanced tight junction proteins, decreased gut permeability, and reduced local and systemic inflammation leading to attenuation of colitis (Figs. 4–8). Even a single dose of UroA/UAS03 exhibited therapeutic efficacies against TNBS-induced colitis. Importantly, prophylactic benefits of UroA/UAS03 on gut barrier function and prevention of colitis development was observed (Fig. 5). The mice pre-treated with UroA/UAS03 prior to TNBS administration significantly reduced gut permeability (Fig. 5e), which is consistent with increased expression of tight junction proteins. Despite not receiving further treatments post-TNBS administration, these mice were protected from disease development suggesting prophylactic effects of these compounds through enhanced barrier function. Moreover, UroA/UAS03 supplementing daily for 7 days induced expression of AhR, Nrf2, and *Cldn4* in the colons of wild-type mice without observable toxicity (Fig. 3f, Supplementary Figs. 3, 11 and 14) suggesting potential translational applications for these compounds. Further, treatment with UroA/UAS03 also mitigated both chronic and acute DSS-induced colitis indicating model independent beneficial activities of these metabolites Fig. 6 and Supplementary Fig. 16). Previously, it was shown that mice lacking AhR or Nrf2 are more susceptible to colitis compared to wild type^{40,49}. In contrast to the toxicity associated with the high affinity AhR ligands such as TCDD, UroA/UAS03 are low affinity non-toxic AhR ligand (partial agonist) like BNF that suppressed the pathogenesis of DSS-induced colitis⁴⁰.

It was suggested that Nrf2 protects from colitis through regulation of pro-inflammatory cytokines and induction of phase II detoxifying enzymes. Kobayashi et al.⁵⁰ demonstrated that Nrf2 suppresses inflammation through redox control, by opposing the transcriptional upregulation of proinflammatory cytokine genes and identified Nrf2 as the upstream regulator of cytokine production. Previously, it was also demonstrated that ablation of Nrf2 leads to enhancement of NF- κ B activation resulting in increased inflammatory cytokines production⁵¹ and severe colitis⁴⁹. We also observed increased basal level of inflammatory mediators in Nrf2^{-/-} mice compared to wild-type mice as well as in Nrf2^{-/-} BMDM. Further, addition of LPS significantly upregulated IL-6 in Nrf2^{-/-} BMDM compared to wild-type BMDM

as well as in TNBS-induced colitis model. UroA/UAS03 failed to repair TNBS-induced barrier dysfunction and colitis in *Nrf2*^{-/-} mice (Fig. 7).

The role of AhR in UroA/UAS03 mediated upregulation of tight junction proteins was demonstrated using AhR siRNA, colon explants from *AhR*^{-/-} mice as well as in vivo treatments in *AhR*^{-/-} mice. Additionally, UroA/UAS03 failed to mitigate TNBS-induced colitis in mice lacking AhR (Fig. 8). Interestingly, UAS03 seems to have some protective role against rapid body weight loss in *AhR*^{-/-} mice that are treated with TNBS. It is not clear at this time, why UAS03 exhibits these beneficial effects. However, it did not protect against other parameters such as shortening colon lengths, increased permeability, and increased inflammatory mediators. We acknowledge the inherent problems of *AhR*^{-/-} mice. *AhR*^{-/-} mice inherently suffer from variety of organ disorders including a decline in the efficacy of their immune system and high sensitivity to inflammatory stimuli⁵². Previously, it was demonstrated that activation of AhR protects against colitis^{41,53} and *AhR*^{-/-} mice develop severe colitis compared to wild type mice and display increased inflammatory mediators⁵⁴. Similarly, our studies also showed that increased susceptibility to TNBS-induced colitis in *AhR*^{-/-} mice compared to wild type. *AhR*^{-/-} mice exhibited rapid body weight loss leading to termination of the experiment at 60 h. Generally, the endogenous ligands of AhR regulate multiple functions in the body via AhR and maintains the homeostasis in wild type mice. In *AhR*^{-/-} mice, the endogenous ligands cannot act as bio-regulatory molecules due to lack of AhR potentially leading to severe colitis phenotype compared to wild type mice. It is therefore possible that failure of UroA/UAS03 mediated protective activities against colitis in *AhR*^{-/-} mice may not provide conclusive evidence for AhR role. Further studies are warranted using *Villin Cre AhR floxed mice*, to tease out involvement of AhR in UroA/UAS03 mediated protective activities in colitis models. Despite plethora effects in *AhR*^{-/-} mice, studies involving colon epithelial cells, siRNA knockdown, *AhR*^{-/-} colon explant studies as well as BMDM studies reinforces the involvement of AhR pathways in mediating UroA/UAS03 barrier and anti-inflammatory activities. Recent study from Dr. Brigitta Stockinger's group⁵⁵ also suggests AhR protects from inflammatory damage by maintaining intestinal stem cell homeostasis and barrier integrity supporting our observations that activation of AhR enhances the barrier integrity. In this paper, they demonstrated that AhR promotes barrier function through direct activity on intestinal epithelial cells (IEC) by using mice that lack AhR in IEC (*Villin^{Cre} AhR^{fl/fl}*). These mice exhibit decreased expression of Muc2 and increased levels of IL-6 suggesting that AhR role in barrier integrity and inflammation⁵⁵.

The current studies highlight the critical requirement for AhR-Nrf2 in protecting from barrier dysfunction. It is possible that UroA/UAS03 are exerting colitis protective activities by two pronged mechanisms of action. These compounds directly act on immune cells (e.g., macrophages) to prevent LPS/bacterial induced inflammation as well as exhibit anti-oxidative activities through AhR-Nrf2 pathways. Most importantly, these metabolites have direct impact on gut epithelium and gut barrier function by upregulating tight junction proteins. Enhanced barrier function reduces the bacterial leakage in the gut leading to significant reduction in systemic inflammation. To delineate the effects on immune cells versus epithelial cells, further in depth studies involving cell specific deletion of AhR and Nrf2 in transgenic mice using Cre/lox methodologies are required. RNA-Seq pathway analysis as well as studies by Ryu et al.²² suggest that UroA plays an important role in regulating mitochondria functions through inducing mitophagy. Several evidences suggest that mitochondrial dysfunction is a major contributor in the

pathophysiology of IBD⁵⁶. It was shown that isolated enterocytes from IBD patients have swollen mitochondria with irregular cristae⁵⁷. The intestinal epithelial cells isolated from experimental colitis mice models also exhibited abnormal mitochondrial structures⁵⁸. Therefore, we speculate that in addition to anti-inflammatory and barrier protective activities, UroA/UAS03 may potentially reduce IBD through regulating mitochondrial dysfunction.

Evolutionarily, human-microbiota developed indigenous mechanisms to protect from external challenges. It is possible that excess use of antibiotics and modern dietary trends led to microbial dysbiosis resulting in the elimination of some bacterial populations that are capable of producing beneficial metabolites. More rigorous and systematic studies are required to assess the beneficial advantages of direct consumption of metabolites in humans both in healthy and disease conditions, whether supplementation of metabolites could overcome the dysbiosis. The current study summarizes one such metabolite, UroA and its analogue, UAS03 with activities in mitigating IBDs by enhancing gut barrier function and reducing inflammation. Existing IBD treatments include utilizing anti-TNF- α antibodies to reduce inflammation; here we suggest that enhancing gut barrier functions in addition to inhibiting inflammation might provide better therapeutic options for control of IBDs. Overall, UroA/UAS03 will not only be efficacious in IBD-related diseases but may also have significant translational implications in other disorders involving barrier dysfunction and inflammation such as alcohol liver diseases, neurological disorders, and colon cancers.

Methods

Materials. General laboratory chemicals and reagent solutions were purchased from Sigma-Aldrich (St. Louis, MO). ELISA kits for IL-6 and TNF- α were purchased from Bio-legend. ELISA kit for CXCL1 was purchased from R&D systems. All antibodies were purchased from Santacruz unless otherwise specified. LPS was purchased from Sigma Aldrich. Colitis grade DSS (36,000–50,000 M.W) was purchased from MP Bio. UroA was custom synthesized as previously described²³.

Mice. C57BL/6 mice were either bred in our animal facility or purchased from Jackson Laboratories. Breeding pairs of *Nrf2*^{-/-} mice (B6.129x1-Nfe2l3^{tm1Ywk/J}, stock # 0170009) were purchased from Jackson Laboratories and bred at U of L animal facility to generate experimental animals. *AhR*^{-/-} mice (Model# 9166) were purchased from Taconic Laboratories. We utilized the mice at the ages of between 7–9 weeks age old for colitis experiments. Mice were kept in specific pathogen-free (SPF) barrier conditions with temperature-controlled room with alternate 12 h cycles of dark and light. Animals were allowed free excess to feed and water ad libitum. All studies were performed under approved protocols from Institutional Animal Care and Use Committee (IACUC), University of Louisville, Louisville, KY, USA. Source Data for all the bar graphs are provided as a Source Data File.

Synthetic procedure for synthesis of UAS03. Chemically UroA (3,8-dihydroxy-6H-dibenzo[b,d]pyran-6-one) structure has a bridge ester, lactone, and two hydroxyl on two phenyl rings. UroA has a lactone (cyclic ester) bond that connects two phenyl rings and leads to the planar structure. Gastric pH or digestive enzymes can hydrolyze the lactone bond leading to opening of the ring. This will result in losing the planar structure, becomes propeller structure, and potentially loses its activities. To generate more stable and potent compounds, we have synthesized non-hydrolyzable cyclic ether derivative, UAS03 by the following procedure (Supplementary Fig. 21).

Sodium borohydride (0.165 g, 4.38 mmol) was added to dry THF (10 ml), and the mixture was cooled 10 °C before borontrifluoride etherate (0.80 g, 5.7 mmol) was added drop wise over a period of 1 h. Then 3,8-dihydroxy-6H-benzo[c]chromen-6-one (Uro-A) (0.5 g, 2.19 mmol) in THF (5 ml) was added over a period of 10 min. The mixture was allowed to stir for 5 h at 50 °C. The completion of reaction was monitored by thin layer chromatography (TLC). The reaction was quenched with methanol. 3 N aqueous HCl solution (10 ml) was added, and the mixture was gently heated to 50 °C for 30 min. The reaction mixture was adjusted to neutral with 10% NaOH solution, and the volatiles were evaporated under reduced pressure. The crude product was purified by column chromatography using 50% ethylacetate in Hexane with 60–120 mesh silica gel to get pure 6H-benzo[c]chromene-3,8-diol product.

MS (M+1) = 215.2. ¹H-NMR (DMSO-d₆): δ : 9.49 (2H, s), 7.51–7.50 (1H, d, J = 6.6 Hz), 7.48–7.47 (1H, d, J = 6.6 Hz), 6.75–6.73 (1H, m), 6.61 (1H, s), 6.48–6.46

(1H, m), 6.32 (1H, s), 4.96 (2H, s). ^{13}C -NMR (DMSO- d_6): δ : 158.10, 156.71, 154.93, 131.88, 123.86, 122.79, 121.66, 115.72, 114.89, 111.84, 110.07, 103.95, 68.18.

Cell cultures. Human colon epithelial carcinoma cell lines, HT29 (ATCC # HTB-38TM) and Caco2 cells (ATCC # HTB-37TM) were maintained in DMEM-high glucose and EMEM-high glucose (Corning; 10-009CV) respectively, supplemented with 10% fetal bovine serum, 1X penicillin-streptomycin solution (100 U/ml penicillin, and 100 $\mu\text{g}/\text{ml}$ streptomycin; Sigma Aldrich) in a humidified atmosphere (5% CO_2 , 95% air, 37 °C). Mouse bone marrow derived macrophages (BMDMs) were isolated and cultured using the following procedure⁵⁹. Briefly, mice were killed by CO_2 anesthesia, rinsed in 70% ethanol and bone marrow was isolated from tibias and femurs. Bone marrow cells were plated (2×10^6 cell/ml) in DMEM-high glucose (HyClone) supplemented with 10% FBS, 1% glutamine, 1X penicillin-streptomycin solution and 50 ng/mL mouse M-CSF (R&D Systems Inc., Minneapolis, MN) for 7 days for differentiation.

Measurements of IL-6 and TNF- α levels in BMDM. BMDM were plated in 96 (10,000 cells/well) and 12 wells (0.1×10^6 cells/well) plate for ELISA and RNA isolation. To evaluate the anti-inflammatory properties, BMDMs were stimulated with *E. coli*-derived lipopolysaccharides (LPS; O55:B5; Sigma) at 50 ng/mL concentration for six hours alone or in combination with UroA or UAS03 at indicated concentrations (0.01, 0.1, 1, 10, 25, and 50 μM) in quadruplicates. For cytokine production via ELISA, the supernatant was collected and centrifuged at $10,000 \times g$ for 10 min at 4 °C to pellet down any cell and cytokines were quantified using IL-6 and TNF- α specific ELISA kit (Biolegend) following manufacturer's instruction.

LPS-induced peritonitis. Male mice (C57BL/6J; 6–8 weeks old) were randomly divided in 3 groups *viz.* vehicle (0.25% sodium carboxymethylcellulose (CMC)), UroA and UAS03. UroA and UAS03 groups received oral gavage of respective compounds (20 mg/kg in 100 μl of volume) at 0, 6, 12, 18, and 24 h. Vehicle group received same volume of CMC at same time. After 24 h, mice were injected intraperitoneally with LPS (2 mg/kg; Sigma-Aldrich). Post 4 h LPS challenge, mice were killed and blood was collected. The serum was prepared using BD Microtainer separator tubes. The serum samples were analyzed for IL-6 and TNF- α using respective ELISA assay kit (Biolegend).

Real-time PCR. Total RNA was isolated from cells/tissue using Maxwell[®] 16 LEV simplyRNA tissue kit (Promega) and reverse transcribed with TaqMan[™] Reverse transcription Kit (Applied Biosystems, CA, USA). The transcribed cDNA (after dilution) was mixed with 100 nM gene specific primers (Real time primers LLC) and 1X SYBR green reaction mix (Power SYBR[®] Green PCR Master Mix; Applied Biosystems, CA, USA). Changes in gene expression was analyzed using CFX96[™] Real-Time System (Bio Rad) and fold change in expression was calculated using $2^{-\Delta\Delta\text{CT}}$ method using GAPDH/ β -actin as house keeping gene and normalized with untreated control.

In vitro permeability study. For in vitro cellular permeability studies, Caco2 cells or HT29 cells (2×10^4 cells/cm²) were seeded in 24-well Transwell[®] plates (Corning; USA), on polyester membrane filters (pore size 0.4 μm , surface area 1.12 cm²)⁶⁰. Culture medium was added to both apical and basal chamber and the medium was changed every other day up to 21 days for Caco2 cells or 5–7 days for HT29 cells. For Caco2 cells, transepithelial electrical resistance (TEER) was calculated using EMD Millipore Millicell-ERS2 Volt-Ohm Meter (Millipore). Filters (with cell monolayer) showing more than 600 $\Omega\cdot\text{cm}^2$ were used for permeability study. After cells reach desired confluence (monolayered cells), cells were pre-treated with vehicle (0.01% DMSO) UroA (50 μM) and UAS03 (50 μM) for 24 h. After treatment, monolayer was washed with PBS to remove any residual drug and 200 μL of LPS (50 ng/ml in HBSS) was added to each well and incubated for 2 h. After LPS treatment, the monolayer was washed with PBS twice and 200 μL of FITC-Dextran (FD-4; Sigma Aldrich, USA) solution (1 mg/mL in HBSS) was added. After 2 h, a sample from the basal chamber was withdrawn and FD4 concentration was determined using fluorescence 96-wells plate reader at excitation and emission wavelengths were 480 and 525 nm, respectively.

RNA sequencing. Total RNA was isolated from HT29 cells treated with vehicle and UroA (50 μM) ($n = 3$) for 24 h and RNA was isolated using Trizol based lysis followed by Qiagen RNeasy kits. The isolated RNA was checked for integrity (RIN>9.5) using the Agilent Bioanalyzer 2100 system (Agilent Technologies, Santa Clara, CA) and quantified using a Qubit fluorometric assay (Thermo Fisher Scientific, Waltham, MA). Poly-A enriched mRNAseq libraries were prepared following Illumina's TruSeq Stranded mRNA LT library preparation protocol (Illumina Inc., San Diego, CA) using 1 μg of total RNA. All 15 samples were individually barcoded and quantitated with the KAPA Library Quantitation Kit for Illumina Platforms (Kapa Biosystems, Wilmington, MA) in conjunction with an Agilent Bioanalyzer DNA 1000 analysis (Agilent Technologies, Santa Clara, CA) for fragment size determination. The average fragment size was approximately 300 bp. 1.8 pM of the pooled libraries with 1% PhiX spike-in was loaded on one NextSeq 500/550 75 cycle High Output Kit v2 sequencing flow cell and sequenced

on the Illumina NextSeq 500 sequencer. The quality of the 1×75 bp sequences was checked using FASTQC (version 0.10.1)⁶¹. Trimming was not necessary with the median quality score above 30 (error probability = 0.001 or 1 base call in 1000 is predicted to be incorrect) across the entire length of the read and the lower quantile above a score of 20 (error probability = 0.01) at the end of the read where there is an expected decrease in quality. The raw reads for each sample were directly aligned to the *Homo sapiens* (hg38) reference genome assembly (hg38.fa) using tophat2 (version 2.0.13)⁶², generating alignment files in bam format. Optional parameters include `-no-coverage-search` and `-library-type fr-firststrand`. The human ENSEMBL⁶³ transcriptome gtf v82 was used for transcript identification, resulting in 60,903 total genes. Supplementary Table 1 indicates the number of raw reads successfully aligned for each of the samples. On average, 26 million reads were aligned per sample with a mean alignment rate of 97%. Following sequence mapping, differentially expressed genes were determined using tuxedo suite of programs including cuffdiff2 (version 2.2.1)^{64,65} with the optional parameter `-library-type fr-firststrand`. The RNA-seq data was deposited in gene data base (GEO # GSE113581).

Immunoblots (western blots). The total protein lysates were collected either from colon tissue/cells using radioimmunoprecipitation assay (RIPA) buffer (Sigma-Aldrich, USA) and quantified using BCA protein quantification kit (Thermo Scientific) as per instructional manual. Total protein (20–50 μg) of was resolved on NuPAGE[™] 4–12% Bis-Tris gel (Novex Life technologies) and transferred to polyvinylidene difluoride membrane (0.22 μm pore; Millipore, USA). After blocking with 5% (w/v) skim milk powder (containing 1X TBS) for 1 h, the membrane was then incubated with respective antibodies at 4 °C overnight (dilutions of respective antibodies is given in Table 1). Next day, respective secondary antibody conjugated with Horseradish peroxidase were probed and the chemiluminescent substrate was used to detect the protein bands (ImageQuant LAS 4000). Densitometry analysis of bands were done using ImageJ software. Anti-bodies for Cldn4, Ocldn, Cldn1, Cyp1A1, AhR, HO1, NQO1, Keap1, β -actin, and Lamin B were purchased from Santa Cruz Biotechnologies (USA) and Nrf2 from Novus Biologicals (USA). Source and list of antibodies are provided in Table 1. The uncropped images of important immunoblots are shown in Supplementary Fig. 22.

Confocal imaging. HT29 or Caco2 or BMDM cells (50,000 cells/well) were plated on to 8-well chambered slides (154534PK; ThermoFisher Scientific) allowed them to grow overnight. The cells were induced with vehicle (0.01% DMSO) or UroA (50 μM) or UAS03 (50 μM) for desired time points and fixed with cold methanol. The AhR or Nrf2 or Cldn4 stained with respective anti-bodies (1:200 dilution) followed by fluorescently labeled (Alexa flour 594 for AhR and Alexa flour 488 for Nrf2 and Cldn4) secondary ab (1:500 dilution; ThermoFisher Scientific). The nucleus was stained with DAPI (Sigma Aldrich). The confocal images were captured using Nikon A1R confocal microscope using $\times 60$ magnification lens with appropriate laser channels.

AhR-reporter assay. AhR-reported assay was performed using AhR Reporter Assay system (Indigo Biosciences). The AhR Reporter cells (expressing luciferase under AhR promoter) as well as positive control MeBio (AhR ligand) compound were provided in the kit. The cells were treated with Vehicle or UroA or UAS03 or ellagic acid or MeBio for 6 h and luminiscence was measured according to manufacture's instructions.

Nrf2-reporter assay. ARE-luciferase plasmid vector was obtained from Cayman Chemicals. HT29 cells were transfected at 50% confluency using lipofectamine 3000 reagent (ThermoFisher Scientific). Briefly, cells were seeded in 6-well plates (0.5×10^6 cells) and grown for 24 h. The transfection complex containing 1 μg of plasmid DNA and transfection reagent was added to each well in absence of FBS. After 6 h medium containing 10% FBS was added and cells were incubated for another 16–18 h. These cells were treated with vehicle (0.01% DMSO) or UroA (50 μM) or UAS03 (50 μM) or sulforaphane (10 μM) for 24 h. After incubation with inducers, cells were lysed and firefly luciferase activities (luminiscence) were measured with Luciferase Assay System (Promega) using multiwell plate luminometer (BMG, LABTECH).

Measurements of Cyp1A1 enzyme activity (ex vivo). Mice were treated with Vehicle or UroA or UAS03, BNF, or FICZ daily for 1 week at indicated concentration either through oral or i.p. route. After 1 week, mice were euthanized and the colon and liver tissues were dissected. Microsomes from these tissues were prepared using the following procedure⁶⁶. For hepatic microsomes, liver was first perfused with 0.9% sodium chloride solution and excised out. Adhering blood and saline was removed by blotting on tissue paper and tissue was homogenized in tissue homogenization buffer (50 mM Tris-HCl, pH 7.4 with 250 mM sucrose). Homogenate was centrifuged at $10,000 \times g$ for 30 min at 4 °C. supernatant obtained was further centrifuged at $105,000 \times g$ for 60 min at 4 °C. The pellet was washed with homogenization buffer and centrifuged again at $105,000 \times g$ for 60 min at 4 °C. The pellet was suspended in homogenization buffer and used for protein and CYP assay. For intestinal microsome preparation, intestine was removed and washed with 0.9% sodium chloride. The intestine was longitudinally cut open to expose

Table 1 List of antibodies used for western blots

Sr no	Antibody	Source	Dilution
1	Nrf2 (NBP1-32822)	Novus Biologicals	1:1000
2	HO-1 (sc-10789)	Santa Cruz Biotechnology	1:500
3	Cldn4 (sc-376643)	Santa Cruz Biotechnology	1:1000
4	ZO-1 (5406)	Cell Signaling Technology	1:2000
5	Ocln (sc-133256)	Santa Cruz Biotechnology	1:1000
6	NQO1 (sc32793)	Santa Cruz Biotechnology	1:1000
7	β -actin (Sc-47778 HRP)	Santa Cruz Biotechnology	1:5000
8	Lamin B (sc-6216)	Santa Cruz Biotechnology	1:100
9	AhR (sc-133088)	Santa Cruz Biotechnology	1:1000
10	Cyp1A1 (H00001543-D01P)	Novus Biologicals	1:100

mucosal layer and mucosa was scrapped with help of glass slide. The scraped tissue was collected in homogenization buffer (50 mM Tris-HCl buffer containing glycerol (20% v/v), protease inhibitor (1%) and heparin (3 U/ml)). This suspended mucosa was homogenized and centrifuged at $10,000 \times g$ for 20 min at 4 °C. Supernatant obtained was further centrifuged at $105,000 \times g$ for 60 min at 4 °C. The pellet was washed with buffer and centrifuged again at $105,000 \times g$ for 60 min at 4 °C. The pellet was suspended homogenization buffer and used for protein and CYP enzymes assays.

Ethoxyresorufin-O-deethylase (EROD) assay. The microsomal proteins (0.5 mg) were mixed with 200 μ L Tris buffer (0.1 M, pH 7.4) containing ethoxyresorufin (0.01 mM). To start reaction, NADPH (0.1 mM) was added and incubated at 37 °C for 10 min. After 10 min, reaction was terminated by adding equal volume of acetonitrile and reaction mixture was centrifuged at $13,000 \times g$ for 10 min at 4 °C. Supernatant was used to determine resorufin by measuring fluorescence (Ex. 530 nm, Em. 580 nm). Pure resorufin (Sigma Aldrich) was used to generate standard curve.

P450-Glo Cyp1A1 luminiscence assay. The above microsomes (20 μ g) were used for P450-Glo Cyp1A1 luminiscence assays as per manufacturer's instructions.

Measurement of Cyp1A1 enzyme activities in vitro. EROD assay: HT-29 cells (15,000 cells/well) treated with vehicle, UroA and UAS03 (24 h), were rinsed with HBSS buffer, and then fresh HBSS buffer was added along with 5 μ M of 7-ethoxyresorufin. Cells were further incubated at 37 °C for 1 h. After the incubation time, fluorescence (Exc. 530 nm, Em. 580 nm) was measured and product (resorufin) formed was calculated from calibration standard and normalized with protein concentration.

P450-Glo Cyp1A1 luminiscence assay: HT29 cells (25,000 cells/well) were plated in 48 well plate. Cell were then treated with UroA (0.1, 1, 10, 25, and 50 μ M) or UAS03 (0.1, 1, 10, 25, and 50 μ M) or FICZ (0.1, 1, 10, 25, and 50 nM) for 24 h. After treatment, cells were washed to remove any residual drugs, and fresh medium containing Cyp1A1 substrate (as per protocol provided with kit Cat.# V8751; Promega) for 3 h. After incubation, 25 μ L of culture medium was removed from each well and transferred to a 96-well white opaque plate and 25 μ L of luciferin detection reagent was added to initiate the luminiscence reaction and plate was incubated at room temperature for 20 min. After incubation, luminiscence was recorded in luminometer. The data reported as fold change over vehicle treatment.

Small interfering RNA (siRNA) mediated knockdown experiment. The AhR siRNA (SR300136) and Cyp1A1 siRNA (SR301093) was purchased from Origene. For knockdown experiments, HT29 cells (0.5×10^6 cells/well) were plated in 6 well plate and grown for 24 h. The AhR, Cyp1A1 and control-siRNA was transfected into HT29 cells using Lipofectamine[®] RNAiMAX reagent (ThermoFisher Scientific) as per instruction given. After 24 h of transfections, cell were induced with vehicle (0.01% DMSO), UroA (50 μ M), and UAS03 (50 μ M) for 24 h. After treatment with inducers, cells were lysed using RIPA buffer and total protein was used to analyse the expression of AhR, Cyp1A1 and Cldn4 by western blot.

Cyp1A1 deletion by CRISPR/Cas9 method. HT29 cells (1.5×10^5) were plated in 6-well in antibiotic free standard growth medium 24 h prior to transfection. At 60% confluency cells, cells were co-transfected with 2 μ g each of CRISPR/Cas9 KO Plasmid (sc-400511-KO-2; Santa cruz) and HDR Plasmid (sc-400511-HDR-2; Santa cruz) using UltraCruz[®] Transfection Reagent (sc-395739; Santa Cruz). Medium was replaced with selective medium (containing 4 μ g/mL puromycin) 96 h post transfection. Transfection was confirmed with fluorescence microscopy and western blot (CYP1A1). The double positive cells for GFP and RFP were sorted using MoFlo XDP sorting instrument (Beckman Coulter). The deletion of Cyp1A1 in these sorted was confirmed by western blots. These cells were then plated in 6-well plate for in standard medium for evaluating the effect of UroA/UAS03 on

Cldn4 expression. After 24 h of UroA/UAS03 treatment cells were harvested for protein and Cldn4 expression was investigated along with normal HT29 cells.

NF- κ B EMSA assay. RAW 264.7 cells or BMDM were plated in 100 mm dishes (1×10^6) in DMEM supplemented with 10% fetal bovine serum (FBS), 100 U/ml penicillin, and 100 U/ml streptomycin. Cells were allowed to grow for 24 h and after incubation, cells were treated with LPS (50 ng/mL) with and without UroA (50 μ M) and UAS03 (50 μ M) for 6 h. After treatments, culture medium was removed and washed with PBS. Cells were scraped and pelleted down in PBS. Supernatant was discarded and pellet was used for isolation of nuclear and cytosolic protein using NE-PER Nuclear and Cytoplasmic kit (Thermo Scientific; Cat #78833). Later nuclear protein (2 μ g) was used for EMSA using Non-Radioactive EMSA Kits with IR Fluor-Probes for Nuclear factor kappa B p65 (Viagene Biotech Inc Cat # IRTF282 60).

Colon explant culture. Colon tissue pieces (0.5–1 cm length) from wild type (C57BL/6) or Nrf2^{-/-} or AhR^{-/-} mice were cultured in triplicates for 24 h in complete DMEM-high glucose medium (supplemented with 10% fetal bovine serum, 1X penicillin-streptomycin solution) in a humidified atmosphere in the presence of vehicle (0.01% DMSO), UroA (50 μ M) or UAS03 (50 μ M). The tissues were processed for protein preparation (tissue lysates with RIPA plus buffer) or total RNA isolation. These tissue lysates or RNA were used to determine the expression of Nrf2, Cldn4 and AhR.

Tissue processing for RNA and protein analysis. Mice were treated with as described in results section. Mice were euthanized with CO₂ asphyxiation followed by cervical dislocation. Colon was dissected out and luminal contents were flushed out with cold PBS (containing PMSF and Sodium orthovanadate). Small portion of colon was snap frozen in liquid nitrogen and stored at -80 °C for RNA analysis. For preparation of protein samples, colon was opened longitudinally and mucosa was scraped in ice-cold 1X PBS using pre-chilled glass slide and centrifuged at $300 \times g$ for 10 min at 4 °C. Supernatant was discarded and pellet was suspended in RIPA buffer (containing 1X protease inhibitor) and vortexed at high speed. After 30 min incubation on ice, samples were centrifuged at $13,000 \times g$ for 20 min at 4 °C. Supernatant was collected and protein was quantified using BCA protein quantification kit. The lysates were used appropriately for western blots.

28-day repeated dose toxicity study. To evaluate toxicity of UroA and UAS03, we performed 28-days repeated dose toxicity study. Mice were fed (oral gavage) with UroA (20 and 40 mg/kg/day) and UAS03 (20 and 40 mg/kg/day) daily for 28 days. Body weight, food, and water intake were assessed weekly. After 28 days, mice were killed and gross examination of all major organs were performed. Blood was collected to obtain serum. Serum alanine aminotransferase (ALT) and aspartate aminotransferase (AST) were analyzed using ALT/ AST kit (BioVision) as per instructional manual.

2,4,6-Trinitrobenzenesulfonic acid (TNBS)-induced colitis. Male C57BL/6 or Nrf2^{-/-} mice (6–8 week old age mice) were anesthetized with ketamine/xylazine (100 mg/12.5 mg/kg IP) mixture and administered with single dose of TNBS (2.5 mg/mice; Sigma Aldrich, USA) in 50% ethanol. After administration of TNBS, mice were held upside down for 30–60 s to ensure proper distribution of TNBS in the colon. Control group received 50% ethanol without TNBS. Mice with TNBS were randomly divided into three groups, viz. vehicle (0.25% sodium carboxymethylcellulose (CMC)), UroA and UAS03. UroA or UAS03 was resuspended in 0.25% sodium-CMC at desired concentrations. The mice were given orally Veh or UroA or UAS03 in 100 μ L at desired concentrations (4 or 20 mg/kg/body weight). The treatment started after 12 h of TNBS administration and every 12 h thereafter up to 72 h. The experiment was terminated post 60 h TNBS, where AhR^{-/-} mice were involved. In some experiments, we treated only once at post 12 h TNBS administration. TNBS administered and control mice were euthanized for tissue

and plasma collection after 80 h of TNBS/ethanol treatment. Mice were examined for colitis phenotype.

DSS-induced colitis. Acute experimental colitis in mice was induced by giving 3% (w/v) colitis grade DSS (MP Biomedicals) in drinking water for 7 days. Control animal received drinking water without DSS. All colitis group mice were randomly divided into three groups *viz.* vehicle treated (0.25% Na-CMC), UroA (20 mg/kg/day) and UAS03 (20 mg/kg/day) on the 4th and 6th day of DSS treatment. After 7 days, animals were put back on regular water for a period of 7 days. For chronic DSS colitis model, we used three cycles of 2.0% (w/v) DSS and each DSS cycle consisted of 7 days followed by 10 days of regular water and mice were treated with UroA (20 mg/kg/day) on every 4th and 6th day of DSS cycle.

Assessment of colitis severity and tissue collection. Mice were evaluated daily for change in body weight, stool consistency, and rectal bleeding and score was given and combined to obtained disease activity index⁶⁷. After euthanasia, the colon was removed and flushed with PBS containing (1 mM PMSF and 0.2 mM sodium orthovanadate). Colon length and colon weight were measured and small parts of colon were excised for myeloperoxidase (MPO) activity and RNA isolation. Tissues for MPO and RNA extraction were snap frozen in liquid nitrogen and stored in -80°C until further analysis. Tissue for histological examination was stored in 10% phosphate buffered saline formalin. Blood was collected and serum was separated by centrifugation at $3500 \times g$ for 15 min. Serum cytokines (IL-6, TNF- α ; Biolegend) and chemokines (CXCL1; R&D Systems) levels were measured by ELISA according to manufacturer's instructions.

In vivo intestinal permeability assay. The gut barrier function was evaluated by in vivo intestinal permeability using FITC-Dextran (MW 4000; FD4, Sigma-Aldrich, USA)⁶⁸. Briefly, mice were orally administered with FITC-dextran (60 mg/100 gm body weight). Mice were fasted for 4 h prior to euthanasia. The FITC-dextran concentration in serum was determined using the standard curve of FITC-dextran in serum (excitation, 485 nm; emission, 525 nm; BMG LABTECH).

Myeloperoxidase (MPO) activity. The MPO activity in the colons was determined using the following procedure⁶⁹. Briefly, colon tissue was homogenized in 0.5% (w/v) hexadecyltrimethylammonium bromide (H6269; Sigma-Aldrich, USA) in 50 mM PBS, pH 6.0. This homogenate underwent 3 freeze-thaw cycles and 10–15 s sonication to obtain homogenous suspension. The supernatant from this suspension was collected after centrifugation at $13000 \times g$ for 20 min at 4°C . The supernatant (10 μl) was then added to 50 mM potassium phosphate buffer (pH 6.0) containing 0.167 mg/ml *o*-dianisidine (Sigma-Aldrich, USA) and 0.0005% H_2O_2 (Sigma-Aldrich USA) and absorbance was taken at 450 nm (BMG, LABTECH) at 2 min interval. Units of MPO in each sample was determined by considering that one unit (U) of MPO = 1 μmol of H_2O_2 split with molar extinction coefficient of 1.13×10^{-2} nm/min and MPO in each sample calculated by using $[\Delta A(t_2 - t_1)] / A_{\text{min}} \times (1.13 \times 10^{-2})$ formula and MPO units were normalized with per mg tissue.

Histopathology. Collected colon tissue were fixed in 10% buffered formaldehyde solution overnight and fixed tissue underwent standard histopathological processing. Briefly, after fixation tissue underwent dehydration and cleaning with xylene before paraffin embedding. The paraffin section of 5 μm were cut (Leica microtome) and stained for H&E staining. The H&E images were captured using Aperio Scanscope. H&E sections were scored blindly using index scoring described by Erben et al.⁷⁰.

Data availability

The RNA-seq data described in this MS is deposited with GEO # GSE113581. The hyperlink for RNA seq as follows: https://urldefense.proofpoint.com/v2/url?u=https-3A_www.ncbi.nlm.nih.gov_geo_query_acc.cgi-3Facc-3DGSE113581&d=DwIBAg&c=OAG1LQNACBDguGvBeNj18Swhr9TMTJS-x4O_KuapPgY&r=gYAe1Rux-xOAAWAT6YX2N_noYeYJBx7FLRBVfJZPt0&m=aQROwFtABYMDtrIp4k7mNRkL77nfCBUH4EqXd2nQLK0&s=RH4q-x-nZSE8JU035mWKJs4mmznYY-E3Nvx9CKs_QKs&e=. The full raw data that support the findings of this study are available from the corresponding author upon reasonable request. The Source Data underlying all the bar graphs in the Figures are provided in the Source Data File.

Received: 9 January 2018 Accepted: 28 November 2018

Published online: 09 January 2019

References

1. Lynch, S. V. & Pedersen, O. The human intestinal microbiome in health and disease. *N. Engl. J. Med.* **375**, 2369–2379 (2016).

2. Levy, M., Kolodziejczyk, A. A., Thaiss, C. A. & Elinav, E. Dysbiosis and the immune system. *Nat. Rev. Immunol.* **17**, 219–232 (2017).
3. Sonnenburg, J. L. & Backhed, F. Diet-microbiota interactions as moderators of human metabolism. *Nature* **535**, 56–64 (2016).
4. Belkaid, Y. & Hand, T. W. Role of the microbiota in immunity and inflammation. *Cell* **157**, 121–141 (2014).
5. Dzutsev, A. et al. Microbes and cancer. *Annu. Rev. Immunol.* **35**, 199–228 (2017).
6. Tamboli, C. P., Neut, C., Desreumaux, P. & Colombel, J. F. Dysbiosis in inflammatory bowel disease. *Gut* **53**, 1–4 (2004).
7. Gopalakrishnan, V., Helmink, B. A., Spencer, C. N., Reuben, A. & Wargo, J. A. The Influence of the gut microbiome on cancer, immunity, and cancer immunotherapy. *Cancer Cell* **33**, 570–580 (2018).
8. Landy, J. et al. Tight junctions in inflammatory bowel diseases and inflammatory bowel disease associated colorectal cancer. *World J. Gastroenterol.* **22**, 3117–3126 (2016).
9. Schulzke, J. D. et al. Epithelial tight junctions in intestinal inflammation. *Ann. N. Y. Acad. Sci.* **1165**, 294–300 (2009).
10. Vindigni, S. M., Zisman, T. L., Suskind, D. L. & Damman, C. J. The intestinal microbiome, barrier function, and immune system in inflammatory bowel disease: a tripartite pathophysiological circuit with implications for new therapeutic directions. *Ther. Adv. Gastroenterol.* **9**, 606–625 (2016).
11. Heber, D. Multitargeted therapy of cancer by ellagitannins. *Cancer Lett.* **269**, 262–268 (2008).
12. Sak, K. Cytotoxicity of dietary flavonoids on different human cancer types. *Pharmacogn. Rev.* **8**, 122–146 (2014).
13. Habauzit, V. & Morand, C. Evidence for a protective effect of polyphenols-containing foods on cardiovascular health: an update for clinicians. *Ther. Adv. Chronic Dis.* **3**, 87–106 (2012).
14. Gbinigie, O. A., Onakpoya, I. J. & Spencer, E. A. Evidence for the effectiveness of pomegranate supplementation for blood pressure management is weak: a systematic review of randomized clinical trials. *Nutr. Res.* **46**, 38–48 (2017).
15. Stockton, A., Farhat, G., McDougall, G. J. & Al-Dujaili, E. A. S. Effect of pomegranate extract on blood pressure and anthropometry in adults: a double-blind placebo-controlled randomised clinical trial. *J. Nutr. Sci.* **6**, e39 (2017).
16. Razani, Z., Dastani, M. & Kazerani, H. R. Cardioprotective effects of pomegranate (*Punica granatum*) juice in patients with ischemic heart disease. *Phytother. Res.* **31**, 1731–1738 (2017).
17. Derosa, G. & Maffioli, P., & Sahebkar, A. Ellagic acid and its role in chronic diseases. *Adv. Exp. Med. Biol.* **928**, 473–479 (2016).
18. Cerda, B., Periago, P., Espin, J. C. & Tomas-Barberan, F. A. Identification of urolithin A as a metabolite produced by human colon microflora from ellagic acid and related compounds. *J. Agric. Food Chem.* **53**, 5571–5576 (2005).
19. Selma, M. V., Beltran, D., Garcia-Villalba, R., Espin, J. C. & Tomas-Barberan, F. A. Description of urolithin production capacity from ellagic acid of two human intestinal *Gordonibacter* species. *Food Funct.* **5**, 1779–1784 (2014).
20. Espin, J. C., Larrosa, M., Garcia-Conesa, M. T. & Tomas-Barberan, F. Biological significance of urolithins, the gut microbial ellagic acid-derived metabolites: the evidence so far. *Evid.-Based Complement. Alternat. Med.* **2013**, 270418 (2013).
21. Tomas-Barberan, F. A. et al. Urolithins, the rescue of 'old' metabolites to understand a 'new' concept: metabotypes as a nexus between phenolic metabolism, microbiota dysbiosis and host health status. *Mol. Nutr. Food Res.* **61**, 1–35 (2016).
22. Ryu, D. et al. Urolithin A induces mitophagy and prolongs lifespan in *C. elegans* and increases muscle function in rodents. *Nat. Med.* **22**, 879–888 (2016).
23. Saha, P. et al. Gut Microbiota conversion of dietary ellagic acid into bioactive phytochemical urolithin A inhibits heme peroxidases. *PLoS One* **11**, e0156811 (2016).
24. Tsukita, S. & Furuse, M. Claudin-based barrier in simple and stratified cellular sheets. *Curr. Opin. Cell Biol.* **14**, 531–536 (2002).
25. Loboda, A., Damulewicz, M., Pyza, E., Jozkowicz, A. & Dulak, J. Role of Nrf2/HO-1 system in development, oxidative stress response and diseases: an evolutionarily conserved mechanism. *Cell. Mol. Life Sci.* **73**, 3221–3247 (2016).
26. Beischlag, T. V., Luis Morales, J., Hollingshead, B. D. & Perdew, G. H. The aryl hydrocarbon receptor complex and the control of gene expression. *Crit. Rev. Eukaryot. Gene Expr.* **18**, 207–250 (2008).
27. Yeager, R. L., Reisman, S. A., Aleksunes, L. M. & Klaassen, C. D. Introducing the "TCDD-inducible AhR-Nrf2 gene battery". *Toxicol. Sci.* **111**, 238–246 (2009).
28. Miao, W., Hu, L., Scrivens, P. J. & Batist, G. Transcriptional regulation of NF-E2 p45-related factor (NRF2) expression by the aryl hydrocarbon receptor-xenobiotic response element signaling pathway: direct cross-talk between

- phase I and II drug-metabolizing enzymes. *J. Biol. Chem.* **280**, 20340–20348 (2005).
29. Antoniou, E. et al. The TNBS-induced colitis animal model: an overview. *Ann. Med. Surg.* **11**, 9–15 (2016).
 30. Smith, P. D. et al. Intestinal macrophages and response to microbial encroachment. *Mucosal Immunol.* **4**, 31–42 (2011).
 31. Bain, C. C. & Mowat, A. M. Macrophages in intestinal homeostasis and inflammation. *Immunol. Rev.* **260**, 102–117 (2014).
 32. Gaya, P., Peiroté, A., Medina, M., Álvarez, I. & Landete, J. M. Bifidobacterium pseudocatenulatum INIA P815: The first bacterium able to produce urolithins A and B from ellagic acid. *J. Funct. Foods* **45**, 95–99 (2018).
 33. Larrosa, M. et al. Anti-inflammatory properties of a pomegranate extract and its metabolite urolithin-A in a colitis rat model and the effect of colon inflammation on phenolic metabolism. *J. Nutr. Biochem.* **21**, 717–725 (2010).
 34. Forster, C. Tight junctions and the modulation of barrier function in disease. *Histochem. Cell Biol.* **130**, 55–70 (2008).
 35. Arrieta, M. C., Bistritz, L. & Meddings, J. B. Alterations in intestinal permeability. *Gut* **55**, 1512–1520 (2006).
 36. Konig, J. et al. Human intestinal barrier function in health and disease. *Clin. Transl. Gastroenterol.* **7**, e196 (2016).
 37. Capaldo, C. T. & Nusrat, A. Cytokine regulation of tight junctions. *Biochim. Biophys. Acta* **1788**, 864–871 (2009).
 38. Esser, C. & Rannug, A. The aryl hydrocarbon receptor in barrier organ physiology, immunology, and toxicology. *Pharmacol. Rev.* **67**, 259–279 (2015).
 39. Stockinger, B., Di Meglio, P., Gialitakis, M. & Duarte, J. H. The aryl hydrocarbon receptor: multitasking in the immune system. *Annu. Rev. Immunol.* **32**, 403–432 (2014).
 40. Furumatsu, K. et al. A role of the aryl hydrocarbon receptor in attenuation of colitis. *Dig. Dis. Sci.* **56**, 2532–2544 (2011).
 41. Goettel, J. A. et al. AHR activation is protective against colitis driven by T cells in humanized mice. *Cell Rep.* **17**, 1318–1329 (2016).
 42. Schiering, C. et al. Feedback control of AHR signalling regulates intestinal immunity. *Nature* **542**, 242–245 (2017).
 43. Gimenez-Bastida, J. A. et al. Ellagitannin metabolites, urolithin A glucuronide and its aglycone urolithin A, ameliorate TNF- α -induced inflammation and associated molecular markers in human aortic endothelial cells. *Mol. Nutr. Food Res.* **56**, 784–796 (2012).
 44. Monteleone, I. et al. Aryl hydrocarbon receptor-induced signals up-regulate IL-22 production and inhibit inflammation in the gastrointestinal tract. *Gastroenterology* **141**, 237–248 (2011). 248 e231.
 45. Shin, S. et al. Nrf2 modulates aryl hydrocarbon receptor signaling: influence on adipogenesis. *Mol. Cell. Biol.* **27**, 7188–7197 (2007).
 46. Hayes, J. D., Dinkova-Kostova, A. T. & McMahon, M. Cross-talk between transcription factors AhR and Nrf2: lessons for cancer chemoprevention from dioxin. *Toxicol. Sci.* **111**, 199–201 (2009).
 47. Mitsuishi, Y., Motohashi, H. & Yamamoto, M. The Keap1-Nrf2 system in cancers: stress response and anabolic metabolism. *Front. Oncol.* **2**, 200 (2012).
 48. Al-Sawaf, O. et al. Nrf2 in health and disease: current and future clinical implications. *Clin. Sci.* **129**, 989–999 (2015).
 49. Khor, T. O. et al. Nrf2-deficient mice have an increased susceptibility to dextran sulfate sodium-induced colitis. *Cancer Res.* **66**, 11580–11584 (2006).
 50. Kobayashi, E. H. et al. Nrf2 suppresses macrophage inflammatory response by blocking proinflammatory cytokine transcription. *Nat. Commun.* **7**, 11624 (2016).
 51. Wardyn, J. D., Ponsford, A. H. & Sanderson, C. M. Dissecting molecular cross-talk between Nrf2 and NF- κ B response pathways. *Biochem. Soc. Trans.* **43**, 621–626 (2015).
 52. Sekine, H. et al. Hypersensitivity of aryl hydrocarbon receptor-deficient mice to lipopolysaccharide-induced septic shock. *Mol. Cell. Biol.* **29**, 6391–6400 (2009).
 53. Benson, J. M. & Shepherd, D. M. Aryl hydrocarbon receptor activation by TCDD reduces inflammation associated with Crohn's disease. *Toxicol. Sci.* **120**, 68–78 (2011).
 54. Fukumoto, S. et al. Identification of a probiotic bacteria-derived activator of the aryl hydrocarbon receptor that inhibits colitis. *Immunol. Cell Biol.* **92**, 460–465 (2014).
 55. Metidji, A. et al. The environmental sensor AHR protects from inflammatory damage by maintaining intestinal stem cell homeostasis and barrier integrity. *Immunity* **49**, 353–362 e355 (2018).
 56. Novak, E. A. & Mollen, K. P. Mitochondrial dysfunction in inflammatory bowel disease. *Front. Cell Dev. Biol.* **3**, 62 (2015).
 57. Delpre, G., Avidor, I., Steinhilber, R., Kadish, U. & Ben-Bassat, M. Ultrastructural abnormalities in endoscopically and histologically normal and involved colon in ulcerative colitis. *Am. J. Gastroenterol.* **84**, 1038–1046 (1989).
 58. Rodenburg, W. et al. Impaired barrier function by dietary fructo-oligosaccharides (FOS) in rats is accompanied by increased colonic mitochondrial gene expression. *BMC Genomics* **9**, 144 (2008).
 59. Kurowska-Stolarska, M. et al. IL-33 amplifies the polarization of alternatively activated macrophages that contribute to airway inflammation. *J. Immunol.* **183**, 6469–6477 (2009).
 60. Kowapradit, J. et al. In vitro permeability enhancement in intestinal epithelial cells (Caco-2) monolayer of water soluble quaternary ammonium chitosan derivatives. *AAPS PharmSciTech* **11**, 497–508 (2010).
 61. Andrews S. FastQC: A Quality Control Tool for High Throughput Sequence Data. (2014).
 62. Kim, D. et al. TopHat2: accurate alignment of transcriptomes in the presence of insertions, deletions and gene fusions. *Genome Biol.* **14**, R36 (2013).
 63. Flicek, P. et al. Ensembl 2014. *Nucleic Acids Res.* **42**, D749–D755 (2014).
 64. Trapnell, C. et al. Differential analysis of gene regulation at transcript resolution with RNA-seq. *Nat. Biotechnol.* **31**, 46–53 (2013).
 65. Trapnell, C. et al. Differential gene and transcript expression analysis of RNA-seq experiments with TopHat and Cufflinks. *Nat. Protoc.* **7**, 562–578 (2012).
 66. Singh, R. et al. Evaluation of memory enhancing clinically available standardized extract of Bacopa monniera on P-glycoprotein and cytochrome P450 3A in Sprague-Dawley rats. *PLoS ONE* **8**, e72517 (2013).
 67. Murthy, S. N. et al. Treatment of dextran sulfate sodium-induced murine colitis by intracolonic cyclosporin. *Dig. Dis. Sci.* **38**, 1722–1734 (1993).
 68. Furuta, G. T. et al. Hypoxia-inducible factor 1-dependent induction of intestinal trefoil factor protects barrier function during hypoxia. *J. Exp. Med.* **193**, 1027–1034 (2001).
 69. Kim, J. J., Shajib, M. S., Manocha, M. M., Khan, W. I. Investigating intestinal inflammation in DSS-induced model of IBD. *J. Vis. Exp.* **60**, 3678 (2012).
 70. Erben, U. et al. A guide to histomorphological evaluation of intestinal inflammation in mouse models. *Int. J. Clin. Exp. Pathol.* **7**, 4557–4576 (2014).

Acknowledgements

This work is financially supported by NIH/NCI (R21CA216090), NIH/NIGMS CoBRE grant (P20GM125504-01) and pilot grants from Microbiology and Immunology (U of L), Rounsavall Foundation and The Jewish Heritage Fund for Excellence Research Enhancement Grant and JGBCC to V.R.J.; V.R.J. and R.S. are partially supported by funds from NIH/NCI (CA191683). Part of RNA-Seq experiment was performed with assistance of the U of L Genomics Facility, which is supported by NIH P20GM103436 (KY IDeA Networks of Biomedical Research Excellence), NIH P30GM106396 (UofL J. G. Brown Cancer Center Phase III CoBRE), the J. G. Brown Foundation, and user fees. We thank JGBCC imaging core facilities at U of L. This work is financially supported by Department of Biotechnology (DBT) (BT/PR12490/AAQ/3/716/2015) to P.K.V., and core-funds from the Institute for Stem Cell Biology and Regenerative Medicine (inStem). P.K.V. is supported by Ramalingaswami ReEntry Fellowship (DBT), India. S.C. is supported by Department of Science and Technology (DST) under the Scheme for Young Scientists and Technologies program (SP/YO/078/2017). A.A.H. is supported by Senior Research Fellowship by Council of Scientific & Industrial Research (CSIR). We thank animal house facility/members and Central Imaging & Flow Cytometry, NMR facilities at inStem and NCBS.

Author contributions

V.R.J. and P.K.V. conceived, designed the experiments, and analyzed the data. R.S., S.C., S.R.B., B.B., B.H., N.G.K., A.A.H., T.S., and P.P. designed, performed the experiments, and analyzed the data. M.V.-K., M.G.I.L., G.M.D., G.W.D., H.-G.Z., and B.H. contributed through invaluable discussions. X.C., E.C.R., and S.J.W. assisted in analyzing RNA-Seq data. A.H. scored the inflammation of colons. R.S., B.H., P.K.V., and V.R.J. wrote the paper, all authors discussed the results. P.K.V. and V.R.J. supervised the project.

Additional information

Supplementary Information accompanies this paper at <https://doi.org/10.1038/s41467-018-07859-7>.

Competing interests: V.R.J., P.K.V., H.B., R.S., S.C., and A.A.H. hold a patent application related to this technology (US patent application number: 62/671,737). P.K.V.'s interests were reviewed and are managed by the Institute for Stem Cell Biology and Regenerative Medicine (inStem) in accordance with their Conflict of Interest policies. The remaining authors declare no competing interests.

Reprints and permission information is available online at <http://npg.nature.com/reprintsandpermissions/>

Journal peer review information: *Nature Communications* thanks the anonymous reviewers for their contributions to the peer review of this work.

Publisher's note: Springer Nature remains neutral with regard to jurisdictional claims in published maps and institutional affiliations.



Open Access This article is licensed under a Creative Commons Attribution 4.0 International License, which permits use, sharing, adaptation, distribution and reproduction in any medium or format, as long as you give appropriate credit to the original author(s) and the source, provide a link to the Creative Commons license, and indicate if changes were made. The images or other third party material in this article are included in the article's Creative Commons license, unless indicated otherwise in a credit line to the material. If material is not included in the article's Creative Commons license and your intended use is not permitted by statutory regulation or exceeds the permitted use, you will need to obtain permission directly from the copyright holder. To view a copy of this license, visit <http://creativecommons.org/licenses/by/4.0/>.

© The Author(s) 2019




Intermittent scavenging of storage lesion from stored red blood cells by electrospun nanofibrous sheets enhances their quality and shelf-life

Received: 18 June 2022

Accepted: 24 November 2022

Published online: 01 December 2022

 Check for updates

Subhashini Pandey ^{1,2,3}, Manohar Mahato ^{1,3}, Preethem Srinath ¹,
Utkarsh Bhutani ¹, Tanu Jain Goap ^{1,2}, Priusha Ravipati ¹ &
Praveen Kumar Vemula ¹ ✉

Transfusion of healthy red blood cells (RBCs) is a lifesaving process. However, upon storing RBCs, a wide range of damage-associated molecular patterns (DAMPs), such as cell-free DNA, nucleosomes, free-hemoglobin, and poly-unsaturated-fatty-acids are generated. DAMPs can further damage RBCs; thus, the quality of stored RBCs declines during the storage and limits their shelf-life. Since these DAMPs consist of either positive or negative charged species, we developed taurine and acridine containing electrospun-nanofibrous-sheets (*Tau-AcrNFS*), featuring anionic, cationic charges and an DNA intercalating group on their surfaces. We show that *Tau-AcrNFS* are efficient in scavenging DAMPs from stored human and mice RBCs ex vivo. We find that intermittent scavenging of DAMPs by *Tau-AcrNFS* during the storage reduces the loss of RBC membrane integrity and reduces discocytes-to-spherocytocytes transformation in stored-old-RBCs. We perform RBC-transfusion studies in mice to reveal that intermittent removal of DAMPs enhances the quality of stored-old-RBCs equivalent to freshly collected RBCs, and increases their shelf-life by ~22%. Such prophylactic technology may lead to the development of novel blood bags or medical device, and may therefore impact healthcare by reducing transfusion-related adverse effects.

Blood transfusion is often a lifesaving practice for patients in the intensive care unit (ICU), where ~50–70% of ICU patients are transfused with blood units during their stay¹. Typical indications for blood transfusion include sickle cell crisis, anemia, and severe blood loss². The highest transfused blood components are red blood cells (RBCs), with >85 million RBC units are transfused annually worldwide^{2,3}. While RBC transfusion has therapeutic benefits, transfusion of storage-aged RBCs may cause deleterious effects on the recipients. These

deleterious effects have been attributed to the storage lesion consisting of damage-associated molecular patterns (DAMPs) generated due to biochemical, morphological, and structural changes in RBCs during the storage-aging process^{4,5}. The most studied DAMPs in this context are as follows: (i) extracellular free-iron and free-hemoglobin (Hb) generated due to lysis of RBCs, (ii) bioactive lipids such as poly-unsaturated fatty acids (PUFAs), (iii) extracellular DNA, and (iv) nucleosomes generated by neutrophils. These DAMPs are a potential

¹Institute for Stem Cell Science and Regenerative Medicine (inStem), GKVK Post, Bellary Road, Bangalore 560065 Karnataka, India. ²The University of Trans-Disciplinary Health Sciences and Technology, Attur (post), Yelahanka, Bangalore 560064 Karnataka, India. ³These authors contributed equally: Subhashini Pandey, Manohar Mahato. ✉e-mail: praveenv@instem.res.in

source of sequelae in vulnerable patients⁶. Based on storage-time-dependent accumulation of DAMPs, stored human RBC units are classified as young RBCs or fresh RBCs (RBCs of <14–21 days of storage) and old RBCs (stored between 21 and 42 days)⁷. Storage of RBCs induces a sequence of biochemical and biomechanical changes in a progressive manner that affect deformability, cell viability, micro-circulatory flow, and oxygen-carrying capability of RBCs⁸; hence, the detrimental effect of RBC storage can negatively impact the transfusion outcomes. Therefore, developing strategies and technologies to enhance the quality and shelf-life of stored RBCs to reduce the incidence of transfusion-related complications will significantly impact healthcare.

The United States Foods and Drug Administration (US-FDA) regulation states that human-packed RBCs (pRBCs) can be stored up to 42 days before transfusion. Post 42 days, the increased DAMPs (extracellular DNA, nucleosomes, Hb, and bioactive lipids) pose a fatal risk to the patient by eliciting an immunomodulatory response^{9,10}. Leukocyte-associated DAMPs, such as extracellular DNA and nucleosomes, are potential immune elicitors in recipients and are implicated in transfusion-related complications¹¹. Leukodepletion of packed RBCs using specialized filters mitigates risk to a large extent, putatively by reducing a load of extracellular DNA and nucleosomes in blood units¹². However, leukodepletion does not remove other critical RBCs-generated DAMPs, such as free-Hb and bioactive lipids, which are also significant mediators of transfusion-related complications. Therefore, in alternative to the leukoreduction process, studies thus far have focused on improving storage conditions by alternative cryopreservation protocols^{13,14}, anaerobic storage^{15,16}, and usage of additives/rejuvenation solutions^{17–19}. Additionally, washing stored RBCs with saline (0.9% NaCl) to remove accumulated bioactive factors is another established strategy approved to use in transfusion medicine^{20,21}. Past investigations suggest that adding preservatives, storing RBCs in an alkaline hypotonic solution with antioxidants, or rendering anaerobic storage conditions improve storage time by up to 10–15 days^{17–19}. Although these approaches have shown encouraging results, efficient technologies to scavenge the spectrum of DAMPs and further reduce their formation in stored RBCs remain an unmet need. Additionally, the leukoreduction process is expensive. Hence, most blood banks in India and developing countries do not routinely use leukoreduction processes. Interestingly, prior to initiating this work, our discussions with blood banks in India revealed that only <10% of blood banks use the leukoreduction process. It is used only in cases where recipients are immunosuppressed/immuno-compromised. Therefore, an important driver for developing new technology is the desire to develop an affordable intervention that could be used in developing and under-resourced countries where non-leukoreduced blood products are the standard inventory.

Here we develop a new approach, demonstrating that intermittent scavenging of DAMPs using electrospun-charged nanofibrous sheets slows the deterioration of stored RBCs, increasing their quality and shelf-life. Critical DAMPs such as extracellular DNA, nucleosomes, free-Hb, and PUFAs are charged molecules with anionic or cationic nature. Therefore, we hypothesized that *charged nanofibrous sheets* made with cationic and anionic polymers may scavenge DAMPs through ionic interactions (Fig. 1a). We have synthesized novel polymers with anionic and cationic nature by introducing poly taurine and poly acridine, respectively. An efficient process to fabricate electrospun nanofibrous sheets with anionic (*Tau*-NFS) and cationic (*Acr*-NFS) charges has been generated. Additionally, the acridine group in *Acr*-NFS may act as a DNA intercalator. We have demonstrated that a combination of *Tau*-NFS and *Acr*-NFS, hereafter *Tau-Acr*NFS, is efficient in scavenging storage lesions such as free extracellular DNA, nucleosomes, Hb, and PUFAs from stored human and mice RBC units, ex vivo. Two major phenomena were demonstrated using *Tau-Acr*NFS;

i) after storage lesion formed in human old RBCs (stored for 42 days), *Tau-Acr*NFS could efficiently scavenge and remove accumulated DAMPs, and ii) the intermittent scavenging of DAMPs using *Tau-Acr*NFS either at 21st or 28th day resulted in significantly less production of DAMPs at maximum storage time (on 42nd day), and reduced the loss of RBC membrane integrity. We have demonstrated that intermittent removal of DAMPs either on 21st or 28th day by *Tau-Acr*NFS enhanced the quality of the blood and increased the shelf-life by ~22%. Additionally, the RBC transfusion studies suggested that the quality of intermittently treated and stored for a maximum allowed 14 days (old RBCs) is equivalent to the quality of freshly collected RBCs without storage. These results are remarkable, and we aim to generate either novel blood bags or an insert-based medical device using *Tau-Acr*NFS, which may have an enormous impact on improving the quality and shelf-life of stored blood.

Results

Charged electrospun nanofibrous sheets efficiently scavenge DAMPs

To synthesize polymers with anionic/cationic charges to generate electrospun nanofibrous sheets, we have selected poly(methyl vinyl ether-*alt*-maleic acid) [PMVEMA, average Mw: 330,000], to which 50% of tetradecylamine was functionalized to impart hydrophobic nature to the polymer. Subsequently, either 25% of taurine or 11% of hexyl acridine were functionalized to obtain anionic (poly-Tau) and cationic (poly-Acr) polymers, respectively. In addition to furnishing cationic charge, acridine can also bind DNA by intercalation, which could enhance the ability of *Acr*-NFS to scavenge extracellular DNA. The detailed synthesis scheme is provided in Supplementary Fig. 1. Anionic (*Tau*-NFS) and cationic (*Acr*-NFS) electrospun nanofibrous sheets were generated through conventional electrospinning of *poly*-Taurine and *poly*-Acridine, respectively (Methods). *Tau*-NFS and *Acr*-NFS are comprised of nanofibers with 100–200 nm width and >50–100 micron length (Fig. 1b). Surface charge measurements confirmed the overall negative and positive charge of *Tau*-NFS and *Acr*-NFS, respectively (Fig. 1c). Furthermore, contact angle measurements show that both NFS are hydrophobic (Fig. 1d), which is critical to prevent aqueous fluid absorption. A 2-h incubation of *Tau*-NFS and *Acr*-NFS in optisol (AS-5) solution that is used as a preservative for storing RBCs suggested that NFS are stable in preservative solution, and the quantification of leached polymers shows that neither polymers have any significant leaching (<0.2%). Scanning electron microscope images of *Tau*-NFS and *Acr*-NFS post-incubation with stored RBCs show that RBCs or neutrophils do not adhere to NFS (Fig. 1e); hence, there will not be any loss of RBC count due to the NFS treatment. Furthermore, to understand whether treatment of *Tau*-NFS and *Acr*-NFS can cause cell loss, we performed a complete blood count (CBC) before and after treatment with *Tau*-NFS and *Acr*-NFS. Quantifying the number of RBCs, white blood cells, platelets, neutrophils and lymphocytes before and after treating with NFS (Supplementary Fig. S2) revealed that there is no loss of cells suggesting that these nanofibrous sheets do not cause any cell death or cell capture. Additionally, the hemolysis rate was measured upon incubation of RBCs with *Tau-Acr*NFS at 37 °C for 1 h. A <1% of hemolysis was observed for *Tau-Acr*-NFS (Fig. 1f). Cumulatively, these results suggest that *Tau-Acr*NFS are stable and do not cause significant hemolysis. However, it should be noted that to evaluate hemocompatibility quantitatively, highly sensitive chemical analyses, such as by untargeted liquid chromatography–mass spectrometry (LC–MS/MS), will be required to determine any biochemical changes following exposure of RBCs to *Tau-Acr*NFS treatment. These experiments will be done in the next study.

Before testing the DAMPs-scavenging efficacy of NFS, we quantified the production of DAMPs (extracellular DNA, Hb, and PUFAs) in stored human non-leukoreduced RBCs in a time-dependent manner for up to 42 days. Various analytical techniques such as PicoGreen

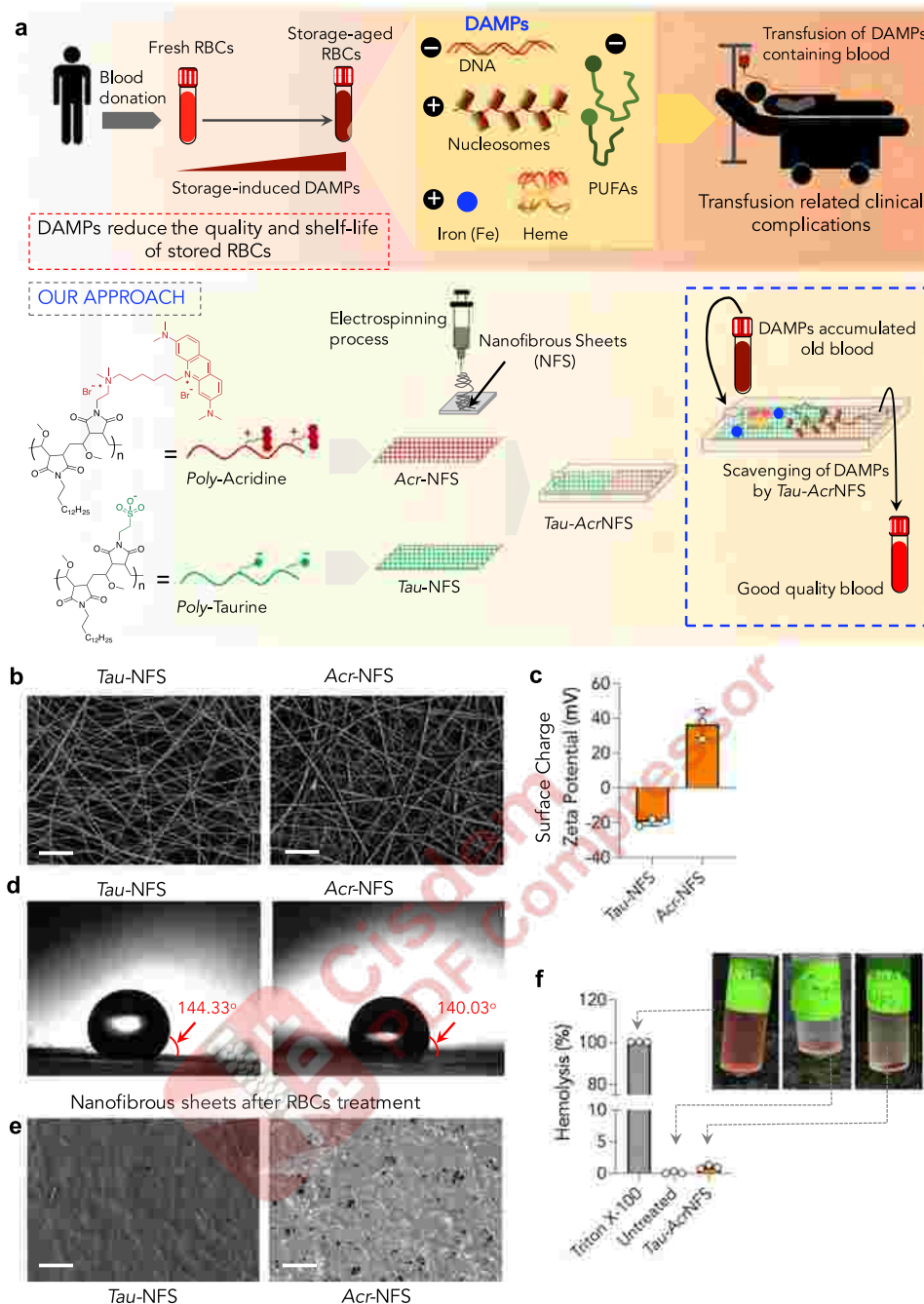


Fig. 1 | Hemocompatible charged nanofibrous sheets scavenge storage lesions to improve the quality of blood. **a** Stored RBCs produce storage lesion or damage-associated molecular patterns (DAMPs) such as DNA, nucleosomes, heme (Hb), iron, and polyunsaturated fatty acids (PUFAs). Transfusion of DAMPs containing RBCs could lead to transfusion-related complications, including systemic inflammation and organ injury. The presence of DAMPs progressively reduces the quality of stored RBCs and limits their shelf-life. All DAMPs consist of positive or negative charge entities. Therefore, *in our approach*, we designed hemocompatible polymers poly-acridine and poly-taurine composed of complementary cationic and anionic charges, respectively. Using these polymers, charge-bearing electrospun nanofibrous sheets (*Tau-NFS* and *Acr-NFS*) were prepared to scavenge charged DAMPs from stored RBCs, which remarkably enhanced the quality and shelf-life of stored RBCs. **b** Scanning electron

microscopy images of *Tau-NFS* and *Acr-NFS* reveal the presence of nanofibrous mesh with a high aspect ratio (scale bar = 2 μm , representative images were selected from 15 images from three independent experiments). **c** Surface charge of *Tau-NFS* and *Acr-NFS* indicate that *Tau-NFS* has a net negative charge (−19.7 mV) and *Acr-NFS* has a net positive charge (+36.7 mV). **d** Contact angle measurements showed that surfaces of *Tau-NFS* and *Acr-NFS* are hydrophobic, which could reduce the absorption of aqueous components during the treatment of stored blood. **e** SEM images of *Tau-NFS* and *Acr-NFS* post-treatment with stored RBCs reveal that except for deposition of DAMPs, no cells have adhered to the NFS (scale bar = 10 μm , representative images were selected from 15 images from three independent experiments). **f** Hemolysis assay revealed that <1% hemolysis was observed upon treatment with *Tau-AcrNFS*. Data are mean \pm s.d. ($n = 3$, from independent experiments). Source data are provided as a Source Data file.

assay, ELISA, Drabkin's assay, and LC-MS were used to quantify extracellular DNA, nucleosomes, Hb, and PUFAs, respectively (Methods). Quantitative elucidation of the storage lesion revealed that DAMPs, including extracellular DNA (Fig. 2a), Hb (Fig. 2b), and

PUFAs such as arachidonic acid (AA, Fig. 2c) and hydroxyeicosatetraenoic acids (5-HETE, 12-HETE, and 15-HETE, Fig. 2d–f) increase over time. For example, on the 42nd day, extracellular DNA and Hb concentration increased by ~150-fold and 40-fold,

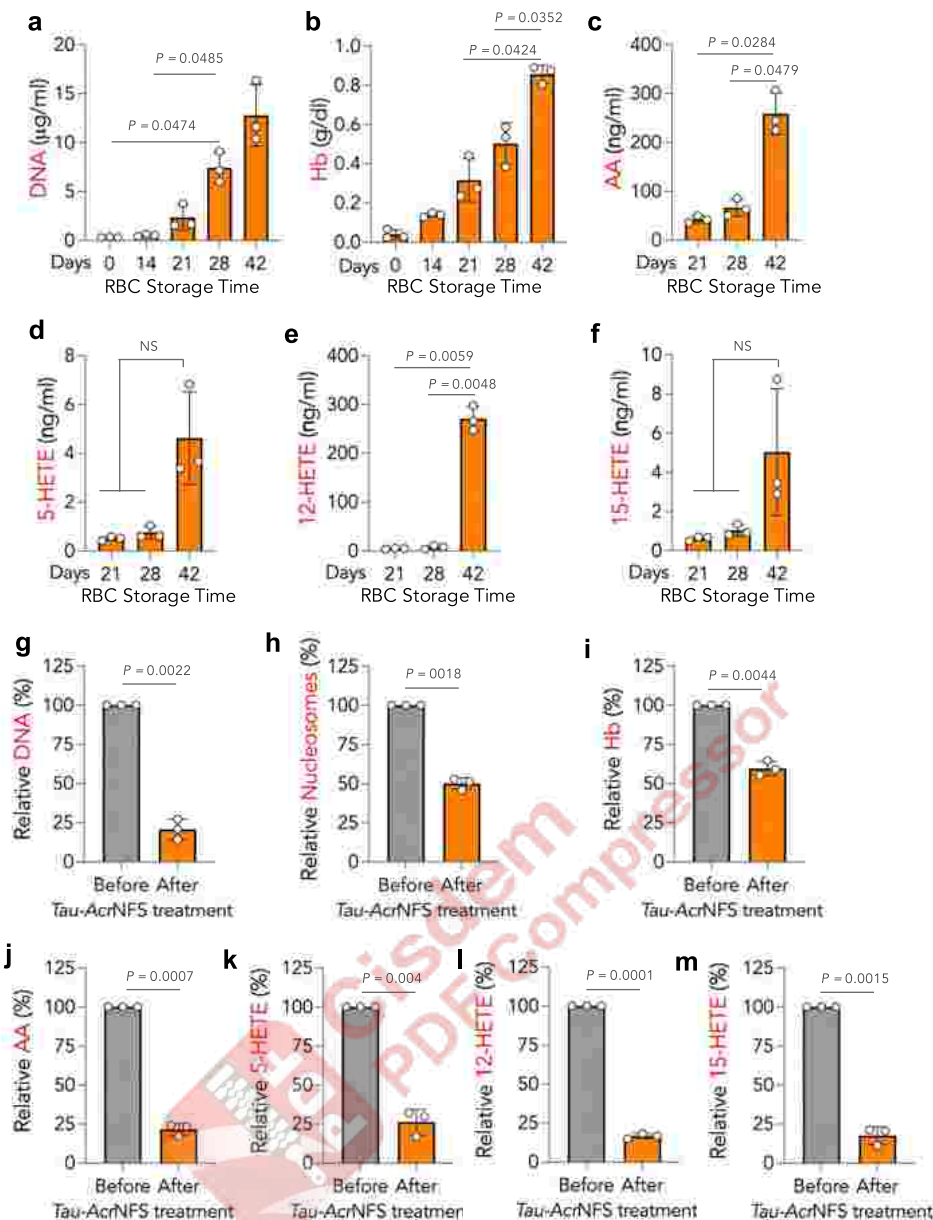


Fig. 2 | Hypothermal storage of human RBCs induced DAMPs production and charged *Tau-AcrNFS* efficiently scavenged DAMPs from stored RBCs.

a–f Storage-induced production of DAMPs as a function of time. RBCs stored at 4 °C progressively produce DNA (**a**), free hemoglobin (Hb, **b**), and polyunsaturated fatty acids (PUFAs) such as AA (**c**), 5-HETE (**d**), 12-HETE (**e**), and 15-HETE (**f**). **g–m**, Incubation of DAMPs accumulated 42 days-stored RBCs with anionic and cationic NFS, *Tau-AcrNFS*, for 5 min at 4 °C efficiently scavenged and reduced the

concentration of DAMPs significantly. The relative concentration of DAMPs before and after *Tau-AcrNFS* treatment has significantly reduced accumulated DNA (**g**), nucleosomes (**h**), Hb (**i**), and PUFAs (**j–m**). Data are mean \pm s.d. ($n = 3$, from independent experiments). For **a–f**, P values were determined by repeated measures one-way ANOVA, and for (**g–m**), by two-tailed Student's t -test with Welch's correction using GraphPad PRISM 9, and exact P values are indicated. NS = not significant. Source data are provided as a Source Data file.

respectively, compared to the 0th day. These observations are in agreement with previous reports^{22–25}.

At the onset, we have systematically optimized the required surface area of nanofibrous sheets and incubation time to scavenge DAMPs. One milliliter of RBCs (42 days stored) were added to the different surface areas of sheets (8, 16, and 24 cm²) and incubated for 30 min at 4 °C. Quantification of extracellular DNA suggested that both nanofibrous sheets could scavenge DNA efficiently with an 8 cm² sheet, and above 8 cm² up to 24 cm² did not increase the scavenging capacity (Supplementary Fig. 3a). Subsequently, RBCs were incubated on 8 cm² nanofibrous sheets for 5, 15, and 30 min to identify the optimum incubation time. Data suggests that *Tau-NFS* and *Acr-NFS* could scavenge the DNA within 5 min of incubation, and

more prolonged incubation did not enhance scavenging capacity (Supplementary Fig. 3b).

To scavenge all DAMPs (extracellular DNA, nucleosomes, Hb, and PUFAs) from old RBCs, 1 ml of 42 days-stored RBCs were incubated with cationic/anionic nanofibrous sheets (*Tau-AcrNFS*) for 5 min at 4 °C. Data in Fig. 2g–m suggests that *Tau-AcrNFS* are efficient in scavenging DAMPs. Upon incubation, nanofibrous sheets scavenged 80% of DNA (Fig. 2g), 50% of nucleosomes (Fig. 2h), 45% of Hb (Fig. 2i), and 75–80% of PUFAs including AA, 5-HETE, 12-HETE, and 15-HETE (Fig. 2j–m). These results suggest that *Tau-AcrNFS* can efficiently scavenge and significantly reduce the concentrations of DAMPs in 42 days of stored old RBCs. SEM images of *Tau-NFS* and *Acr-NFS* post-treatment with stored RBCs (Fig. 1e) shows a gummy layer on the

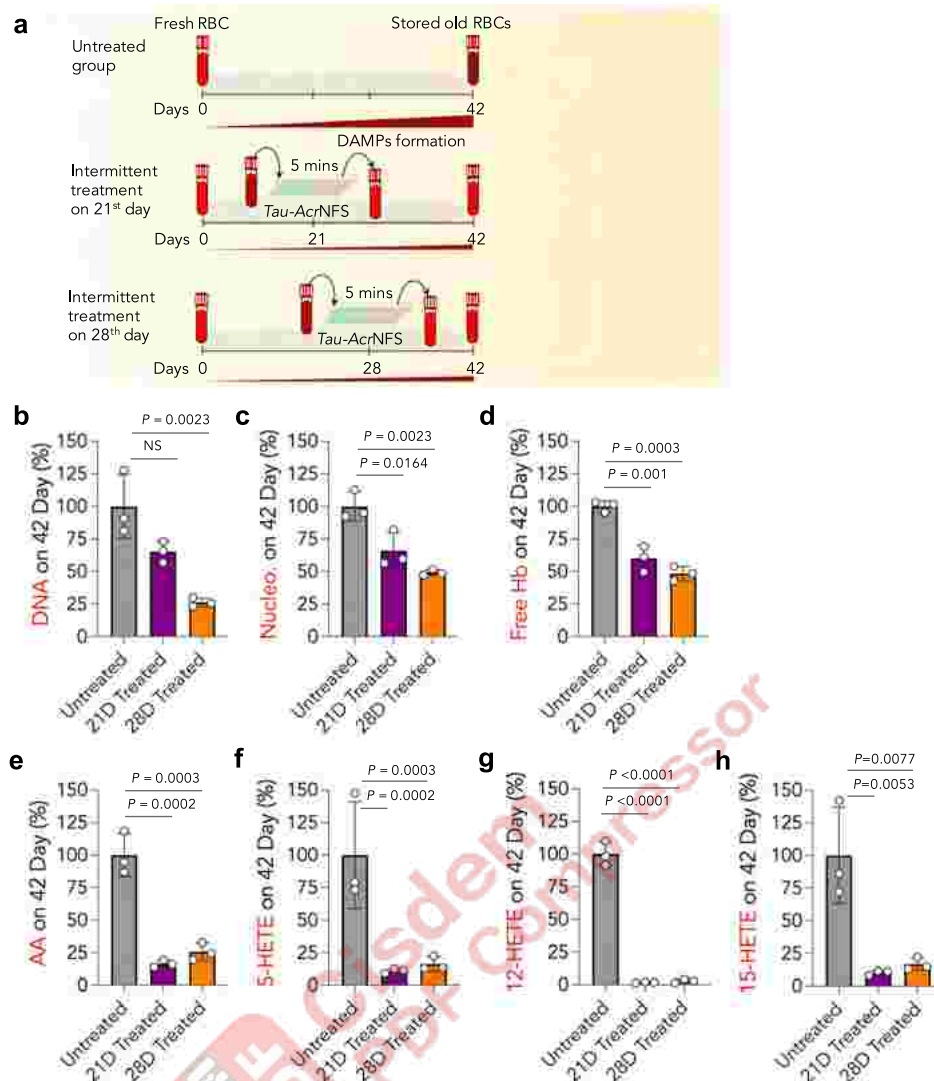


Fig. 3 | Intermittent scavenging of DAMPs using *Tau-AcrNFS* from stored RBCs can reduce the accumulation of DAMPs at 42 days of stored human RBCs.

a Schematic of DAMPs production in untreated and *Tau-AcrNFS* treated stored RBCs. In the untreated group, RBCs were stored at 4 °C for 42 days, in treated groups, RBCs were incubated with *Tau-AcrNFS* for 5 min on either the 21st or 28th day, and stored at 4 °C for 42 days, and DAMPs were quantified on 42nd day for all

groups (**b–h**). Intermittent treatment of stored RBCs with *Tau-AcrNFS* on either the 21st or 28th day significantly reduced the accumulation of DNA (**b**), nucleosomes (**c**), Hb (**d**), and PUFAs (**e–h**) on the 42nd day. Data are mean \pm s.d. ($n = 3$, from independent experiments); P values were determined by ordinary one-way ANOVA with Tukey's post hoc analysis using GraphPad PRISM 9, and exact P values are indicated. Source data are provided as a Source Data file.

surface, which could be due to the accumulation of sequestered proteins and lipids on the nanofibrous sheets.

Intermittent scavenging of DAMPs by *Tau-AcrNFS* significantly enhances the quality of stored old RBCs

The data in Fig. 2a–f suggest that DAMPs formation is minimal until 28 days of storage; subsequently, an exponential production of DAMPs occurs. It is reasoned that the accumulated DAMPs, until 28 days, might have a synergistic effect on accelerating the deterioration of stored human RBCs; hence, large quantities of DAMPs are produced within 42 days. Therefore, we envisaged that intermittent removal of DAMPs either on the 21st or 28th-day using *Tau-AcrNFS* would reduce further damage to RBCs and enhance the quality of 42 days-stored RBCs. To test this hypothesis, either on the 21st or 28th day, stored RBCs were incubated with *Tau-AcrNFS* for 5 min (Fig. 3a), stored back at 4 °C, and measured the DAMPs on the 42nd day. The data in Fig. 3b–h suggest that intermittent removal of DAMPs either on the 21st or 28th day significantly reduces the number of DAMPs present on the 42nd day. Furthermore, intermittent treatment either on the 21st or 28th day has

remarkably reduced the formation of cell-free DNA, nucleosomes, cell-free Hb, and PUFAs by 75, 50, 50, and 75–98%, respectively, compared to 42 days of stored untreated RBCs (Fig. 3b–h).

RBCs' shape and membrane rigidity play critical roles in their quality, function, and fate, such as gas transport capacity and RBC clearance from circulation^{26,27}. RBCs should stretch/elongate and undergo deformation to pass through capillaries. Hence to retain function, they should be mechanically stable and withstand extensive passive deformation²⁸. DAMPs are known to have a deleterious effect on RBCs' quality. The morphology of RBCs progressively deteriorates throughout hypothermic storage. While discocytes are considered healthy RBCs, upon storage, they progressively convert into spherocytes and echinocytes due to loss of the membrane and reduced surface area (Fig. 4a). Storage-aged RBCs have fewer discocytes and more spherocytes. Therefore, we investigated whether intermittent DAMPs scavenging either on the 21st or 28th day by *Tau-AcrNFS* can prevent/reduce the transformation of discocytes into spherocytes. Fresh RBCs and storage-aged RBCs (42nd day) were imaged through a field-emission scanning electron microscope

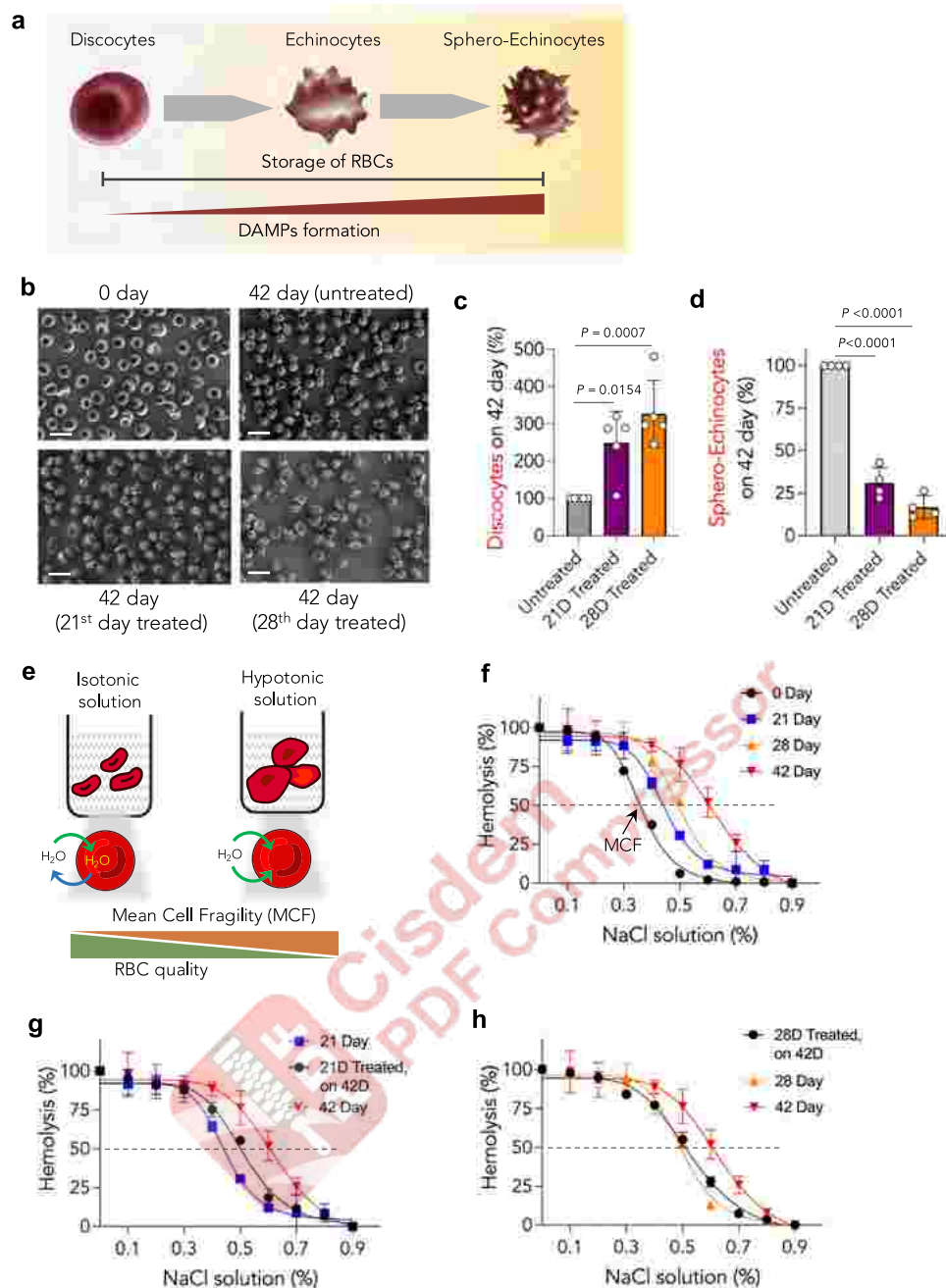


Fig. 4 | Intermittent scavenging of DAMPs using *Tau-AcrNFS* prevents structural and morphological damage to stored human RBCs. **a** Schematic of storage-induced structural transformation of healthy discocytes into non-healthy echinocytes and spherocytes. **b** SEM images of freshly collected RBCs (0th day), and storage-aged RBCs on the 42nd day. RBCs were stored for 42 days either without treatment or intermittently treated with *Tau-AcrNFS* either on the 21st or 28th day (**b**). Scale bar = 10 μ m. The relative number of discocytes present on the 42nd day (**c**) revealed that intermittent scavenging of DAMPs using *Tau-AcrNFS* has increased by 250% and 350% for the 21st and 28th day treated RBCs, respectively ($n = 5$, from independent experiments). The relative number of spherocytes present on the 42nd day (**d**) revealed that intermittent scavenging of DAMPs using *Tau-AcrNFS* has decreased their number to 30% and 15% for the 21st and 28th day treated RBCs, respectively ($n = 4$, from independent experiments). The number was calculated from

10,000 RBCs in each sample. **e–h** Osmotic fragility test revealed that intermittent treatment had enhanced membrane integrity of stored RBCs. Schematic of osmotic fragility test to measure the mean cell fragility (MCF) by placing RBCs in a hypotonic solution, where RBC swells and undergoes hemolysis (**e**). The lower MCF values are equivalent to higher membrane integrity. MCF values of stored RBCs progressively increased as a function of storage time (**f**), suggesting that loss of membrane integrity of RBCs during the storage. MCF values of 42 days of stored RBCs that were intermittently treated were lower than untreated stored old RBCs (**f, g**), suggesting that intermittent removal of DAMPs reduced the damage of RBCs and enhanced the membrane integrity of stored old RBCs ($n = 3$, from independent experiments). Data in **c, d, f–h** are mean \pm s.d., P values in data **c** and **d** were determined by ordinary one-way ANOVA with Tukey's post hoc analysis using GraphPad PRISM 9, and exact P values are indicated. Source data are provided as a Source Data file.

and estimated the number of discocytes and spherocytes. The images revealed that most RBCs were transformed into either spherocytes or spherocytes, while healthy discocytes reduced significantly (Fig. 4b).

The number of discocytes present in untreated 42 days of stored RBCs sample was considered 100% (counted from 10,000 cells, Fig. 4c). Similarly, the number of discocytes and spherocytes were counted in 42 days of stored RBCs samples that were untreated

and intermittently treated with *Tau-AcrNFS* on either the 21st or 28th day (Fig. 4b–d). The intermittent treatment has increased total discocytes on the 42nd day by 250 and 350%, respectively (Fig. 4c). On the contrary, compared to untreated samples, intermittent treatment on the 21st or 28th day has decreased the total number of spherocytocytes on the 42nd day to 30 and 15%, respectively (Fig. 4d). These results suggest that intermittent removal of DAMPs using *Tau-AcrNFS* reduces the conversion of healthy discocytes into spherocytocytes, hence, improves the quality of stored RBCs.

Furthermore, we have conducted the osmotic fragility test to characterize RBC membrane integrity by subjecting stored RBCs to a hypotonic solution (Fig. 4e). Mean cell fragility (MCF) is the concentration of NaCl at which 50% hemolysis occurs. The quality of the RBC membrane is inversely proportionate to the MCF value. We have observed 0 and 100% hemolysis in 0.9% (isotonic) and 0.1% (hypotonic) NaCl solutions, respectively. The MCF values for 0, 21, 28, and 42 days of stored RBCs were 0.36, 0.45, 0.5, and 0.64% NaCl, respectively (Fig. 4f), suggesting that the membrane integrity of RBCs progressively deteriorates upon storage. Interestingly, MCF values for 42-day RBCs, which were intermittently treated with *Tau-AcrNFS* either on the 21st or 28th day, were 0.5 and 0.51%, respectively (Fig. 4g, h), suggesting that intermittent removal of DAMPs slows down the deterioration of RBC membrane quality.

Transfusion quality of *Tau-AcrNFS* treated stored old RBCs is comparable to freshly collected RBCs

Post RBCs transfusion, measuring the duration of transfused RBCs remaining in circulation (in vivo recovery) is a gold standard for quantifying the quality of stored RBCs²⁹. A higher % of RBCs stay longer in circulation, which signifies the better quality of transfused RBCs. According to the FDA guidelines, transfusion of stored human RBCs is considered as successful when $\geq 75\%$ of transfused human RBCs survive in circulation after 24 h²⁹. Hence, similar standards were adopted to quantify the efficiency of the transfusion of stored mouse RBCs into mice³⁰. Therefore, as a proof-of-concept, we measured the transfusion efficiency of *Tau-AcrNFS* treated stored mouse RBCs into mice, in vivo.

The shelf life of C57BL/6J mice RBCs is reported to be 14 days, equivalent to 42 days stored human RBCs³¹. First, we demonstrated that stored mouse RBCs generate DAMPs, such as cell-free Hb and cell-free nucleosomes, as a function of storage time (Fig. 5a, b). Subsequently, intermittent scavenging of DAMPs from stored mouse RBCs on the 5th and 10th days using *Tau-AcrNFS* reduced the production of DAMPs on the maximum allowed storage time, i.e., 14 days (Fig. 5c, d). To optimize intermittent treatment for RBC recovery experiments, mouse RBCs were intermittently treated with *Tau-AcrNFS* either once (on the 5th day or 10th day) or twice (on the 5th and 10th days), and DAMPs were measured on the 14th day (Supplementary Fig. 4). Data in Supplementary Fig. 4 suggest that total DAMPs on 14th day were significantly lower in samples that were treated twice (5th and 10th days), compared to samples treated once on either 5th or 10th day. Therefore, for RBC recovery experiments, stored mouse RBCs were intermittently treated on the 5th and 10th days. Cumulatively, these results suggest that intermittent scavenging of DAMPs might prevent progressive damage to RBCs and enhance transfusion efficiency.

In RBCs transfusion experiments, we labeled RBCs with biotin, in vivo. Intravenous administration of sulfo-NHS-biotin covalently binds and labels RBC membrane proteins with biotin³². After 48 h of post-administration of sulfo-NHS-biotin (1 mg/mouse), blood was collected from the same mouse. The biotinylated RBCs were transfused into a different mouse to study transfusion efficiency (Fig. 5e). Blood was collected at 1, 24, 48, and 72 h post-transfusion of biotin-labeled RBCs. The collected RBCs were complexed with Streptavidin APC-eFluor™ and quantified by flow cytometry to measure the % of labeled transfused RBCs that remain in circulation. Interestingly, ~95% of transfused fresh RBCs have remained in circulation for 72 h (Fig. 5f,

Supplementary Fig. 5), suggesting that freshly collected RBCs have the highest quality. To test the effect of storage, the biotin-labeled mouse RBCs were stored for 14 days, either without treating or intermittently treating with *Tau-AcrNFS* on the 5th and 10th days (Fig. 5e). After 14 days, biotinylated RBCs were transfused into mice, and tracked their circulation time. A total of 90% of untreated transfused RBCs were in circulation for 24 h, which was reduced to <40% at 48 h (Fig. 5g, Supplementary Fig. 6), suggesting that the quality of stored old RBCs deteriorated significantly. On the contrary, *Tau-AcrNFS* treated stored old RBCs remain >90% in circulation even at 72 h, similar to fresh RBCs (Fig. 5h, Supplementary Fig. 7), suggesting that intermittent treatment slows down stored RBC aging, and prevents their clearance from circulation by the spleen. Remarkably, these findings indicate that intermittent scavenging of DAMPs reduced the deterioration of stored RBCs, and the quality of 14 days-stored old RBCs is equivalent to freshly collected RBCs.

Intermittent scavenging of storage lesion with *Tau-AcrNFS* enhances the shelf-life of stored old RBCs

In situ-generated DAMPs deteriorate RBC quality during storage, limiting their maximum shelf-life to 42 and 14 days for human and mouse RBCs, respectively. Intermittent removal of DAMPs by *Tau-AcrNFS* treatment enhanced the quality of RBCs; therefore, we envisaged that enhanced quality of RBCs may increase the shelf-life of stored old RBCs.

Initially, the phospholipid architecture of RBCs was studied to understand their shelf-life. Storage-associated loss of phospholipid asymmetry results in phosphatidylserine (PS) exposure in the outer leaflet of the RBC membrane^{33–35}. PS exposure serves as an ‘eat-me’ signal to phagocytes to clear the RBCs from circulation^{33,36} (Fig. 6a). PS exposure increases with storage and is linked with DAMPs production³⁷, hence, the low survivability of stored RBCs in circulation. Therefore, the number of RBCs expressing PS on the outer leaflet of their membrane was determined as described elsewhere³⁸. In untreated stored RBCs, we found that 4, 20, and 40% of PS-exposed RBCs were present in 5, 14, and 17 days of stored mouse RBCs, respectively (Fig. 6b and Supplementary Fig. 8). On the contrary, intermittent scavenging of DAMPs by *Tau-AcrNFS* has significantly reduced PS-exposed RBCs on days 14 and 17 (Fig. 6c and Supplementary Fig. 9). Hence, the overall quality of RBCs is higher in the intermittently treated samples even on the 17th day, which is three days longer than the maximum allowed 14 days.

Furthermore, we have conducted RBC recovery experiments using long-term stored mouse RBCs. As described in the previous section, biotinylated murine RBCs were stored for up to 18 days either without treating or intermittently treated with *Tau-AcrNFS* on the 5th and 10th days. The different days of stored biotinylated RBCs (15–18 days) were transfused into mice, and measured the percentage of transfused RBCs in circulation (Fig. 6d–g and Supplementary Figs. 10–16). As expected, when DAMPs were not scavenged, 15–17 days-stored RBCs could not remain longer in circulation, and the number of transfused RBCs reduced to <30% within 24 h, which is well below the accepted 75% range. On the contrary, 15–17 days-stored RBCs when they were intermittently treated with *Tau-AcrNFS*, post-transfusion, >95% of transfused RBCs remained in circulation after 24 h (Fig. 6d–f). However, whether treated or not, 18 days-stored RBCs could not remain in circulation for 24 h (Fig. 6g), suggesting that the upper limit for storing the intermittently treated RBCs is 17 days. Therefore, the maximum shelf life of murine RBCs was increased from 14 days to 17 days.

Post-blood transfusions, DAMPs are known to cause systemic immunomodulation. Hence, we tested the efficacy of *Tau-AcrNFS* treatment to prevent transfusion-induced immunomodulation. To test that, we have transfused fresh RBCs (0 day), untreated and intermittently treated 17 days-stored RBCs in C57BL/6J mice (8–12 weeks).

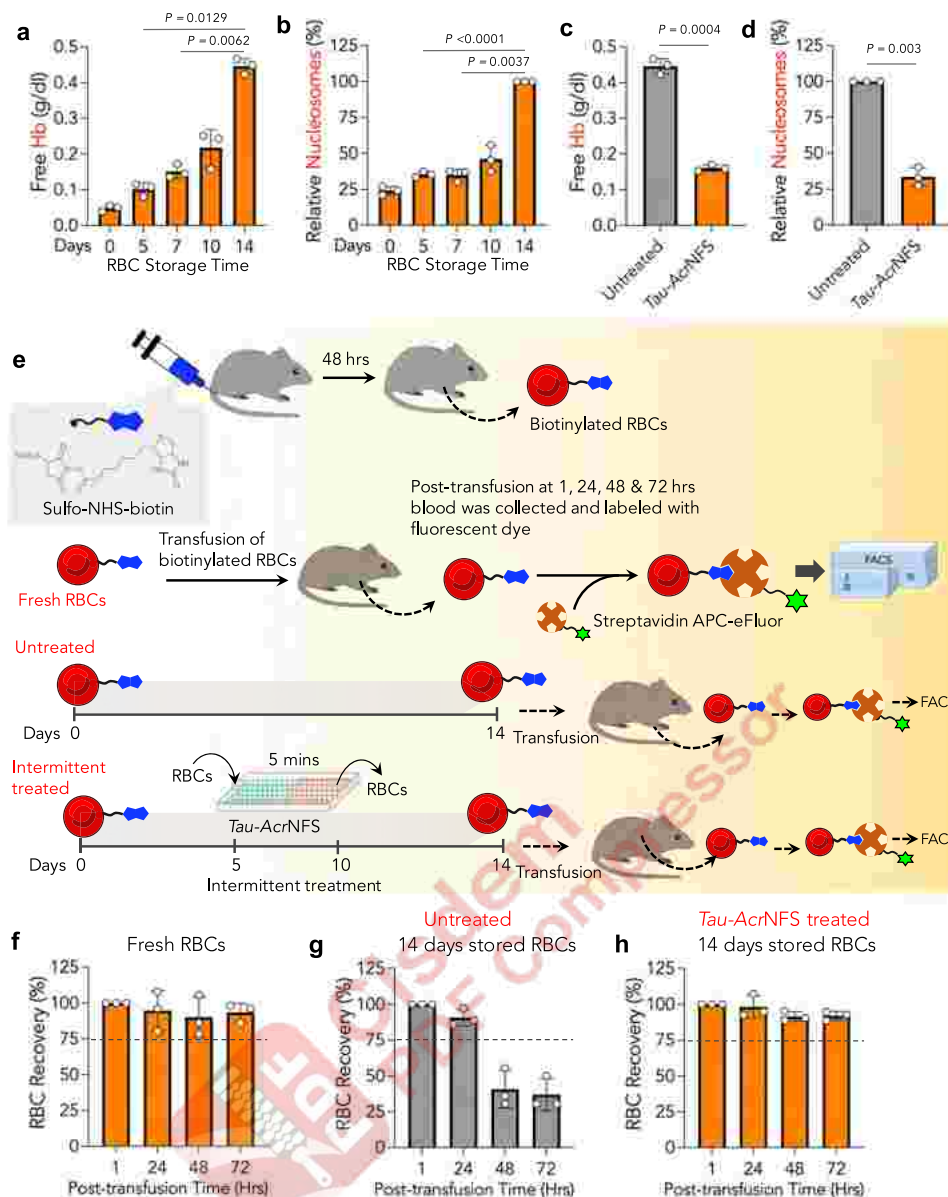
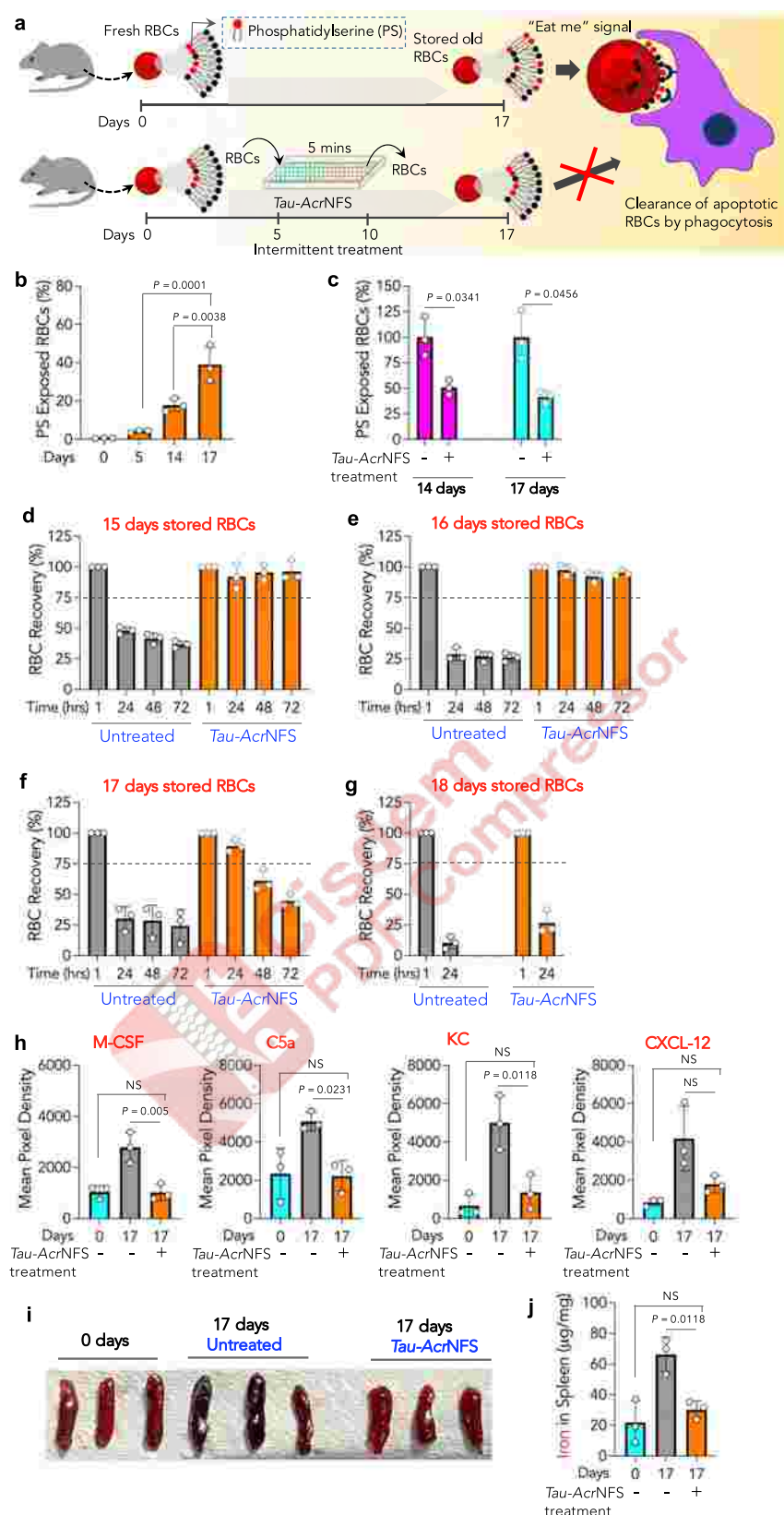


Fig. 5 | Mice RBCs generate DAMPs during their storage, and intermittent treatment with *Tau-AcrNFS* enhanced the quality of stored old RBCs equivalent to fresh RBCs in vivo. **a, b** Stored mice RBCs produced DAMPs such as free hemoglobin and nucleosomes. **c, d** The relative concentration of DAMPs before and after *Tau-AcrNFS* treatment has significantly reduced accumulated Hb (**c**), and nucleosomes (**d**). **e–h** Biotinylation of RBCs, and post-transfusion recovery of RBCs, in vivo. Schematic of RBC recovery experiments, in vivo (**e**). After 48 h of intravenous administration of Sulfo-NHS-biotin (1 mg/mouse) in C57BL/6j mice (8–12 weeks), biotin-labeled RBCs containing blood were collected. In the fresh RBCs recovery group, freshly collected biotinylated RBCs were transfused into C57BL/6j mice (8–12 weeks) and collected the blood post-transfusion times 1, 24, 48, and 72 h. The collected RBCs were labeled with Streptavidin APC-eFluor™ and quantified via flow cytometry to measure the % of labeled transfused RBCs that remain in circulation. The number of labeled RBCs present in circulation has been

quantified (**f**). Similarly, 14 days-stored biotinylated RBCs, either untreated or intermittently treated with *Tau-AcrNFS*, were transfused into mice, collected blood at post-transfusion 1, 24, 48, and 72 h, and labeled with Streptavidin APC-eFluor™, and quantified via flow cytometry (**g** and **h**, $n = 3$, from independent experiments). In untreated stored RBCs, ~90% of RBCs were in circulation for 24 h but rapidly cleared thereafter (**g**). On the contrary, post-transfusion of intermittently treated RBCs, >90% of transfused-RBCs were found in circulation even at 72 hrs (**h**), suggesting that intermittent treatment has increased the quality of stored old RBCs equivalent to fresh RBCs. Data in **a–d**, and **f–h** are mean \pm s.d. ($n = 3$, from independent experiments). For **a, b**, P values were determined by Repeated Measures one-way ANOVA, and for (**c, d**), by Student's t -test with Welch's correction using GraphPad PRISM 9, and exact P values are indicated. Source data are provided as a Source Data file.

Two hours post-transfusion, blood was collected, and cytokines/chemokines in plasma were quantified using Mouse Cytokine Array Panel A (Methods, Fig. 6h, Supplementary Fig. 17). Transfusion of untreated 17 days-stored RBCs has elevated expression of stromal cell-derived factor1 (CXCL12), macrophage-colony-stimulating factor (M-CSF), complement component 5A(C5A), and keratinocyte-derived chemokine/CXCL1 (KC/CXCL1). Transfusion of untreated 17 days-stored RBCs has led to 2–3 fold higher cytokine production levels than either fresh

RBCs or intermittently treated 17-days-stored RBCs (Fig. 6h). Additionally, mice spleens were collected 2 h post-transfusion, and spleens were significantly darkened when transfused with untreated RBCs compared to treated RBCs (Fig. 6i). The darkening of the spleen is associated with iron deposition after transfusing poor quality RBCs, loaded with free Hb, which corroborated by Fe^{2+} quantification using ICP spectroscopy (Fig. 6j). These results suggest that intermittent scavenging of DAMPs using *Tau-AcrNFS* enhanced the quality of stored



old RBCs equivalent to fresh RBCs and significantly enhanced their shelf-life.

Discussion

Transfusion of RBCs is a lifesaving practice, which is limited by the progressive deterioration of stored RBCs as a function of time. In situ

generated DAMPs such as cell-free DNA, cell-free nucleosomes, free Hb, free iron, and polyunsaturated fatty acids are the primary cause of declining RBCs condition. Large observational studies have reported a mean duration of RBC storage of between 16 and 21 days, with a maximum storage duration before transfusion is limited to 42 days with standard preservative solutions³⁹. Until now, existing strategies are

Fig. 6 | Intermittent scavenging of DAMPs using *Tau-AcrNFS* enhances the shelf-life of stored old RBCs and prevents systemic inflammation in vivo.

a–c During the storage, exposure of phosphatidylserine (PS) on the outer leaflet of the RBC membrane serves as an ‘eat-me’ signal, thus, RBCs will be eliminated from circulation by phagocytes. Intermittent scavenging of DAMPs by *Tau-AcrNFS* reduces PS exposure, therefore, keeping RBCs in circulation for longer periods (**a**). Time-dependent PS exposure on mice RBCs (**b**), intermittent treatment reduced PS exposure on RBCs (**c**). **d–g** Recovery of storage-aged RBCs either untreated or intermittently treated with *Tau-AcrNFS* on the 5th & 10th days. The maximum allowed storage time for mice blood is 14 days. Recovery data suggests that the quality of untreated RBCs that are stored for 15–17 days declines drastically, and RBCs are eliminated from circulation immediately after transfusion. Only 15–20% of transfused RBCs were found in circulation after 24 h (**d–f**), which is well below the accepted 75%. On the contrary, intermittently treated RBCs, even after storing for

17 days, >95% of transfused RBCs were found in circulation at 24 hrs (**d, e, and f**), suggesting that intermittent removal of DAMPs has decreased RBC damage, and enhanced the shelf-life of RBCs at least by 22%. However, irrespective of whether intermittent treatment or not, 18 days-stored RBCs were eliminated from circulation, with only 25% of RBCs found after 24 h (**g**), suggesting the upper limit of intermittent treatment. **h–j**, Fresh RBCs, or 17 days-stored RBCs, either untreated or intermittently treated, were transfused into C57BL/6J mice (8–12 weeks). Two hours of post-transfusion, serum inflammatory cytokines were quantified (**h**), spleens were collected and imaged (**i**), and iron in the spleens was quantified using ICP-AES (**j**). Data are mean \pm s.d. ($n=3$, from independent experiments). For **b, h, j**, P values were determined by ordinary one-way ANOVA with Tukey's post hoc analysis and for (**c**), by two-tailed Student's t -test with Welch's correction using GraphPad PRISM 9, and exact P values are indicated. NS = not significant. Source data are provided as a Source Data file.

limited to developing preservatives and rejuvenating solutions. Additionally, engineered-proteins-containing filters have been developed to absorb pathogen-specific toxins^{40,41}. However, there was no effort made to scavenge DAMPs during RBC storage to prevent RBC damage. Interestingly, these DAMPs carry either cationic or anionic charges⁴². Therefore, we have designed polymers with an appropriate hydrophilicity/hydrophobicity balance, and carrying anionic (due to taurine) or cationic (due to acridine) charges. Robust electrospun nanofibrous sheets (*Tau-AcrNFS*) were generated using these polymers. The charged *Tau-AcrNFS* do not cause hemolysis, and upon incubation, RBCs or any other cells do not adhere to these sheets, suggesting that *Tau-AcrNFS* are robust and consist of key parameters that play a critical role in translating this technology into a medical device.

Interestingly, scavenging DAMPs using *Tau-AcrNFS* has a dual advantage. When *Tau-AcrNFS* treatment is used terminally at the end of the storage, they efficiently scavenge in situ generated DAMPs from stored blood. On the other hand, intermittent treatment of stored blood using *Tau-AcrNFS* can prevent the damage of RBCs, hence, significantly lowering the production of DAMPs until their maximum storage time. We have identified a suitable storage day for intermittent treatment through systematic time-dependent experiments. We found that 28th-day treatment results in a maximum reduction of DAMPs and retains healthier RBCs on the 42nd day. This observation could be because the accelerated deterioration of RBCs majorly occurs between the 28th day and to 42nd day of storage.

The structural integrity of RBCs plays a vital role in increasing their post-transfusion circulation time. The osmotic fragility measurements revealed that compared to untreated RBCs, removal of DAMPs on the 28th day using *Tau-AcrNFS* enhanced 42 days stored human RBC's membrane integrity and reduced PS-exposure on the outer leaflet of the membrane to reduce ‘eat-me’ signals. It was envisaged that maintaining membrane integrity should lead to extended survival in circulation. Post-transfusion recovery of murine RBCs affirmed this hypothesis. Murine RBCs can be stored a maximum of 14 days, akin to 42 days for human RBCs. Remarkably, mouse RBCs recovery suggested that intermittent removal of DAMPs enhanced the quality of 14 days-stored old RBCs equivalents to freshly collected RBCs. In addition to improving the quality, intermittent removal of DAMPs has increased the shelf-life by at least 22%. Systemic immunomodulation is one of the hallmarks of the transfusion of stored old RBCs. As we demonstrated here, intermittent removal of DAMPs has lessened the accumulation of DAMPs in stored old RBCs and ultimately reduced immunomodulation. Therefore, it is anticipated that this approach would reduce transfusion-related complications. We are designing a *Tau-AcrNFS*-based insert in blood bags as a medical device, which will be feasible to use in the blood bank processing setting without the need for multiple interventions during the storage of RBCs.

In summary, our study implicates in situ generated DAMPs in causing accelerated deterioration of RBCs. We establish a novel

approach to slow down the damage of stored RBCs through intermittent scavenging of the storage lesion. In the future, treating with the nanofibrous sheets before the transfusion could significantly reduce DAMPs and prevent transfusion-related complexities. Furthermore, the intermittent treatment adds a new dimension to maintaining RBC quality. Finally, our investigation establishes the concept of scavenging DAMPs during storage, leading to increased quality and shelf-life of RBCs. Furthermore, the use of charged electrospun nanofibrous sheets may lead to the development of novel blood bags or an insert-based medical device. Therefore, it may significantly impact healthcare by improving the RBC transfusion quality.

Methods

Ethics

Our research involved in preclinical study and human volunteers for blood collection complies with all relevant ethical guidelines. Human blood was collected according to the approved protocols from the Institutional Human Ethical Committee (inStem/IEC-10/003) of the Institute for Stem Cell Science and Regenerative Medicine (inStem). Informed consent has been obtained from the participants. Blood donors are both male ($N=3$, age 26–30 years) and female ($N=3$, age 25–28 years). All mouse studies strictly adhered to institutional and national guidelines for humane animal use. The experimental protocols were approved by the Institutional Animal Ethics Committee (IAEC) at the Institute for Stem Cell Science and Regenerative Medicine (INS-IAE-2020/16(R1)).

Materials

Poly (methoxy vinyl ether-alt-maleic anhydride) average Mw-330,000 (PMVEMA), was used in all synthesis procedures. Tetrahydrofuran (THF), tetradecylamine, taurine, sodium bicarbonate, ethyl acetate, 3,6-bis(dimethylamino) acridine hemi (zinc chloride) salt, benzene, methanol, and ammonium hydroxide, N,N -dimethyl ethylene diamine, 1,6-dibromohexane, sodium sulfate, toluene, dimethylformamide (DMF), triton X-100, chamber slides (HI Media), blood collection tubes (BD Vacutainer), citric acid monohydrate, trisodium citrate dihydrate, sodium dihydrogen phosphate, dextrose, sodium chloride, glucose anhydrous, mannitol, adenine, APTMS (3-(Aminopropyl)trimethoxysilane), glutaraldehyde, cacodylate buffer, osmium tetroxide, hexamethyldisilazane, ethanol, double distilled water and deionized water were used. Unless mentioned otherwise, all chemicals were procured from Sigma-Aldrich.

Synthesis of anionic and cationic scaffolds

A detailed scheme for the synthesis is described in Supplementary materials.

PMVEMA -C₁₄. The PMVEMA (500 mg, 3.2 mmol) was added to tetrahydrofuran (THF) (10 ml) in a pressure tube and stirred at 80 °C until dissolution. Subsequently, tetradecylamine (345 mg, 1.6 mmol) in THF

(10 ml) was added to the previous mixture. The reaction mixture was heated at 80 °C for 3 h. The solvent was finally removed using a rotavapor to get the polymer in dry powder form (800 mg, ~90% yield). ¹H-NMR (CD₃OD, 600 MHz), δ: 3.0–3.51 (Br, 9H, -OCH₃, -O-CH, PMVEMA and -NH-CH₂ alkyl protons), 1.47 (Br, 2H, alkyl protons), 1.22 (Br, 22H, alkyl protons), 0.845 (t, 3H, alkyl protons). As per NMR data, ~50% of PMVEMA polymer was substituted with tetradecyl amine. FTIR (cm⁻¹): 3354, 2926, 1858, 1782, 1733, 1697

Poly-Taurine: PMVEMA-C₁₄-Tau. A solution of taurine (100 mg, 0.8 mmol) and sodium bicarbonate was prepared (84 mg, 1.0 mmol) in deionized water (1 ml). This solution was added dropwise to the solution of PMVEMA-C₁₄(50%) (800 mg) in THF (20 ml) and left for stirring at 80 °C for 16 h. The reaction mixture was subjected to rotavapour to concentrate. Subsequently, it was sequentially triturated with ethylacetate and deionized water to remove the residual tetradecylamine & taurine. The final polymer was obtained in a gel form, which was lyophilized to a white powder (720 mg, ~75% yield). ¹H-NMR (CD₃OD, 800 MHz), δ: 3.9–4.1 (Br, 1H, taurine), 2.7–3.5 (Br, 5H, -OCH₃, -O-CH, PMVEMA and -NH-CH₂ alkyl protons), 1.95 (Br, 2H, PMVEMA protons), 1.4 (Br, 1H, alkyl protons), 1.1–1.2 (Br, 11.5H, alkyl protons), 0.8 (t, 1.5H, alkyl protons). As per the NMR data, PMVEMA was approximately substituted by 50% of C₁₄H₂₉NH₂ and ~25% of taurine. FTIR (cm⁻¹): 3209, 3046, 2946, 1722, 1616, 1037.

Acridine hexyl bromide. 3,6-bis(dimethylamino) acridine hemi (zinc chloride) salt (10 g, 27.02 mmol) was dissolved in methanol (50 ml), and excess ammonium hydroxide (50 ml) was added. Acridine orange (AO) base was extracted from benzene and dried over sodium sulfate; the AO base (5 g) was recovered from benzene using rotavapor. The AO base (2.65 g, 10 mmol) was dissolved in anhydrous toluene (100 ml), and 1,6-dibromohexane (7.7 ml, 50 mmol) was added to the solution and refluxed at 120 °C overnight. The bright red precipitate in the reaction mixture was filtered and dried (yield- 2.1 g, 41.2%). ¹H-NMR (CDCl₃, 600 MHz) δ: 8.7 (s, 1H), 7.9 (d, 2H), 7.08 (m, 2H), 6.75 (s, 2H), 5.0 (t, 2H), 3.4 (t, 2H), 3.3 (s, 12H), 2.048 (m, 2H), 2.029 (m, 2H), 1.96 (m, 2H), 1.94 (m, 2H).

Poly-Acridine

PMVEMA-C₁₄-Acr. The solution of *N,N*-dimethyl ethylene diamine (87 μl, 0.8 mmol) in THF (10 ml) was added dropwise to the solution of PMVEMA-C₁₄(50%) (800 mg) in THF (20 ml) in a pressure tube. The mixture was allowed to stir at 80 °C for 12 h. After its dissolution, THF in the reaction mixture was reduced until a viscous solution appeared using rotavapour. Dry DMF (10 ml) was added to this viscous solution, followed by the addition of Acridine-hexyl bromide (243 mg, 0.48 mmol) in DMF (5 ml). The resulting mixture was stirred at 50 °C for 16 h. The polymer was triturated thoroughly with deionized water to remove unreacted Acr-Hexyl-Bromide and DMF. Further, the polymer was lyophilized to an orange powder (800 mg, ~80%) ¹H-NMR (CDCl₃, 800 MHz), δ: 6.5–8.6 (Br, 0.77H, acridine protons), 3.0–3.5 (Br, 4H, PMVEMA protons), 0.98–1.7 (Br, 9.5H, alkyl protons), 0.87 (Br, 3H, alkyl protons). As per the NMR data, approximately 50% of tetradecylamine (C₁₄H₂₉NH₂) and ~11% of acridine hexyl bromide were substituted on PMVEMA polymer.

Fabrication of electrospun nanofibrous sheets

The electrospinning solutions were prepared by dissolving *poly*-Taurine (20%, w/v) and *poly*-Acridine (15%, w/v) in dry DMF at room temperature (RT). These solutions were stirred overnight before electrospinning. During the electrospun procedure using the Espin device (ES2, Espin nanotech, India), a 2-mL plastic syringe (Dispo Van, India), and a blunt 22 G needle (Dispo Van, India) were used. The solutions were pumped via a syringe pump at a constant flow rate of 0.5 ml/h (*poly*-Taurine) and 0.3 ml/h (*poly*-Acridine). The electrospun

nanofibrous sheets (*Tau*-NFS and *Acr*-NFS) were collected on an aluminum foil placed 15 cm away from the needle (where 15 kV voltage was applied). All experiments were carried out at 25 °C and less than 55% relative humidity (RH). The electrospun mats with a length and width of approximately 10 cm × 10 cm were stored in a desiccator until further use.

Field emission scanning electron microscopy

The morphology of the *Tau*-NFS and *Acr*-NFS was investigated by FESEM (Carl Zeiss MERLIN VP compact). Dried electrospun mats were mounted on aluminum stubs and sputter-coated with gold (Pelco® SC-7 Auto sputter coater). The gold-coated mats were imaged at a voltage of 2 kV. The scaffolds treated with pRBCs were imaged to investigate the adherence of blood cells.

Contact angle measurement

The wettability of *Tau*-NFS and *Acr*-NFS was studied using the sessile drop method. The scaffolds were cut uniformly and placed on a glass slide before the measurement. Water droplets (5 μL) ~2 mm in diameter were dropped on the electrospun NFS, and the images were acquired. The images were processed using ImageJ software (V1.53).

Hemolysis assay

A hemolysis assay was performed to evaluate the hemolytic nature of *Tau*-*Acr*-NFS. The blood was collected in a tube containing anticoagulant sodium citrate. The collected blood was centrifuged (500 G, 10 min), and the supernatant was discarded. These washed RBCs were used to prepare 2% hematocrit in saline and added to *Tau*-*Acr*-NFS fixed in a chamber slide (16 cm²) prewashed with double distilled water. The RBCs were further resuspended in saline and pelleted down. This setup was kept on an incubator shaker (37 °C and 100 rpm) for 1 hour. After 1 hour, the hematocrit was transferred into a 2 ml centrifuge tube and centrifuged at 500 G for 10 min at RT. A 100% lysis sample of the untreated RBC specimen was prepared with 0.1% Triton-X100 in 2% hematocrit. The concentration of Hb in a 100% lysed RBCs sample was determined by cyanmethemoglobin (Drabkin's) method, which is considered as 100%. Afterward, a series of dilutions was prepared from lysed sample to generate a standard curve. The level of hemolysis of the *Tau*-*Acr*-NFS-treated RBCs is then derived from the standard curve using Drabkin's method. For Drabkin's method, the absorbance was recorded at 540 nm using Varioskan LUX Multimode Microplate Reader (ThermoFisher, Massachusetts, USA).

Polymer leaching test

Acr-NFS (8 cm²) was fixed on the chamber slide and incubated in Optisol (AS-5) solution [composition: sodium chloride (8.77 mg/mL), glucose anhydrous (8.18 mg/mL), mannitol (0.01% w/v) and adenine (0.03 mg/mL)]. The sheets were incubated for 2 h. The optisol solution was removed after both incubations and lyophilized to recover the leached *poly*-Acridine from the sheets. The lyophilized *poly*-Acridine was dissolved in DMF and estimated using a fluoro spectrophotometer (Horiba Fluoro log QM, France). Fluorescence intensities were recorded as a function of time with excitation at 502 nm and emission at 535 nm. The Leaching (%) was determined via a pure *poly*-Acridine polymer standard curve prepared at the excitation and emission wavelengths mentioned above.

Packing of human RBC

Blood was collected according to the approved protocols from the Institutional Human Ethical Committee (inStem/IEC-10/003) of the Institute for Stem Cell Science and Regenerative Medicine (inStem). Informed consent has been obtained from the participants. RBC units were prepared from human whole blood (both male and female, *n* = 3) of different blood groups collected in 20 ml vacutainers containing citrate-phosphate-dextrose with adenine (CPD-A) that contains citric

acid monohydrate (3.577 mg/mL), trisodium citrate dihydrate (29.972 mg/mL), sodium dihydrogen phosphate (2.496 mg/mL) and dextrose (25.5 mg/mL). The whole blood was centrifuged for 20 min at 500g, and the supernatant was removed. The removal of supernatant was followed by the addition of optisol (AS-5, preservative) that contains sodium chloride (8.77 mg/mL), glucose anhydrous (8.18 mg/mL), mannitol (0.01% w/v) and adenine (0.03 mg/mL) to obtain a hematocrit of ~65%, which was transferred into standard PVC bags, and stored at 4 °C in the dark.

Scavenging of DAMPs from stored human RBCs using *Tau*-NFS and *Acr*-NFS, in vitro

On different days of, stored RBCs (0, 14, 21, 28, and 42) were incubated with *Tau*-NFS and *Acr*-NFS individually and in combination for 5 min in total to scavenge DAMPs. In both treatment conditions, the nanofibrous sheets were prewetted with distilled water for 30 min before the addition of RBCs. The scavenging experiments were performed on ice under the aseptic condition. *Tau*-*Acr*NFS was mounted on the chamber slides, and the blood samples were added. It was made sure that the blood should cover the entire surface area and be in contact with nanofibers. The total surface area of the scaffold was kept at 24 cm² for each experiment. Scaffold treatment of RBCs was done at 4 °C for 5 min to keep the cold chain storage.

Quantification of free Hb using Cyanmethemoglobin (Drabkin's) method. Drabkin's reagent lyses RBCs and oxidizes all forms of Hb, except for the minimally present sulphaemoglobin, to the stable HiCN⁴³. The supernatant of the stored RBCs unit (scaffold-treated or untreated) was diluted (1:10) with Drabkin's reagent (Sigma, St. Louis, MO, USA). Human Hb diluted with Drabkin's reagent (1:10) (Sigma Aldrich, USA) was used to prepare the standards (0–40 mg/ml) and the calibration curve. The samples and standards were incubated in the dark at RT for 15 min. Absorbance was recorded at 550 nm using a Varioskan LUX Multimode Microplate Reader (ThermoFisher, Massachusetts, USA). The Hb concentration of each sample was calculated from the human Hb calibration curve.

Quantification of free DNA by PicoGreen assay. RBC supernatants from scaffold-treated and untreated groups were thawed on ice. Supernatants were diluted (1:50) with PicoGreen[®] reagent and Tris-EDTA (TE) buffer (Quant-iT[™] PicoGreen[™] dsDNA Assay Kit, Invitrogen, USA), followed by 5 min incubation in the dark. Free-DNA estimation was performed using a fluoro spectrophotometer (Horiba Fluoro log QM, France)⁴⁴.

Quantification of nucleosomes. Stored RBC supernatant was diluted in PBS (1:5). The Anti-Histone-Biotin-Monoclonal antibody (cloneH11-4) and Anti-DNA-POD-Monoclonal antibody from mouse (clone MCA-33) was used for quantifying nucleosomes by ELISA (Catalog No. I1920685001, Cell Death Detection kit, Roche, Indianapolis, IN), according to manufacturer's instructions.

Osmotic fragility test

The stored RBC units (treated and untreated group) were added to 9 tubes containing saline concentration series ranging from 0% (distilled water) (Tube 1) to 0.9% (Tube 9). The tubes were gently mixed and incubated at room temperature for 30 min. The incubation was followed by centrifugation at 500g for 20 min, and supernatants were collected. The optical density of the supernatant was measured by Varioskan LUX Multimode Microplate Reader (ThermoFisher, Massachusetts, USA) at 540 nm. Hemolysis in each tube was expressed in percentage. The maximum absorbance value of haemolyzed RBCs was taken at 100% in the distilled water. The erythrocytes treated with normal saline were used as a negative control (0% hemolysis).

Primary and secondary fixation of RBCs for SEM

Glass coverslips were sonicated in acetone and cleaned. They were further dipped in 2% APTMS (3-(Aminopropyl)trimethoxysilane), and diluted in acetone to impart a coating of APTMS. RBCs were primarily fixed with 2% glutaraldehyde (GTA), incubated for 30 min in the dark, and washed with PBS. The primary fixed RBCs were incubated on APTMS-coated coverslips for 1 h. After 1 h, the coverslips were rinsed twice with PBS and incubated with 0.1 M cacodylate buffer for 10 min. Secondary fixation was achieved via 1% (w/v) Osmium tetroxide (OsO₄) in 10 min to 16 hours. The secondary fixed coverslips were then rinsed with MilliQ water (10 min), followed by a dehydration step that involves a gradient ethanol wash, ranging from 40 to 100%. The dehydration step is followed by HMDS (Hexamethyldisilazane) drying. Finally, dried samples were mounted on aluminum stubs, sputter-coated with gold, and imaged under FESEM (Carl Zeiss MERLIN VP compact).

Bioactive lipid estimation by LCMS

Chemicals and standards. Eicosanoids; 5(S)-HETE, 12(S)-HETE, 15(S)-HETE, and AA were purchased from Cayman Chemical Co. (Ann Arbor, Michigan, USA). 5(S)-HETE-d8 (Cayman Chemical Co) was used as an internal standard (IS) for this study. Acetonitrile (Baker analyzed[®] LC-MS reagent), water (Baker analyzed[®] LC-MS reagent), formic acid, ethanol, ethyl acetate (EtOAc), and glacial acetic acid were used in sample preparations for LC-MS/MS measurements.

Preparation of stock solutions. 5-(S)-HETE, 12(S)-HETE, 15(S)-HETE, AA, and IS 5(S)-HETE-d8 were constituted in ethanol by the provider. 5, 12 & 15 (S)-HETE was further processed and serially diluted to obtain solutions ranging from 0.05 to 100 ng/ml. AA solutions ranged from 0.5 to 1000 ng/ml. The working concentration of the pure IS was 1000 ng/ml.

Sample preparation. Lipid extraction from stored RBCs supernatant was performed by gently mixing the samples with 0.5 mL of EtOAc containing 0.13% acetic acid (v/v). All samples were spiked with 5 µl of the IS. After 10 min of vigorous shaking (1500 rpm), samples were centrifuged (10,000 rpm, 10 min, 4 °C), and 450 µl of the organic layer was transferred to fresh tubes and evaporated in speed vac (Scan Vac, Labogene, Denmark) at 4 °C. The dry residue was reconstituted in 25 µL of nitrogen-purged EtOH and then directly injected (2 µl) into the LC-MS/MS system.

LC-MS/MS conditions. HPLC analysis was done using a Shimadzu Prominence HPLC system. The instrument was equipped with a communication module (CBM-20A), degassing unit (DGU-20A5R), solvent delivery units (LC-30AD), column oven (CTO-20AC), and an autosampler (SIL-30AC). The temperature of the column oven was maintained at 40 °C while the autosampler was set at 4 °C. The lipids were separated using an Acquity UPLC[®] BEH C18 1.7 µm column (2.1 × 50 mm). The mobile phase comprised solvent A, i.e., water with 0.1% formic acid (FA) and acetonitrile with 0.1% FA as solvent B. The flow rate was maintained at 0.2 ml/min, and the injection volume was 2 µl. The gradient for lipid elution (20.10 min) was set as 50% A and 50% B for one minute. This was followed by a linear gradient to 20% A and 80% B for 8 min to elute 5, 12, and 15 HETE. This was further followed by a linear gradient to 100% B for 2 min and kept for 5 min to elute AA. Finally, the column was equilibrated at 50% A and 50% B for 4 min before the next injection. LC-MS analysis was performed by QTRAP 5500 (Sciex, Framingham, Massachusetts, USA), a triple quadrupole mass spectrometer. LC-MS analysis was performed by MultiQuant[™] 3.0.3 Software (SCIEX). The operating parameters for the mass spectrometer were as follows: declustering potential (DP): −209.8 V, entrance potential (EP): −5.7 V, collision cell exit potential (CXP): −16.9 V, ion spray voltage: −4500 V, source temperature: 500 °C,

curtain gas: 35 psi, ion source gas 1: 40 psi and ion source gas 2: 50 psi. All the spectra of lipids were recorded and quantified in multiple reaction monitoring (MRM) mode. Negative electrospray ionization was employed for all the lipids, and the deuterated IS. The ion Q1/Q3 transitions and other parameters can be seen in Supplementary Table 1.

In vivo experimental design

Mice. Both male and female C57BL/6J mice of age 8–12-weeks-old were used for the experiments. The animals were housed in the animal facility at the National Center for Biological Sciences, Bengaluru. Animals were caged (maximum, four per cage) during the experiment, food and water were provided *ad libitum*. Mice were housed in facility that was subjected to 12/12 h light/dark cycle, at a temperature of 20–25 °C and humidity of 35–65%. All mouse studies strictly adhered to institutional and national guidelines for humane animal use. The experimental protocols were approved by the Institutional Animal Ethics Committee (IAEC) at the Institute for Stem Cell Science and Regenerative Medicine (INS-IAE-2020/16(R1)).

Packaging and storage of mice RBCs and their treatment with Tau-AcrNFS to scavenge DAMPs. Blood collected in CPD was immediately transferred and centrifuged at 500g for 20 min at 4 °C. Plasma was carefully aspirated, and the pRBCs were pooled together. Optisol (AS-5) was added to the pRBCs at 65% hematocrit. Totally 550 µL and 250 µL blood units were finally aliquoted from these pRBCs and stored in sterile Eppendorf tubes (0.6 and 0.3 ml). Mouse pRBCs were treated with *Tau-AcrNFS* (24 cm²) for 5 min on the 5th and 10th day of storage at 40 °C. After the scavenging procedure, the RBCs were again transferred into autoclaved 2 ml Eppendorf tubes, leaving a small residual space, and stored till the 17th day. Its supernatant was taken for extracellular Hb and nucleosome estimation.

Quantification of PS on RBCs by Annexin V (AV). The number of erythrocytes expressing PS on their outer membrane was determined as described elsewhere³⁸. Briefly, labeling with AV was performed by adding 5 µL of AV-Alexa Fluor™ 568 conjugate (Invitrogen, USA) in 10⁶ erythrocytes in 100 µL Annexin binding buffer. The binding buffer was prepared by adding 140 mM and 2.5 mM CaCl₂ in 10 mM HEPES Buffer (all from Sigma-Aldrich). After incubation on ice for 15 min, cells were diluted four times with binding buffer and analyzed on a BD LSR Fortessa cytometer (BD Biosciences). Data was collected with FACSDiva v8.02, and data analysis was performed FlowJo v10.0.8. The erythrocyte population with exposed PS labeled with AV-Alexa Fluor™ 568 conjugate was measured as a percentage of Annexin V-positive RBCs.

Quantification of pro-inflammatory cytokine levels in serum. C57BL/6J mice (8–12 weeks, *n* = 3) were transfused with either fresh RBCs or RBCs stored for 17 days (untreated or intermittently treated with *Tau-AcrNFS*). After 2 h of transfusion, blood was collected and plasma was separated and analyzed for pro-inflammatory markers at 1:10 dilution with array buffer. Cytokines/chemokines, including stromal cell-derived factor1 (CXCL12), macrophage-colony-stimulating factor (M-CSF), complement component 5A(C5A), and keratinocyte-derived chemokine/CXCL1 (KC/CXCL1) were quantified using Mouse Cytokine Array Panel A (R&D Systems, Minnesota, USA, Serial No. 893560) following the manufacturer's instruction.

Transfusion of RBCs

Biotinylation of RBCs, in vivo. Briefly, Sulfo-NHS Biotin (Thermo-fisher Scientific, US) powder was dissolved in sterile PBS, vortexed, and passed through a 0.22 µm filter. It was diluted to a final concentration of 1 mg biotin-sulfo-NHS per 300 µL 1× PBS. Mice were restrained, and the biotin reagent solution was administered through intravenous injection. After 48 h of the biotin administration, under mild

anesthesia, around 1 ml of biotinylated blood was collected through a cardiac puncture in CPD-containing vials and immediately centrifuged at 500g for 20 min at 4 °C. Plasma was carefully aspirated, and pRBCs were pooled together. The biotin-labeled blood was processed and stored using Optisol as a preservative in sterile Eppendorf tubes (0.5 and 1 ml).

Treatment of Biotin-labeled RBCs with Tau-AcrNFS

Functionality tests. Biotin-labeled RBCs were divided into treated and untreated groups. The treatment group (*n* = 3) pRBC units were treated with *Tau-AcrNFS* on the 5th and 10th days of storage and then packed until 18 days. The untreated group pRBCs units (*n* = 3) were not treated with sheets during the storage timeline. Both groups were analyzed for PS exposure during storage.

Evaluating the enhanced shelf-life of biotin-labeled RBCs by recovery experiment. On different days of storage (0, 7, 14, 15, 16, 17, and 18 days), biotinylated pRBC units with and without treatment were diluted (1:1) with PBS. Totally, 200 µL of diluted biotinylated pRBC was administered to the restrained mice via intravenous injection⁴⁵. At specific time points, 6 µL of blood was collected via tail snip and stored in microfuge tubes containing 250 µL of sterile PBS.

To detect biotinylated RBCs through flow cytometry, approximately 10⁶–10⁸ RBCs (100 µL of the diluted sample) were added to 0.125 µg of streptavidin- APC-eFluor® 780 Conjugate (1:20 of 0.2 mg/mL; eBioscience™). Samples were incubated in the dark for 5 min, washed with 400 µL PBS, and centrifuged at 1000 g for 4 min. The RBC pellet was resuspended in 200 µL PBS. Samples were analyzed using BD LSR Fortessa cytometer (BD biosciences, USA). The red laser was used to excite the dye (λ emission = 780 nm) with a bandpass filter of 780/60. The following formula was used to calculate the post-transfusion survival (%).

$$\frac{\text{Post transfusion RBC recovery (\%)} \text{ at } t(t)}{\text{Post transfusion RBC Recovery at } t(1h)} \times 100$$

where (*t*) stands for pdst-transfusion time point, i.e., 1, 24, 48, and 72 h. This formula is used for all pRBCs units stored for different days and then transfused in a different set of mice. The data was collected with FACSDiva v8.02 and data analysis was performed FlowJo v10.0.8.

Quantification of total iron in the spleen

Sample digestion and preparation. Splenectomy was performed in mice after 2 h of transfusion. Spleen from all the groups was taken in a tared 2 ml Eppendorf, and the dry weight was recorded. Then, 1 ml protein precipitation solution and 1 ml (8%) nitric acid were added to the spleen tube and homogenized for 2 min. The protein precipitation solution was prepared with 0.53 N HCl and 5.3% trichloroacetic acid in HPLC water. The solution containing a homogenized spleen with a closed lid was boiled at 2000C for 30 min. Cooled in RT for 2 min, and caps were opened to release air bubbles. Finally, the solution was centrifuged at full speed for 10 min. For total iron quantification, the supernatant from all the groups (*n* = 3) was taken.

ICP-MS method. The optimized operating conditions used for ICP-MS (Shimadzu-2030) are summarized in Supplementary Table 2. A peristaltic pump was used to deliver the samples (0.1 mL/min) to the nebulizer, converting the sample into a spray mist using argon (Ar) gas. Automated adjustments were made for torch alignment, detector voltage, and ion lens voltages for optimized resolution, sensitivity, and stability across a broad range of atomic masses. The doubly charged ion/charge ratio (Ce²⁺ 69.95 to Ce 139.90) and oxide ratio (CeO⁺ 155.90 to Ce139.90) were also monitored and were maintained below 3% and 2.5% (intensity), respectively. The Prep Fast system was interfaced with the ICP-MS and auto-diluted the stock solutions to generate the

calibration curves and QC samples. The 30-ppb Indium (In) solution was also mixed in-line by the Prep-Fast during the analysis as an internal standard to all the analyzed samples and standards. The method was evaluated for its selectivity, sensitivity, linearity, precision, and accuracy.

Statistical analysis

In experiments with multiple groups, ordinary one-way ANOVA with Tukey's post hoc test was used. In experiments with multiple groups, which are time-course studies, repeated measures of one-way ANOVA were used. The two-tailed Student's *t*-test with Welch's corrections was used to compare two experimental groups. The probability value (*P*) < 0.05 was considered as a statistically significant difference. Statistical analysis and graphing were performed with GraphPad PRISM 9.

Reporting summary

Further information on research design is available in the Nature Portfolio Reporting Summary linked to this article.

Data availability

All data generated or analyzed during this study are included in this published article and its supplementary information files or are available from the corresponding author upon reasonable request. Source data are provided with this paper.

References

- Netzer, G. et al. Transfusion practice in the intensive care unit: a 10-year analysis. *Transfusion* **50**, 2125–2134 (2010).
- Sharma, S., Sharma, P. & Tyler, L. N. Transfusion of blood and blood products: indications and complications. *Am. Fam. Phys.* **83**, 719–724 (2011).
- Remy, K. E. & Spinella, P. C. Red blood cell storage age—what we know from clinical trials. *Expert. Rev. Hematol.* **9**, 1011–1013 (2016).
- Hovav, T., Yedgar, S., Manny, N. & Barshtein, G. Alteration of red cell aggregability and shape during blood storage. *Transfusion* **39**, 277–281 (1999).
- Bennett-Guerrero, E. et al. Evolution of adverse changes in stored RBCs. *Proc. Natl Acad. Sci. USA* **104**, 17063–17068 (2007).
- Roback, J. D. Vascular effects of the red cell storage lesion. *Hematol. Am. Soc. Hematol. Educ. Program* **2011**, 475–479 (2011).
- Arese, P., Turrini, F. & Schwarzer, E. Band 3/complement-mediated recognition and removal of normally senescent and pathological human erythrocytes. *Cell Physiol. Biochem.* **16**, 133–146 (2005).
- Orlov, D. & Karkouti, K. The pathophysiology and consequences of red blood cell storage. *Anaesthesia* **70**, 29–37 (2015).
- Rapido, F. et al. Prolonged red cell storage before transfusion increases extravascular hemolysis. *J. Clin. Invest.* **127**, 375–382 (2017).
- Yoshida, T., Prudent, M. & D'Alessandro, A. Red blood cell storage lesion: causes and potential clinical consequences. *Blood Transfus.* **17**, 27–52 (2019).
- Bakkour, S. et al. Manufacturing method affects mitochondrial DNA release and extracellular vesicle composition in stored red blood cells. *Vox Sang.* **111**, 22–32 (2016).
- Blumberg, N. et al. An association between decreased cardiopulmonary complications (transfusion-related acute lung injury and transfusion-associated circulatory overload) and implementation of universal leukoreduction of blood transfusions. *Transfusion* **50**, 2738–2744 (2010).
- Henkelman, S., Noorman, F., Badloe, J. F. & Lagerberg, J. W. Utilization and quality of cryopreserved red blood cells in transfusion medicine. *Vox Sang.* **108**, 103–112 (2015).
- Chang, A. L. et al. Previous cryopreservation alters the natural history of the red blood cell storage lesion. *Shock* **46**, 89–95 (2016).
- Burns, J. M. et al. Deterioration of red blood cell mechanical properties is reduced in anaerobic storage. *Blood Transfus.* **14**, 80–88 (2016).
- Dumont, L. J., D'Alessandro, A., Szczepiorkowski, Z. M. & Yoshida, T. CO₂-dependent metabolic modulation in red blood cells stored under anaerobic conditions. *Transfusion* **56**, 392–403 (2016).
- Hess, J. R. et al. Successful storage of RBCs for 10 weeks in a new additive solution. *Transfusion* **40**, 1012–1016 (2000).
- Pallotta, V., Gevi, F., D'Alessandro, A. & Zolla, L. Storing red blood cells with vitamin C and *N*-acetylcysteine prevents oxidative stress-related lesions: a metabolomics overview. *Blood Transfus.* **12**, 376–387 (2014).
- Vani, R. et al. Prospects of vitamin C as an additive in plasma of stored blood. *Adv. Hematol.* **2015**, 961049 (2015).
- Schmidt, A., Refaai, M., Kirkley, S. & Blumberg, N. Proven and potential clinical benefits of washing red blood cells before transfusion: current perspectives. *Int. J. Clin. Transfus. Med.* **4**, 79–88 (2016).
- Bennett-Guerrero, E. et al. Randomized study of washing 40–42 day stored red blood cells. *Transfusion* **54**, 2544–2552 (2014).
- Fuchs, T. A. et al. Neutrophils release extracellular DNA traps during storage of red blood cell units. *Transfusion* **53**, 3210–3216 (2013).
- Vlaar, A. P. J. et al. Accumulation of bioactive lipids during storage of blood products is not cell but plasma derived and temperature dependent. *Transfusion* **51**, 2358–2366 (2011).
- Silliman, C. C. et al. Identification of lipids that accumulate during the routine storage of prestorage leukoreduced red blood cells and cause acute lung injury. *Transfusion* **51**, 2549–2554 (2011).
- D'Alessandro, A. & Zolla, L. Biochemistry of red cell aging in vivo and storage lesions. *Haematologica* **7**, 389–396 (2013).
- Bosman, G. J., Were, J. M., Willekens, F. L. & Novotny, V. M. Erythrocyte ageing in vivo and in vitro: structural aspects and implications for transfusion. *Transfus. Med.* **18**, 335–347 (2008).
- Ho, J., Sibbald, W. J. & Chin-Yee, I. H. Effects of storage on efficacy of red cell transfusion: when is it not safe? *Crit. Care Med.* **31**, S687–S697 (2003).
- Chasis, J. A. & Mohandas, N. Erythrocyte membrane deformability and stability: two distinct membrane properties that are independently regulated by skeletal protein associations. *J. Cell Biol.* **103**, 343–350 (1986).
- Roussel, C., Buffet, P. A. & Amireault, P. Measuring post-transfusion recovery and survival of red blood cells: strengths and weaknesses of Chromium-51 labeling and alternative methods. *Front. Med.* **5**, 1–8 (2018).
- Gilson, C. R. et al. A novel mouse model of red blood cell storage and posttransfusion in vivo survival. *Transfusion* **49**, 1546–1553 (2009).
- Hod, E. A. et al. Transfusion of red blood cells after prolonged storage produces harmful effects that are mediated by iron and inflammation. *Blood* **115**, 4284–4292 (2010).
- Mock, D. M. et al. Development, validation, and potential applications of biotinylated red blood cells for posttransfusion kinetics and other physiological studies: evidenced-based analysis and recommendations. *Transfusion* **58**, 2068–2081 (2018).
- Kuypers, F. A. & de Jong, K. The role of phosphatidylserine in recognition and removal of erythrocytes. *Cell Mol. Biol. (Noisy -le-Gd.)* **50**, 147–158 (2004).
- Verhoeven, A. J. et al. Prolonged storage of red blood cells affects aminophospholipid translocase activity. *Vox Sang.* **91**, 244–251 (2006).
- Bosman, G. J. et al. Susceptibility to hyperosmotic stress-induced phosphatidylserine exposure increases during red blood cell storage. *Transfusion* **51**, 1072–1078 (2011).
- Segawa, K. & Nagata, S. An apoptotic 'eat me' signal: phosphatidylserine exposure. *Trends Cell Biol.* **25**, 639–650 (2015).

37. Dinkla, S. et al. Phosphatidylserine exposure on stored red blood cells as a parameter for donor-dependent variation in product quality. *Blood Transfus.* **12**, 204–209 (2014).
38. Burger, P., De Korte, D., Van Den Berg, T. K. & Van Bruggen, R. CD47 in erythrocyte ageing and clearance—the dutch point of view. *Transfus. Med. Hemotherapy* **39**, 348–352 (2012).
39. Lelubre, C. & Vincent, J.-L. Relationship between red cell storage duration and outcomes in adults receiving red cell transfusions: a systematic review. *Crit. Care* **17**, R66 (2013).
40. Rimmelé, T. & Kellum, J. A. Clinical review: blood purification for sepsis. *Crit. Care* **15**, 1–10 (2011).
41. Didar, T. F. et al. Improved treatment of systemic blood infections using antibiotics with extracorporeal opsonin hemoadsorption. *Biomaterials* **67**, 382–392 (2015).
42. Land, W. G. Transfusion-related acute lung injury: the work of DAMPs. *Transfus. Med. Hemotherapy* **40**, 3–13 (2013).
43. Han, V., Serrano, K. & Devine, D. V. A comparative study of common techniques used to measure haemolysis in stored red cell concentrates. *Vox Sang.* **98**, 116–123 (2010).
44. Singer, V. L., Jones, L. J., Yue, S. T. & Haugland, R. P. Characterization of PicoGreen reagent and development of a fluorescence-based solution assay for double-stranded DNA quantitation. *Anal. Biochem.* **249**, 228–238 (1997).
45. Dholakia, U., Bandyopadhyay, S., Hod, E. A. & Prestia, K. A. Determination of RBC survival in C57BL/6 and C57BL/6-Tg(UBC-GFP) mice. *Comp. Med.* **65**, 196–201 (2015).

Acknowledgements

This work was supported by core funds from the Institute for Stem Cell Science and Regenerative Medicine (DBT-inStem). S.P. was supported by Senior Research Fellowship from the Lady Tata Memorial Trust. U.B. was supported by National Postdoctoral Fellowship under the Nano-mission of the Department of Science Technology (DST), Govt. of India. Animal work in the inStem/NCBS Animal Care and Resource Centre was partially supported by the National Mouse Research Resource (NaMoR) grant (grant no. BT/PR5981/MED/31/181/2012:2013-2016;2018) from the Department of Biotechnology. We thank the animal house facility/members and Central Imaging & Flow Cytometry facility (CIFF) at inStem and NCBS. We thank the NMR facility at NCBS. P.K.V. thanks Dr. Sandip Patil and E-Spin Nanotech Pvt. Ltd., India, for their generous gift of a Super ES-1 device.

Author contributions

P.K.V. conceived and designed the experiments. S.P., M.M., P.S., U.B., and R.P. designed, performed the experiments, and analyzed the data. M.M., S.P., and T.J. synthesized the polymers. S.P., M.M., P.S., U.B., and

R.P. performed in vitro and in vivo experiments. S.P. and P.K.V. wrote the paper, all authors discussed the results. P.K.V. supervised the project.

Competing interests

P.K.V., S.P., M.M., P.S., and U.B. hold a patent related to this technology: “Composition and methods to enhance the quality and shelf-life of biological material” (IPP Application no: 202241014827, provisional application). The patent applicant is the Institute for Stem Cell Science and Regenerative Medicine. All compositions and methods of use described in this manuscript were covered in the patent application. T.J.G. and R.P. do not have any competing interests.

Additional information

Supplementary information The online version contains supplementary material available at <https://doi.org/10.1038/s41467-022-35269-3>.

Correspondence and requests for materials should be addressed to Praveen Kumar Vemula.

Peer review information *Nature Communications* thanks Rosemary Sparrow, Vani Rajashekaraiah, and the other, anonymous, reviewer(s) for their contribution to the peer review of this work. Peer reviewer reports are available.

Reprints and permissions information is available at <http://www.nature.com/reprints>

Publisher's note Springer Nature remains neutral with regard to jurisdictional claims in published maps and institutional affiliations.

Open Access This article is licensed under a Creative Commons Attribution 4.0 International License, which permits use, sharing, adaptation, distribution and reproduction in any medium or format, as long as you give appropriate credit to the original author(s) and the source, provide a link to the Creative Commons license, and indicate if changes were made. The images or other third party material in this article are included in the article's Creative Commons license, unless indicated otherwise in a credit line to the material. If material is not included in the article's Creative Commons license and your intended use is not permitted by statutory regulation or exceeds the permitted use, you will need to obtain permission directly from the copyright holder. To view a copy of this license, visit <http://creativecommons.org/licenses/by/4.0/>.

© The Author(s) 2022